

**Titre:** Thermoplastic Vulcanizate Nanocomposites Based on Polypropylene/Ethylene Propylene Diene Terpolymer (PP/EPDM) Prepared by Reactive Extrusion  
**Title:**

**Auteur:** Amin Mirzadeh  
**Author:**

**Date:** 2012

**Type:** Mémoire ou thèse / Dissertation or Thesis

**Référence:** Mirzadeh, A. (2012). Thermoplastic Vulcanizate Nanocomposites Based on Polypropylene/Ethylene Propylene Diene Terpolymer (PP/EPDM) Prepared by Reactive Extrusion [Thèse de doctorat, École Polytechnique de Montréal]. PolyPublie. <https://publications.polymtl.ca/782/>  
**Citation:**

 **Document en libre accès dans PolyPublie**  
Open Access document in PolyPublie

**URL de PolyPublie:** <https://publications.polymtl.ca/782/>  
PolyPublie URL:

**Directeurs de recherche:** Charles Dubois, Pierre Lafleur, & Musa R. Kamal  
**Advisors:**

**Programme:** Génie chimique  
**Program:**

UNIVERSITÉ DE MONTRÉAL

THERMOPLASTIC VULCANIZATE NANOCOMPOSITES BASED ON  
POLYPROPYLENE/ETHYLENE PROPYLENE DIENE TERPOLYMER  
(PP/EPDM) PREPARED BY REACTIVE EXTRUSION

AMIN MIRZADEH

DÉPARTEMENT DE GÉNIE CHIMIQUE  
ÉCOLE POLYTECHNIQUE DE MONTRÉAL

THÈSE PRÉSENTÉE EN VUE DE L'OBTENTION  
DU DIPLÔME DE PHILOSOPHIAE DOCTOR  
(GÉNIE CHIMIQUE)

JANVIER 2012

UNIVERSITÉ DE MONTRÉAL

ÉCOLE POLYTECHNIQUE DE MONTRÉAL

Cette thèse intitulée:

THERMOPLASTIC VULCANIZATE NANOCOMPOSITES BASED ON  
POLYPROPYLENE/ETHYLENE PROPYLENE DIENE TERPOLYMER (PP/EPDM)  
PREPARED BY REACTIVE EXTRUSION

présentée par: MIRZADEH Amin

en vue de l'obtention du diplôme de : Philosophiae Doctor

a été dûment acceptée par le jury d'examen constitué de :

Mme DESCHÊNES Louise, Ph.D., présidente

M. DUBOIS Charles, Ph.D., membre et directeur de recherche

M. LAFLEUR Pierre, Ph.D., membre et codirecteur de recherche

M. KAMAL Musa R., Ph.D., membre et codirecteur de recherche

M. FAVIS Basil, Ph.D., membre

M. CASSAGNAU Philippe, Ph.D., membre

## **DEDICATION**

To my Family

## ACKNOWLEDGMENTS

I would like to express my deep and sincere gratitude to my research supervisors, Prof. Charles Dubois, Prof. Pierre Lafleur and Prof. Musa Kamal for believing in my potential and for providing me the great opportunity to study under their supervision. Their innovative and questioning approach, encouragement, patience and broad knowledge helped me throughout my study at the École Polytechnique de Montréal.

Thanks to Prof. Philippe Cassagnau, Prof. Basil Favis and Prof. Louise Deschênes for taking part in my thesis committee.

During my study, I had the chance to attend and present my results in rheology meetings. I would like to thank Prof. Pierre J. Carreau and Prof. Marie-Claude Heuzey and all the students in their research group for the valuable comments and suggestions.

I shall also thank to the National Science and Engineering Research Council of Canada whose generous financial support made this research possible.

I would like to appreciate Dr. Prashant Bhadane and Dr. Shant Shabbikian who worked on the same field before me. It was a great privilege to have a discussion with them about the scientific issues.

Thanks to all the technical staff of Chemical Engineering department, especially Mr. Jacques Beausoleil, Mr. Guillaume Lessard, Mr. Gino Robin, Ms. Martine Lamarche, Mr. Carol Painchaud and Mr. Lionel Valero. An especial thank to Ms. Mélina Hamdine for all the training, suggestions and her patience. I would also like to thank Ms. Leelapornpisit Weawkamol for experimental assistance particularly for microscopy parts.

I would like to thank my friends with whom I had wonderful time during these years; Majid, Tara, Daniel, Leila, Sina, Babak, Khatereh, Farrokh, with special thanks to Camilia who has been there for me in any condition and helped me for the French translation.

And last but not the least, all my deepest gratitude to my family for their unconditional love and support.

## RÉSUMÉ

Les élastomères thermoplastiques (TPEs) représentent un groupe important de matériaux polymères, plus précisément des mélanges de polymères, qui possèdent un comportement élastique similaire aux matériaux caoutchouteux mais contiennent des liens thermoréversibles les rendant faciles à manipuler via des procédés de traitement des thermoplastiques. Une catégorie importante de TPEs consiste en des matériaux à base de polyoléfine, dont de polypropylène (PP) et de terpolymère éthylène-propylène-diène (EPDM) qui sont connus dans le marché pour leurs propriétés physique et mécanique intéressantes obtenues grâce à leur faible tension interfaciale ( $\sim 0.3$  mN/m) et à leur compatibilité de phase. Durant les dernières décennies les mélanges d'EPDM/PP ont, en raison de l'importance commerciale, attiré l'attention des milieux industriels et académiques afin d'améliorer leur comportement élastique et /ou leurs propriétés techniques, et étendre leurs champs d'application.

Cette thèse s'intéresse principalement à l'usage des nanotechnologies par l'incorporation de la nano-argile dans la phase thermoplastique de ces matériaux. Elle étudie l'effet de différents niveaux de dispersion de la nano-argile sur la co-continuité des mélanges réactifs et la liaison interfaciale des mélanges préparés par l'extrusion réactive. De plus, la recherche portée dans ce travail a aussi pour but de déterminer le comportement élastique de ces mélanges en présence de la nano-argile et cela en relation avec le niveau de dispersion de ces particules dans les mélanges. Par conséquent, le développement morphologique et les propriétés fonctionnelles et techniques des nanocomposites thermoplastiques vulcanisés (TPV) ont été investigués. Pour ce travail, différentes sortes de polymères polypropylène-g-maléique anhydride ont été utilisées afin d'élucider l'effet de l'agent de comptabilisation sur le niveau de dispersion de la nano-argile dans la phase thermoplastique. Les analyses par diffractométrie de rayons X (XRD), la microscopie électronique à transmission (TEM), et la microscopie électronique à balayage (SEM) des mélanges préparés confirment que les nanocomposites PP se modifient d'une structure intercalée vers une coexistence des tactoïdes intercalés et des couches exfoliées nommées des nanocomposites 'partiellement exfoliées'. Parmi les différents paramètres de performance de l'agent de comptabilisation, sa relaxation se corrèle directement avec les résultats de la caractérisation des nanocomposites; un temps de relaxation plus long de l'agent de comptabilisation est associé avec une meilleure dispersion de la nano-argile dans les mélanges.

Pour étudier la co-continuité du développement des mélanges non-réactifs, l'EPDM et les nanocomposites PP ont été mélangés à l'état fondu avec différentes compositions en utilisant un mélangeur interne. Basé sur la mesure de continuité des TPEs et de leurs nanocomposites associées pour la phase thermoplastique et élastique, il est déduit que la présence de nano-argile réduit la plage de composition de la co-continuité et altère ses caractéristiques symétriques. Toutefois, cet effet est plus prononcé plus chez les nanocomposites intercalées que chez les nanocomposites partiellement exfoliées. Une meilleure dispersion de la nano-argile limite la réduction de la continuité de la phase thermoplastique de sorte que l'indice de continuité de la phase thermoplastique des nanocomposites TPE partiellement exfoliées préparées avec un contenu plus élevé d'EPDM (*i.e.* à 70 wt%) devient plus importante que celle des TPEs sans nano-argile. Ces résultats montrent qu'il est possible d'utiliser plus d'EPDM dans les mélanges en utilisant des nanocomposites partiellement exfoliées avant la formation de la matrice de dispersion de structure qui limite la production du TPV. Néanmoins, il s'avère important de mentionner que les radiations gamma ont été utilisées pour stabiliser la morphologie d'EPDM et estimer la continuité du PP en utilisant des extractions solubles et des techniques de gravimétrie.

De plus, l'effet de la continuité sur le comportement rhéologique des nanocomposites TPE a été étudié. La viscosité transitoire s'est montrée plus sensible à l'indice de continuité que les autres fonctions matérielles obtenues en utilisant un balayage en fréquence, des essais de relaxation de contrainte, et les essais de fluage. Il a été montré qu'un indice de continuité d'EPDM plus élevé amène à une baisse de viscosité transitoire normalisée quand la phase thermoplastique est continue; car la déformation des domaines d'EPDM est plus facile que l'altération dans une matrice continue. D'un autre côté, basé sur les expériences d'extraction et des micrographes SEM, il existe des preuves qui démontrent que l'argile reste principalement dans la phase PP. Les résultats de balayage par la calorimétrie différentielle (DSC) montrent que la présence de nano-argile dans la phase thermoplastique augmente la température de la cristallisation (jusqu'à ~20 °C), ce qui peut s'avérer bénéfique pour les applications de moulage par injection grâce à une solidification plus rapide et un temps de cycle plus court.

L'objectif ultime de ce travail est de maximiser le comportement élastique en contrôlant la morphologie du mélange et son niveau de réticulation. Par conséquent, cette étude couvre aussi les effets de la présence de nano-argile et son niveau de dispersion sur la réaction de réticulation des nanocomposites TPV préparées par une extrusion réactive. Ici, la phase élastique a été

vulcanisée d'une manière dynamique en utilisant une résine phénolique de diméthylol ou une résine d'octylphénol-formaldéhyde avec du chlorure d'étain déshydraté comme catalyseur. Dans cette étude, la vulcanisation dynamique des TPVs préparés et ses nanocomposites correspondant a été caractérisée en utilisant différents critères tels que : le contenu en fraction soluble, la viscosité et le module élastique  $G'$  en déformation dynamique, , la largeur du signal de résonance magnétique nucléaire (RMN), le contenu d'agent de réticulation et la concentration en diène résiduelle. La combinaison de ces paramètres a été jugée suffisante pour décrire le système.

Contrairement aux mélanges préparés dans un mélangeur interne dans lequel le niveau de réticulation des nanocomposites TPV est toujours plus bas que celui des TPVs, l'effet de la présence de nano-argile dans les échantillons préparés par extrusion réactive s'avère plus compliqué. Il appert que la différence entre la taille de la réaction de réticulation entre les TPVs et les nanocomposites TPV est plus prononcée pour les échantillons préparés avec une vitesse de vis plus élevée (400 tour par minute (rpm), temps de résidence ~ 65 s). Néanmoins, il n'existe pas de différence significative pour les échantillons préparés avec une vitesse de vis plus basse (200 rpm, temps de résidence ~ 45 s).

Pour ces mélanges réactifs, l'analyse de la courbe du couple de mélange en fonction du temps, ainsi que l'analyse des mesures sur la fraction soluble et des micrographes SEM à différentes positions dans l'extrudeuse confirment que la structure co-continue existe au moins avant la deuxième zone de mélange dans une extrudeuse bi-vis en fonctionnement co-rotatif. Autrement dit, la co-continuité des mélanges avant la deuxième zone de mélange n'est pas seulement contrôlée par la vulcanisation dynamique, mais aussi par la présence de nano-argile. Considérant ce fait et basé aussi sur le calcul de la conversion chimique par la mesure des valeurs de concentration de la diène résiduelle obtenu par RMN, il est suggéré que la présence de nano-argile affecte la réaction de réticulation principalement par son influence sur la continuité de la phase d'EPDM dans la structure co-continue qui se forme lors de l'étape initiale du processus de mélange. Il a été démontré qu'une plage de réticulation plus élevée est associée avec un indice de continuité d'EPDM plus haut. À son tour, le niveau de la co-continuité dépend aussi du degré de dispersion de nano-argiles. Aussi, quand la continuité de la phase d'EDPM des deux mélanges est similaire, l'effet de barrière des nano-argiles intensifie la réaction de réticulation par l'augmentation de la concentration de l'agent curatif local. Nos travaux montrent que si l'EPDM dans le système correspondant non-réactif est une phase continue, le niveau de la réaction de

réticulation devient plus dépendant de la vitesse de rotation des vis. En autres mots, plus le temps de résidence est long, plus élevé est l'étendue de réticulation. De plus, il est important de mentionner que la valeur de la largeur de base du pic principal en spectroscopie RMN peut seulement être utilisée pour comparer l'étendue de réticulation dans des TPVs dû à l'influence du nano-argile sur la mobilité de la chaîne principale de l'EPDM dans les nanocomposites TPV.

L'analyse des mélanges du point de vue de structure des nanocomposites révèle que l'interaction des chaînes de polymères dans les galeries inter-couches des nano-argiles est plus prononcée pour les nanocomposites TPV comparé aux nanocomposites TPE dû à une contrainte de cisaillement plus élevée exercée sur les couches nano-argiles durant la vulcanisation dynamique. Aussi, en augmentant le contenu d'EPDM, l'intercalation du polymère n'a pas été significativement améliorée. Pour les nanocomposites TPV préparés à une vitesse de vis plus élevée (400 rpm), le premier pic de la caractéristique du nano-argile en diffraction rayon X ( $2\theta = 2.85^\circ$ , l'espace-d correspondant est 3.1 nm) s'est déplacé à un angle plus bas ( $2\theta = 0.94^\circ$ , l'espace-d correspondant est 9.3 nm), tandis que celui des nanocomposites TPV basés sur une composition partiellement exfoliée a complètement disparu.

La dernière partie de cette thèse se penche sur la question de l'influence du niveau de dispersion des nano-argiles, et conséquemment l'étendue de réticulation, sur le comportement élastique et la morphologie des TPVs. Une méthode récemment développée, s'appelant le balayage de la température de relaxation de contrainte (TSSR), a été utilisée pour estimer l'indice d'élasticité des TPVs et des nanocomposites TPV. Cette méthode donne de l'information satisfaisante sur l'étendue de réaction de réticulation. Le comportement élastique des mélanges contenant 50 p/p % et 60 p/p% d'EPDM- dans lesquelles les études morphologiques suggèrent la présence des gouttes élastiques dans le voisinage des particules élastiques de formes irrégulières avec un niveau d'inter-connectivité bas- corrèle avec la taille de la gouttelette élastique. Par conséquent, la présence de nano-argile influence la valeur de l'indice d'élasticité par son effet sur la taille des gouttelettes élastiques qui contrôle le nombre des points de rétraction dans le mécanisme de fluage proposé durant l'essai TSSR. Il faut prendre note que l'augmentation du contenu d'EPDM abaisse le nombre des gouttes et augmente aussi la formation des particules élastiques avec des formes irrégulières. D'un autre côté, la relation directe entre les valeurs de l'indice élastique et la densité de réticulation est seulement observée pour des séries de TPVs qui

montrent un réseau extensif bien développé entre les gouttes de forme irrégulière (mélanges contenant 70wt% d'EPDM). Finalement, l'effet de la présence de nano-argile et son niveau de dispersion sur le comportement élastique se démontre par son influence sur la densité de réticulation.

## ABSTRACT

Thermoplastic elastomeric materials (TPEs) are an important class of copolymers or polymer blends that exhibit the typical advantages of conventional rubbers but can be processed with the thermoplastic processing methods. Among different kind of thermoplastic elastomer, those based on polypropylene (PP) and ethylene propylene diene terpolymer (EPDM) are known to have more interesting properties due to the relatively low interfacial tension between PP and EPDM ( $\sim 0.3$  mN/m). Considering the commercial significance of the mentioned blends, different approaches have been used during the last few decades to improve their rubber like behaviour and/or their engineering properties to expand their fields of applications. In this regard, in the present dissertation, the use of nanotechnology by incorporating the nanoclay in the thermoplastic phase is the major interest subject. The effects of different nanoclay dispersion levels on the co-continuity of non reactive blends and the extent of crosslinking in the blends prepared by reactive extrusion are studied. This research intends to tailor the rubber like behaviour by the nanoclay presence and its dispersion level. Therefore the morphology development along the screw axis and the functional and engineering properties of the prepared thermoplastic vulcanizates nanocomposites are also investigated.

For this work, different grades of polypropylene-g-maleic anhydride polymers were chosen to elucidate the effect of compatibilizer on the nanoclay dispersion level in thermoplastic phase. X-ray diffraction (XRD) patterns along with transmission electron microscopy (TEM) and scanning electron microscope (SEM) micrographs confirmed that prepared PP nanocomposites ranged from intercalated structure to a coexistence of intercalated tactoids and exfoliated layers namely “partially exfoliated” nanocomposite. Among various factors affecting the compatibilizer performance, it is shown that only the relaxation behaviour of compatibilizer correlates directly with the nanocomposites characterization results; higher relaxation times of the compatibilizer are associated with better dispersion of nanoclay.

To study the co-continuity development of the nonreactive blends, EPDM and the mentioned PP nanocomposites at various compositions were melt blended using an internal mixer. Based on continuity measurements of TPEs and TPE nanocomposites for both thermoplastic and rubber phase, it is shown that the presence of nanoclay decreases the co-continuity composition range and alters its symmetrical feature. However, this effect is more

pronounced in the intercalated nanocomposites than in partially exfoliated nanocomposites. It seems that better nanoclay dispersion limits the reduction of the thermoplastic phase continuity in a manner that the continuity index of the thermoplastic phase for partially exfoliated TPE nanocomposite prepared at high EPDM content (i.e. at 70 wt%) is greater than that of corresponding TPE without nanoclay. According to these results, it is possible to shift to higher EPDM content using partially exfoliated system before formation of matrix-dispersed particle structure which limits thermoplastic vulcanizate production. This should be mentioned that gamma irradiation was carried out in order to fix the EPDM morphology to estimate the continuity of PP using the solvent extraction and gravimetry technique. Additionally, the effect of continuity on rheological behaviour of TPE nanocomposites was investigated. The stress growth viscosity was found to be more sensitive to the continuity index than other material functions obtained using frequency sweep, stress relaxation and creep experiments. It seems that a higher EPDM continuity index leads a lower overshoot of normalized stress growth viscosity when thermoplastic phase is continuous because deformation of the separated domains of EPDM is easier than alteration in a continuous network structure.

On the other hand, based on extraction tests and SEM micrographs, there are some evidences that clay remain mainly in the PP phase. According to differential scanning calorimetry (DSC) results, the presence of nanoclay in the thermoplastic phase increases the crystallization temperature (up to  $\sim 20$  °C) that could be beneficial for molding applications, because of the faster solidification and shorter cycle time.

The ultimate goal in this field is to maximize the rubber like behaviour by controlling the blend morphology and the level of crosslinking. Therefore, this study also covers the effects of nanoclay presence and its dispersion level on the crosslinking reaction of thermoplastic vulcanizate nanocomposites prepared by reactive extrusion. Here, the rubber phase was dynamically vulcanized using dimethylol phenolic resin or octylphenol-formaldehyde resin along with stannous chloride dihydrate as the catalyst. In the present study, the dynamic vulcanization of the prepared TPVs and corresponding nanocomposites are characterized using different criteria, such as gel content, viscosity and normalized storage modulus in the time sweep tests, nuclear magnetic resonance (NMR) signal line width, bound curative content and residual diene concentration. The combination of the above parameters appears to be sufficient to provide a clear description of the systems.

Contrary to the blends prepared in internal batch mixer in which the extent of crosslinking in TPV nanocomposites is always lower than that of TPVs, however, the effect of nanoclay presence in the samples prepared by reactive extrusion is more complicated. It seems that the difference in the extent of crosslinking reaction between TPVs and TPV nanocomposites is more pronounced for the samples prepared at higher screw speed (400 rpm, residence time of ~ 45 s). Whereas, there is no significant difference was found for the samples prepared at lower screw speed (200 rpm, residence time of ~ 65 s).

The torque-time curve analysing obtained from internal batch mixer, gel content experiments and SEM micrographs along the extruder axis for the reactive blends confirm that the co-continuous structure exists at least before the second mixing zone of the twin screw extruder. In other words, the co-continuity of the blends before the second mixing zone is not only controlled by dynamic vulcanization but also by the presence of nanoclay. Considering this fact and based on the bound curative content and residual diene concentration values obtained by solid state NMR, it is suggested that nanoclay presence affects the extent of crosslinking reaction mainly through its effect on the continuity of the EPDM phase in the co-continuous structure forming in the initial stage of the mixing process. It is shown that the higher extent of crosslinking is associated with higher continuity index of EPDM. In turn, the level of co-continuity, as mentioned earlier, depends on the degree of dispersion of nanoclay. On the other hand, when the continuity of EPDM phase of two blends is similar, the barrier effect of nanoclays intensifies the crosslinking reaction by increasing the local concentration of curing agent. In our experimental window, if EPDM in the corresponding non-reactive system is a continuous phase, the extent of crosslinking reaction appears to be more dependent on the screw speed. Otherwise, higher residence time would increase the extent of crosslinking. Moreover, it should be mentioned that the backbone peak base width values may be used only to compare the extent of crosslinking in the TPVs due to the influence of nanoclay on the mobility of the backbone of EPDM in TPV nanocomposites.

The investigation of the blends, from nanocomposite structure point of view, reveals that intercalation of polymer chains into the interlayer galleries of the nanoclays is more pronounced for the TPV nanocomposites compared to TPE nanocomposites due to the higher shear stress which is exerted on the nanoclay layers during dynamic vulcanization. It should be mentioned that by increasing EPDM content, polymer intercalation was not enhanced significantly. For the

TPV nanocomposites based on intercalated system prepared at higher screw speed (400 rpm), the first characteristic peak of nanoclay ( $2\theta=2.85^\circ$ , corresponding d-spacing is 3.1 nm) shifted to the lower angle ( $2\theta=0.94^\circ$ , corresponding d-spacing is about 9.3 nm) while that of TPV nanocomposites based on partially exfoliated system disappeared.

The last part of the present study is devoted to find how the dispersion level of nanoclay and consequently the extent of crosslinking change the rubber like behaviour and the morphology of the prepared TPVs. Therefore, recently developed method named temperature scanning stress relaxation (TSSR) was used to estimate the rubber indices of TPVs and TPV nanocomposites. The mentioned method also successfully provided information about the extent of crosslinking reaction. It is shown that the rubber like behaviour of the blends containing 50wt% and 60wt% of EPDM in which morphological studies suggest the presence of the rubber droplets in vicinity of irregular shape rubber particles with a low level of interconnectivity, correlates with the rubber droplet size. Therefore, the nanoclay presence affects the rubber index values mainly through its effect on the size of the rubber droplets that controls the number of retraction points in the proposed buckling mechanism during the TSSR test. It should be mentioned that by increasing the EPDM content, the number of the droplet like domains decreases and more irregular shape rubber particles is formed. On the other hand, the direct relation between rubber index values and the crosslink density is observed only for those series of TPVs showing the fully developed extensive network between irregular shape rubber domains (blends containing 70wt% of EPDM). Hence, the nanoclay dispersion level influences the rubber like behaviour through its effect on the crosslink density.

## TABLE OF CONTENTS

DEDICATION .....	III
ACKNOWLEDGMENTS .....	IV
RÉSUMÉ .....	V
ABSTRACT.....	X
TABLE OF CONTENTS .....	XIV
LIST OF TABLES .....	XX
LIST OF FIGURES.....	XXI
NOMENCLATURE.....	XXV
Chapter 1 INTRODUCTION AND OBJECTIVES.....	1
1.1 Introduction .....	1
1.2 Objectives .....	3
1.2.1 Main Objective.....	3
1.2.2 Specific Objective .....	4
Chapter 2 LITERATURE REVIEW .....	5
2.1 Morphology Formation in Dynamically Vulcanized PP/EPDM.....	5
2.1.1 Co-continuity and its Importance on the Final TPVs Morphology .....	7
2.1.2 Factors Influencing the Co-continuity and Final Morphology of TPVs .....	9
2.1.2.1 Viscosity .....	9
2.1.2.2 Interfacial Tension.....	13
2.1.2.3 Processing Conditions and Other Parameters .....	13
2.1.3 Equations for the Phase Inversion and Co-continuous Composition.....	15
2.2 Crosslinking Systems .....	19
2.2.1 Extent of Crosslinking Reaction .....	22

2.2.1.1	Solvent Swelling .....	22
2.2.1.2	Gel Content .....	23
2.2.1.3	Solid State NMR .....	24
2.2.1.4	AFM Force Modulation Amplitude .....	27
2.3	Mechanical and Viscoelastic Properties.....	27
2.3.1	Elastomeric Properties Characterization .....	29
2.3.1.1	Modified Hysteresis Tensile Analysis.....	29
2.3.1.2	Temperature Scanning Stress Relaxation Test (TSSR).....	30
2.4	Rheological Properties .....	31
2.5	Reactive Extrusion of TPVs .....	33
2.6	Polymer Layered Silicate Nanocomposites.....	38
2.6.1	Nano-clay.....	39
2.6.2	Surface Treatment .....	40
2.6.3	Preparation Methods of Nanocomposites.....	41
2.6.3.1	In-situ Polymerization .....	41
2.6.3.2	Solution Mixing.....	41
2.6.3.3	Melt Mixing .....	42
2.6.4	Nanocomposites Characterization.....	42
2.6.4.1	Wide angle X-ray Scattering Analysis .....	43
2.6.4.2	Transmission Electron Microscopy.....	44
2.6.5	Properties of Nanocomposites .....	44
2.7	TPV Nanocomposites.....	45
2.8	Summary and Limitations of the Previous Works.....	47
Chapter 3	ORGANIZATION OF THE ARTICLES.....	50

Chapter 4 THE EFFECT OF COMPATIBILIZER ON THE CO-CONTINUITY AND  
NANOCCLAY DISPERSION LEVEL OF TPE NANOCOMPOSITES BASED ON PP/EPDM 52

4.1	Abstract .....	53
4.2	Introduction .....	54
4.3	Experimental.....	56
4.3.1	Materials .....	56
4.3.2	Blend Preparation and Nomenclature .....	57
4.3.2.1	Masterbatch Preparation .....	57
4.3.2.2	Nanocomposite Preparation .....	58
4.3.2.3	TPE Nanocomposites Preparation.....	58
4.3.3	Characterization Steps.....	59
4.3.3.1	Thermogravimetric Analysis.....	59
4.3.3.2	Differential Scanning Calorimetry .....	59
4.3.3.3	X-ray Diffraction.....	59
4.3.3.4	Electron Microscopy.....	59
4.3.3.5	Solvent Extraction and Gravimetry for Continuity .....	60
4.3.3.6	Rheological Measurements .....	61
4.4	Results and Discussion.....	61
4.4.1	Thermogravimetry.....	61
4.4.2	Differential Scanning Calorimetry and Crystallinity. ....	62
4.4.3	Clay Dispersion in PP and TPE Nanocomposite. ....	63
4.4.4	Correlation between Rheological Behavior of PP-g-MA and Nanoclay Dispersion. ....	67
4.4.4.1	Thermal Stability of PP-g-MA During Rheological Tests. ....	67
4.4.4.2	Determination of Linear Zones in Rheological Tests.....	68
4.4.4.3	Correlation between Compatibilizer Viscosity and Clay Dispersion.....	69

4.4.4.4	Correlation between Compatibilizer Relaxation Time and Clay Dispersion ....	70
4.4.5	Effect of Nanoclay Dispersion Level on Co-continuity and Morphology of TPEs...	71
4.4.5.1	Rubber Phase Continuity in TPEs.....	71
4.4.5.2	Thermoplastic Phase Continuity. ....	75
4.5	Conclusion.....	77
4.6	References .....	79
Chapter 5	THE EFFECTS OF NANOCCLAY DISPERSION LEVELS AND PROCESSING PARAMETERS ON THE DYNAMIC VULCANIZATION OF TPV NANOCOMPOSITES BASED ON PP/EPDM PREPARED BY REACTIVE EXTRUSION.....	81
5.1	Abstract .....	82
5.2	Introduction .....	83
5.3	Experimental Procedures.....	86
5.3.1	Materials .....	86
5.3.2	Blend Preparation and Nomenclature .....	86
5.3.3	Sample Preparation and Characterization Steps .....	88
5.3.3.1	X-ray Diffraction.....	88
5.3.3.2	Electron Microscopy.....	89
5.3.3.3	Determination of Gel Content along the Screw Axis.....	89
5.3.3.4	Rheological Measurements .....	90
5.3.3.5	Solid State NMR .....	90
5.4	Results and Discussion.....	90
5.4.1	Nanocomposite Characterization .....	90
5.4.2	The Extent of Crosslinking.....	93
5.4.2.1	Curve Analyzing and Gel Content Experiments.....	93
5.4.2.2	Rheological Characteristics .....	96

5.4.2.3	Solid State NMR Analysis .....	98
5.5	Conclusion.....	104
5.6	References .....	105
Chapter 6	MORPHOLOGY EVOLUTION AND THERMO MECHANICAL CHARACTERISTICS OF TPV NANOCOMPOSITES BASED ON PP/EPDM PREPARED BY REACTIVE EXTRUSION .....	107
6.1	Abstract .....	108
6.2	Introduction .....	108
6.3	Experimental Procedures.....	111
6.3.1	Materials .....	111
6.3.2	Blend Preparation and Nomenclature .....	111
6.3.3	Sample Preparation and Characterization Steps .....	112
6.3.3.1	X-ray Diffraction.....	112
6.3.3.2	Electron Microscopy.....	112
6.3.3.3	Temperature Scanning Stress Relaxation (TSSR) and Tensile Testing .....	113
6.4	Results and Discussion.....	113
6.4.1	Nanocomposite Characterization .....	113
6.4.2	Crosslink Density of TPVs.....	117
6.4.3	Correlation between Morphology and Rubber like Behavior .....	119
6.4.3.1	TPVs Containing 50 wt% and 60 wt% of EPDM.....	119
6.4.3.2	TPVs Containing 70 wt% of EPDM .....	123
6.4.4	Tensile Properties.....	125
6.5	Conclusion.....	126
6.6	References .....	127
Chapter 7	GENERAL DISCUSSIONS AND CONCLUSIONS.....	130

7.1 Scientific Contributions and Concluding Remarks ..... 130

7.2 Recommendations..... 134

REFERENCES..... 136

## LIST OF TABLES

Table 4-1. Properties of Compatibilizers.....	57
Table 4-2. Nomenclature of TPE nanocomposites based on their compositions.....	58
Table 4-3. Nanoclay content for the masterbatches and nanocomposites obtained by TGA.....	61
Table 4-4. Percent of crystallinity and crystallization temperature .....	63
Table 4-5 . Change in storage modulus and complex viscosity after one hour at 200 °C. ....	68
Table 4-6. Stress values at three sequences for frequency sweep tests.....	68
Table 4-7. Characteristic relaxation time at 200 °C, $\omega=1$ Hz. ....	70
Table 5-1. Processing conditions and the elements used in screw profile .....	87
Table 5-2. . Nomenclature of TPV nanocomposites and their compositions. ....	88
Table 5-3. The continuity indices of EPDM from non-crosslinked specimens.....	101
Table 5-4. The backbone peak base width for the TPV and TPV nanocomposites.....	102
Table 6-1. Tensile properties of TPVs and TPV nanocomposites.....	125

## LIST OF FIGURES

Figure 2-1. Types of morphology in immiscible blends. (a) dispersed structure; (b) Matrix-fiber structures; (c) lamellar structure; (d) co-continuous structure(Potschke & Paul, 2003) .....	6
Figure 2-2. Co-continuous structure composition range using definition 1 and definition 2 (Potschke & Paul, 2003) .....	8
Figure 2-3. Relation between the volume range of co-continuous structures and viscosity ratio (M. Van Duin & Machado, 2005) .....	9
Figure 2-4. Schematic representation of the two dispersion mechanisms: Left, the stepwise equilibrium mechanism of repeated breakup at $Ca_{critical}$ ; right, the transient mechanism of thread breakup during extension (Janssen & Meijer, 1993). .....	11
Figure 2-5. Distortion growth rate at dominant wavelength and dominant wave length vs $\lambda$ (Potschke & Paul, 2003) .....	12
Figure 2-6. Comparison of effect of viscosity ratio on critical shear in rotational and irrotational shear fields (Grace 1982). .....	12
Figure 2-7. Continuity index of EPDM in non-plasticized and plasticized PP/EPDM blends (Shant. Shahbikian, 2010). .....	14
Figure 2-8. Phase inversion predictions for different viscosity based-models as well as the .....	18
Figure 2-9. Simplified mechanism of $SnCl_2$ -activated resole crosslinking of ENB-EPDM (M. Van Duin & Machado, 2005) .....	21
Figure 2-10. Change of the extent of EVA crosslinking in the internal mixer (Agnès Verbois, 2004) .....	24
Figure 2-11 $^1H$ MAS NMR spectrum of thermoset rubber (before extraction) (Ellul, Tsou, & Hu, 2004). .....	25
Figure 2-12. $^1H$ MAS spectra of EPDM samples (after extraction), with Different phenolic resin content (Ellul, Tsou, & Hu, 2004) .....	26
Figure 2-13. Schematic representation of deformation mechanism in TPVs (C. Boyce, Socrate, Kear, Yeh, & Shaw, 2001). .....	28

Figure 2-14. Strain-permanent set curve generated from the modified hysteresis tensile test (Cai, Reid, Srinivasan, & Vennemann, 2004). .....	30
Figure 2-15. Temperature-recoverable stress ratio curve from a TSSR test (Cai, Reid, Srinivasan, & Vennemann, 2004).....	31
Figure 2-16. Storage modulus and dynamic viscosity of <i>EPDM/PP TPVs</i> of different compositions at 220°C: 20/80 ◆; 40/60 ▼; 60/40 ● , (w/w) (Goharpey, Nazockdast, & Katbab, 2005) .....	32
Figure 2-17. Torque evolution during the reaction between EMA and pentanediol at different temperatures and DBTO contents (Pesneau, Champagne, & Huneault, 2002).....	34
Figure 2-18. Different rheological results on the bulk EVA cross-linking at different temperatures and catalyst concentration (Verbois, Cassagnau, Michel, Guillet, & Raveyre, 2004). .....	35
Figure 2-19. Evolution of dynamic viscosity with time for non reactive blend as compared to the same system, dynamically cross-linked at 78% insoluble (Pesneau, Champagne, & Huneault, 2002). .....	36
Figure 2-20. TEM micrographs of samples taken at L/D= 8, 9, 10 and 15 upon dynamic vulcanization of PE/EPDM blend (50/50; w/w) (M. Van Duin & Machado, 2005).....	38
Figure 2-21. Schematic illustration of atoms arrangement in a typical MMT layer (Sinha Ray & Okamoto, 2003).....	39
Figure 2-22. Schematic representation of clay surface treatment (Dell'Anno, 2004).....	40
Figure 2-23. Principle of X-ray diffraction (Kornmann, 1999). .....	43
Figure 4-1. Thermo-gravimetric analysis of Cloisite 15A.....	62
Figure 4-2. XRD patterns of Cloisite 15A and nanocomposites at different scan range. ....	64
Figure 4-3. TEM micrographs of PP nanocomposites. ....	65
Figure 4-4. SEM images of PP Nanocomposites after removing the amorphous phase.....	66
Figure 4-5. XRD patterns of TPE nanocomposites at different EPDM content. ....	67
Figure 4-6. Complex viscosity as a function of angular frequency for pure compatibilizers.....	69

Figure 4-7. Normalized stress relaxation modulus as a function of time for pure compatibilizers. .....	71
Figure 4-8. . Complex viscosity as a function of angular frequency for PP nanocomposites. ....	72
Figure 4-9. The continuity indices of EPDM (a) from non-crosslinked specimens and PP (b) from irradiated samples (corrected for thermoplastic phases solubility in cyclohexane at room temperature, and irradiated EPDM solubility in xylene). ....	73
Figure 4-10. SEM micrographs of TPE nanocomposites after partial PP matrix dissolution. (a) exfoliated system TPEN3.50, (b) intercalated system TPEN4.50.....	73
Figure 4-11. Normalized stress growth viscosity as a function of time for (a)TPENx.50 and (b) TPENx.70 .....	74
Figure 4-12. Micrographs of TPE nanocomposites after PP dissolution for (a) semi exfoliated system TPEN1.70, (b) intercalated system TPEN4.70 .....	76
Figure 4-13. Micrographs of irradiated TPE nanocomposites after complete PP dissolution (Bright spots show accumulated nanoclay agglomerates). ....	77
Figure 5-1. XRD patterns of Cloisite 15A and nanocomposites at different scan range. ....	91
Figure 5-2. TEM micrographs of PP nanocomposites. ....	92
Figure 5-3. SEM images of PP Nanocomposites after removing the amorphous phase.....	93
Figure 5-4. Torque-time curves and temperature profiles of the reactive blends. ....	94
Figure 5-5. Gel content upon dynamic vulcanisation along the screw axis for the samples containing 60wt% (a), 70 wt% (b) and 50 wt% (c) of EPDM. ....	95
Figure 5-6. Figure 6. Evolution of the normalized storage modulus with time for the various reactive blends prepared by twin screw extruder, prepared by internal batch mixer at 200 °C (black) and 170 °C (gray) using 50wt% (a) and 70 wt% (b) of EPDM.....	97
Figure 5-7. The evolution of dynamic viscosity and storage modulus with frequency. ....	98
Figure 5-8. <sup>1</sup> H MAS NMR spectrum of EPDM and TPVN3. The upper curves are the same spectrums as the lower curves but with higher amplification factor. ....	99
Figure 5-9. Residual diene contents of TPVs and TPV nanocomposites.....	100

Figure 5-10. Aromatic area ratio of TPVs and TPV nanocomposites after extraction. ....	103
Figure 6-1. XRD patterns of Cloisite 15A, PP nanocomposites and TPV nanocomposites prepared at screw speed of 200 rpm (gray) and 400 rpm (black).....	115
Figure 6-2. TEM micrographs of N4 (a) and N3 (b and c) polypropylene nanocomposites.....	116
Figure 6-3. SEM images of N3 (a) and N4 (b) polypropylene nanocomposites after removing the amorphous phase. ....	116
Figure 6-4. Crosslink density values of the TPVs and TPV nanocomposites containing 50 wt%(white), 60 wt%(gray) and 70 wt%(black) of EPDM prepared by twin screw extruder. ....	118
Figure 6-5. SEM micrographs of TPV60 (X <sub>1</sub> ; the first row ), TPVN3.60 (X <sub>2</sub> :the second row) and TPVN4.60 (X <sub>3</sub> :the third row) for the samples taken at the first mixing zone (a), the second mixing zone (b), the third mixing zone (c) and the die exit (d). ....	120
Figure 6-6. Normalized force – temperature curves of TPVs and TPV nanocomposites samples containing 50 wt%(a), 60 wt%(b) and 70 wt%(c) of EPDM obtained from TSSR measurements. ....	122
Figure 6-7. Figure 7. SEM micrographs of TPV70 (X <sub>1</sub> ; the first row ), TPVN4.70 (X <sub>2</sub> :the second row) and TPVN3.70 (X <sub>3</sub> :the third row) for the samples taken at the first mixing zone (a), the second mixing zone (b), the third mixing zone (c) and the die exit (d).....	124

## NOMENCLATURE

**English letters:**

B	Diameter of the Elongated Thread
Ca	Capillary Number
$D_n$	Number Average Diameter
$D_v$	Volume Average Diameter
G	Shear Modulus
G'	Storage Modulus
G''	Loss Modulus
$G_v$	Volume Swelling Rate
l	Distortion Wavelength
$M_c$	Molecular Weight Between Two Crosslinks
$N_2$	Second Normal Stress Difference
p	Viscosity Ratio
p'	Hydrostatic Pressure
q	Instability Coefficient
R	Universal Gas Constant
$R_0$	Starting Sphere Radius
RI	Rubber Index
t	Time
T	Absolute Temperature
$V_1$	Molar Volume of the Solvent
$\Delta H$	Latent Heat of Fusion

**Greek letters:**

$[\eta]$	Intrinsic Viscosities
$\alpha_0$	Amplitude of the Initial Distortion
$\dot{\gamma}_p$	Shear Rate
$\delta$	Solubility Parameter
$\epsilon_{crit}$	Critical Strain

$\eta^*$	Complex Viscosity
$\eta_m$	Matrix Viscosity
$\kappa$	Temperature Coefficient
$\lambda$	Viscosity Ratio Or Strain Ratio
$\lambda_l$	Wavelength
$\mu$	Crosslink Density
$\rho$	Density
$\sigma$	Interfacial Tension
$\tau_i$	Gel Content
$v$	Volume Fraction
$\chi$	Flory-Huggins Interaction Parameter
$\Omega$	Tomokita Function
$\omega$	Frequency
$\Phi$	Continuity Index or Continuity Fraction

#### List of Abbreviations:

CEC	Charge Exchange Capacity
DBTO	Dibutyltin Oxide
DCPD	Dicyclopentadiene
DMA	Dynamic Mechanical Analysis
DSC	Differential Scanning Calorimetry
EMA	Ethylene Methacrylate
ENB	Ethylidene Norbornene
EPDM	Ethylene Propylene Diene Terpolymer
EPR	Ethylene Propylene Rubber
EVA	Ethylene-Vinyl Acetate
FTIR	Fourier Transform Infrared Spectroscopy
HD	Hexadiene
IPB	Interpenetrating Polymer Blends
IPN	Interpenetrating Polymer Network
IPS	Interpenetrating Phase Structure

MMT	Montmorillonite
NMR	Nuclear Magnetic Resonance
NR	Natural Rubber
PE	Polyethylene
PLS	Polymer Layered Silicate
PP	Polypropylene
PP-g-MA	Polypropylene-Grafted-Maleic Anhydride
PSA	Pressure Sensitive Adhesives
PVC	Polyvinyl Chloride
SBR	Styrene Butadiene Rubber
SBS	Styrene Butadiene Styrene
SEBS	Styrene Ethylene/Butylene Styrene
SEM	Scanning Electron Microscope
SIS	Styrene Isoprene Styrene
TEM	Transmission Electron Microscopy
TGA	Thermogravimetric Analysis
TPE	Thermoplastic Elastomeric Material
TPV	Thermoplastic Vulcanizate
TSSR	Temperature Scanning Stress Relaxation
VNB	Vinylidene Norbornene
XRD	X-Ray Diffraction

## Chapter 1 INTRODUCTION AND OBJECTIVES

### 1.1 Introduction

Thermoplastic Elastomeric Materials (TPEs) are a class of copolymers or polymer blends which show the processing characteristics of a thermoplastic and functional performance of a conventional thermoset rubber. TPEs usually have a two-phase structure, an elastomeric phase giving the material the rubber-like properties and a stiffer thermoplastic phase that operates as a physical cross-linker for the rubber phase. This phase melts at elevated temperature and TPE becomes processable (Borcea, 2008).

No curing step during processing, the ease of tailoring the properties by adjusting the hard/soft ratio and by the addition of processing oil and/or solid fillers, simple and fast processing, low energy consumption and recycle ability are some advantages of TPEs compared to thermoset rubbers. Some disadvantages also exist, for example, elastomeric recovery may not be as good as thermoset rubbers, another one is related to the application temperature of these compounds due to the physical nature of the cross-links in the TPEs (Lebel, 1994).

Generally, depending on the connection of the soft and the hard phases thermoplastic elastomers can be classified into two main categories: Block copolymers and thermoplastic elastomer blends. Block copolymers are the most widely used TPEs. They are characterized by their molecular architecture, which has a “hard” thermoplastic segment (block) and a “soft” elastomeric segment (block). The formation of the two phase structure occurs by the lack of miscibility of the hard and soft segments or by crystallization of the hard segments. The properties of these TPEs can be tailored by the choice of monomer types, the hard/soft ratio and the positions of the hard and soft segments within the polymer chain (Drobny, 2007). Styrenic block copolymers and thermoplastic polyurethanes are well-known examples of common TPEs. Styrenic TPEs are usually styrene ethylene/butylene styrene (SEBS), styrene butadiene styrene (SBS) and styrene isoprene styrene (SIS). The polystyrene end-blocks form a reversible physical network that provides thermo-plasticity feature for processing. With cooling, the reformation and hardening of the polystyrene domains create a rubber network in position. Principal styrenic TPE markets are : extruded film/sheet and wire/cable covering, pressure sensitive adhesives (PSA),

grips, molded shoe soles and other footwear, kitchen utensils, hot-melt adhesives and asphalt modifiers (Drobny, 2007; Sengers, 2005).

The second most widely used TPEs on a tonnage basis (worldwide consumption of about 687000 tons with an annual average growth rate of about 7% in 2009) are thermoplastic elastomer blends that are made by melt mixing of a thermoplastic polymer such as polypropylene (PP), polyethylene (PE), polyvinyl chloride (PVC) or a polyamide with an elastomer such as ethylene propylene rubber (EPR), ethylene propylene diene monomer (EPDM), styrene butadiene rubber (SBR), ethylene-vinyl acetate (EVA) or natural rubber (NR) (Drobny, 2007; M. Van Duin & Machado, 2005). TPE blends are all phase separated systems in which their two-phase structures are obtained by the lack of miscibility of the rubber and the thermoplastic phase. A prerequisite for these blends is that the thermoplastic polymer is continuous (Bhadane, 2005).

Among the different types of thermoplastic elastomer blends, thermoplastic vulcanizates (TPVs) with the improved rubber like behavior are prepared by dynamic vulcanization which was claimed first by Gessler et al. and Fischer (Fischer & Woodbury, 1974; Gessler & Haslee, 1962). By definition, the process of dynamic vulcanization consists of crosslinking an elastomer during its melt blending with a thermoplastic polymer, which often leads to fully vulcanized and finely dispersed rubber droplets in the thermoplastic matrix (Ellul, Tsou, & Hu, 2004; Harrats, Thomas, & Groeninckx, 2006). Coran and Patel showed that, in theory, a large number of elastomers and thermoplastics could be dynamically vulcanized to produce different TPVs. However, practically the best chemical and physical properties of these materials were obtained with a TPV based on ethylene-propylene diene terpolymer EPDM and polypropylene PP (Aubert Y. Coran & Patel, 1978). The focus lies here on this type of TPEs that have gained wide acceptance because of their rubber-like properties. TPV based on PP and EPDM is one of the most studied TPVs in the literature; the ultimate goal of these studies is to enhance their elasticity by shifting the TPV compositions towards higher EPDM contents, adjusting the level of crosslinking chemicals, molecular weight of thermoplastic phase, processing conditions and so on.

On the other hand, polypropylene layered silicate nanocomposites have similarly received much attention, due to their high performance. These two complementary technologies can come together to form TPV nanocomposites, with interesting properties that significantly depend on the final morphology in the material.

Since, nanocomposite formation is thermodynamically driven, it can occur only with a negative free energy change. Therefore, maleic anhydride-grafted polypropylene (PP-g-MA) is generally used as a compatibilizer and its effect on nanocomposite structure and mechanical properties has been investigated extensively. Nevertheless, more questions have been raised about which of the compatibilizers properties could be a good predictor of the compatibilizer effectiveness. The use of PP-g-MA affects the viscosity ratio, interfacial tension, mobility of the interface and the degree of exfoliation. Consequently, the co-continuous composition range changes. Thus, the effect of the different compatibilizers on the blend morphology should be addressed.

It should be mentioned that a number of studies, related to the TPV nanocomposites field, investigated the effect of nanoclay presence on non-reactive systems and/or in processing reactive systems in internal batch-mixers. Therefore, more studies are needed to obtain better insight into the effect of nanoclay presence and its dispersion level in reactive extrusion of these materials while dynamic vulcanization in extruders proceeds quite differently from that in batch mixers. It is necessary to make the crosslinking kinetics compatible with the shorter residence times used in the extruder.

It was indicated that increasing the cross-link density results in enhanced TPV nanocomposite elasticity, but only to a certain level. An important research question is how can the elasticity be further improved to the level of thermoset elastomers, in order to exploit the TPV nanocomposite to their maximum potential and to develop their fields of applications?

In view of the above considerations, the following objectives are identified for the present research project.

## **1.2 Objectives**

### **1.2.1 Main Objective**

The main objective of this study is *to determine the fundamental parameters affecting the elasticity of thermoplastic vulcanizate nanocomposites prepared by reactive extrusion for molding applications.*

### 1.2.2 Specific Objective

To achieve this objective, the following scientific and technical issues are addressed as the specific objectives. The various components of the project are guided by available literature and the results are analyzed in light of theoretical and quantitative principles.

- i. To determine a compatibilizer (PP-g-MA) property as a good predictor of the compatibilizer effectiveness.
- ii. To investigate the influence of the compatibilizer on co-continuous composition range.
- iii. To study the thermal and rheological characteristics of TPE and TPV nanocomposites prepared with different compatibilizers.
- iv. To study the dynamic vulcanization and morphology evolution along the extruder axis.
- v. To assess the effects of nanoclay dispersion level in thermoplastic phase on dynamic vulcanization of TPV nanocomposites prepared by reactive extrusion.
- vi. To investigate the rubber like behavior and functional/mechanical properties of TPV nanocomposites.
- vii. On the basis of the above findings, to propose a combination of composition(s) and processing variables to produce superior TPVs for molding applications.

## Chapter 2 LITERATURE REVIEW

### 2.1 Morphology Formation in Dynamically Vulcanized PP/EPDM

Most commercial polymer blends are known as immiscible blends forming multi-phase structures due to their high molecular weight and unfavorable interactions. Different parameters determine the properties of multiphase materials. The most important one is the blend morphology created during the melt mixing process. On the other hand, morphology development is controlled by the rheological properties of the components, by the blend composition, by the interfacial tension and by the processing conditions. According to Potschke and Paul (Potschke & Paul, 2003), the final morphology obtained after mixing of immiscible polymer pairs can be grouped into four basic structures (Figure 2.1):

- i. Matrix-dispersed particle structure
- ii. Matrix-fiber structures
- iii. Lamellar structures
- iv. Co-continuous structures

Dynamic vulcanization is the major step dictating morphology development of TPVs (especially in the co-continuous structure composition range), however, it should be noted that this process is not the initial step in TPV production process. Normally, thermoplastic and elastomer components are melt blended in the first stage and consequently the cross-linking agents are introduced into the mixture (Goharpey, Katbab, & Nazockdast, 2001). Therefore, the first stage of TPV production is not indeed different from TPE blends production.

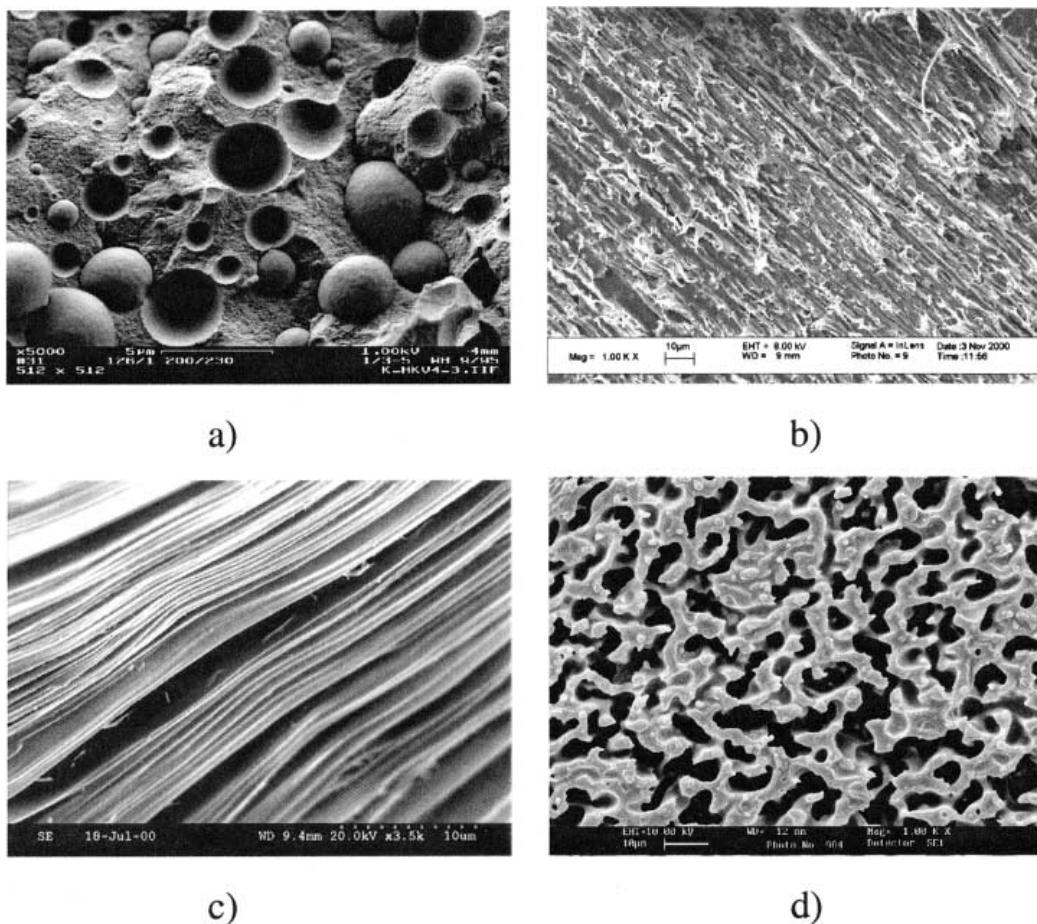


Figure 2-1. Types of morphology in immiscible blends. (a) dispersed structure; (b) Matrix-fiber structures; (c) lamellar structure; (d) co-continuous structure (Potschke & Paul, 2003)

Ideally, the elastomer should be present as finely dispersed particles in a small amount of polymer. The cross-linked elastomer particles promote the blend elasticity and prevent coalescence. In contrast, if the cured elastomer phase is continuous, the resulting compound cannot be reprocessed. Therefore, in cases where the elastomer is the major component, the development of co-continuity is critically important, since the dynamic vulcanization can be considered as the driving force for phase inversion, i.e., when the morphology changes from a dispersed-matrix type to a co-continuous type or vice versa (Potschke & Paul, 2003).

To have a better insight about the co-continuous structure composition range, the co-continuous structure is defined in the next section.

### 2.1.1 Co-continuity and its Importance on the Final TPVs Morphology

According to Paul and Potschke, there are two definitions of the co-continuous structure. The classic definition describes an ideally co-continuous structure as the coexistence of at least two continuous structures within the same volume; in other words co-continuous structures would be observed when both components have three-dimensional spatial continuity on some finite scale of mixing. In the literature, co-continuous phase structures are also described as interpenetrating polymer networks (IPNs), interpenetrating phase structures (IPs) or interpenetrating polymer blends (IPBs) (Potschke & Paul, 2003). There is general agreement in the literature that co-continuity is related to this definition.

The second definition is based on the percolation threshold theory and considers that the structures formed by melt mixing of polymers represent a coexistence of different structure types rather than an ideal network. Lyngaae-Jorgensen et al. (Lyngaae-Jorgensen, Lunde Rasmussen, Chtcherbakova, & Utracki, 1999) define a co-continuous structure as one wherein at least a part of each phase forms a coherent continuous structure permeating the whole volume. This definition also allows some part of the components to exist in separate domains that are not part of the network structure.

Figure 2.2 shows the critical volume fraction  $\phi_{cr}$ , or percolation threshold is the volume fraction at which the transition from a structure containing only discrete domains of one phase to a system containing one infinite structure (and discrete domains) takes place. Increasing of the proportion of the minor component incorporated in the percolation structure makes a fully co-continuous structure. Lyngaae-Jorgensen et al. define the continuity index or continuity fraction ( $\phi_c$ ) that stands for the portion of a component that is part of percolating structure. The first definition is a special case of the second, when the continuity fraction is equal to one for both phases (Lyngaae-Jorgensen & Utracki, 2003).

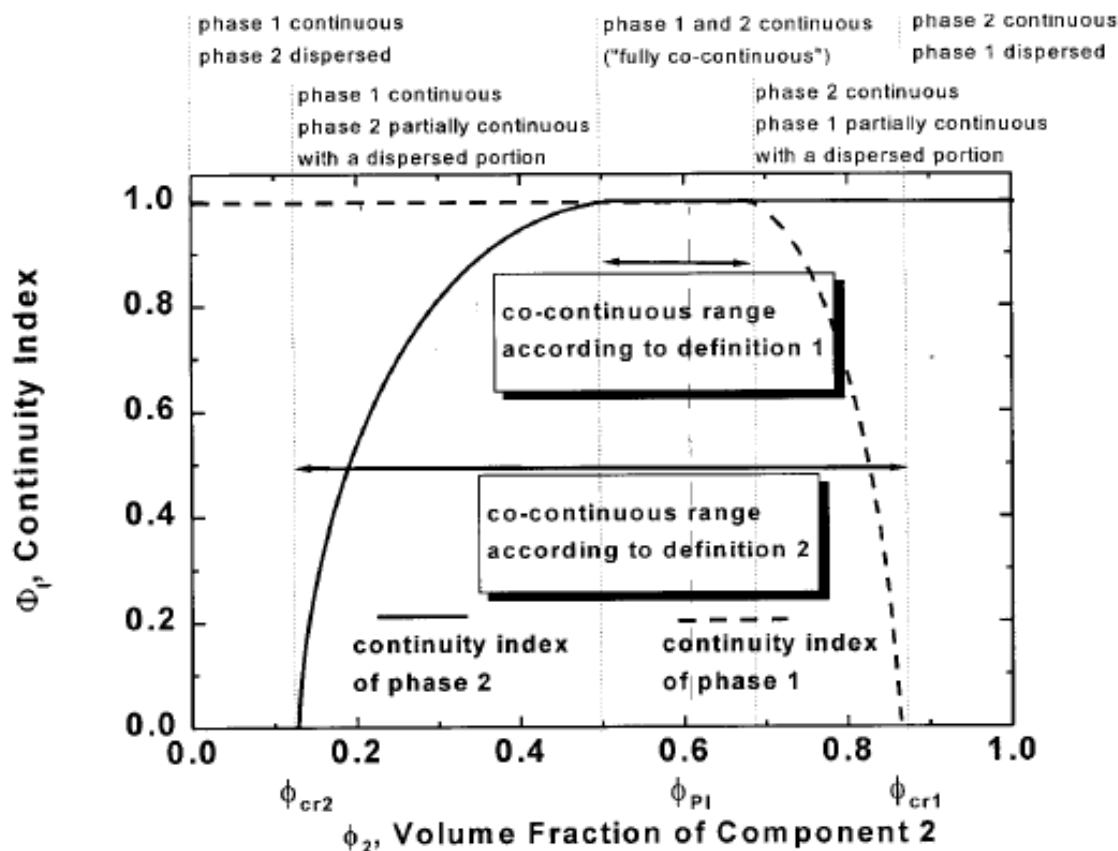


Figure 2-2. Co-continuous structure composition range using definition 1 and definition 2  
(Potschke & Paul, 2003)

It is desirable to shift the TPV composition towards higher EPDM contents in order to have TPVs with enhanced elasticity. However, melt processability requires a certain degree of thermoplastic phase continuity. As seen later in the present study, the co-continuous structure forming in the initial step of TPV production is an important factor affecting the dynamic vulcanization. It should be noted that the elastomer phase changes from a viscous fluid to an elastic solid due to the dynamic vulcanization. The elastomer becomes rigid and cannot adapt to the applied stress. As a result, this phase breaks up into micron-sized elastomer particles and continuity index of the rubber phase decreases in a reactive blend (Radusch & Pham, 1996). Parameters influencing on co-continuous structure will be discussed in the next section.

## 2.1.2 Factors Influencing the Co-continuity and Final Morphology of TPVs

### 2.1.2.1 Viscosity

Rigorous mixing of two molten polymers in a shear field can produce co-continuous structure, when the viscosities and volume fractions of the two components are equal. Equal volume fraction maximizes the opportunity for maintaining connectivity, because neither component is present in a minor amount. However, in most systems, the viscosities of the components are different. To minimize the energy dissipation during the mixing, the low-viscosity phase tends to be continuous. Therefore to keep the connectivity of the phases and to counterbalance this tendency, the volume fraction of the higher-viscosity component has to be increased (Potschke & Paul, 2003). This fact is the basis for some of the phase inversion equations (Figure 3). So the viscosity ratio is one of the most important parameters to control the final morphology.

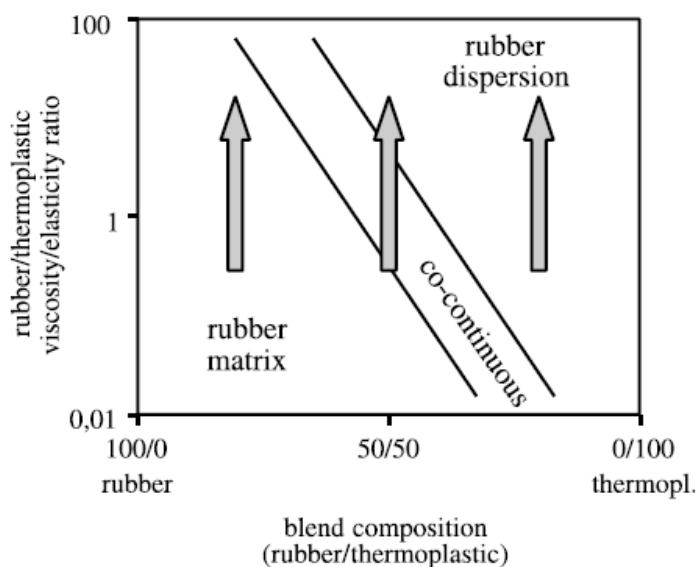


Figure 2-3. Relation between the volume range of co-continuous structures and viscosity ratio  
(M. Van Duin & Machado, 2005)

In the case of PP/EPDM blends this would mean that if the viscosity of the PP is reduced, a higher amount of rubber can be dispersed before rubber-matrix state is reached. Even when the rubber-matrix is reached, crosslinking can develop the co-continuity, for example Abdou-Sabet et al. studied the morphology of PP/EPDM blends containing 80 vol% rubbers. In the uncured

blends, polypropylene was the minor component, dispersed in the EPDM matrix. However, the morphology of the TPVs showed that in the initial step of the dynamic vulcanization of the rubber phase, co-continuous structure was first produced and, as the degree of vulcanization of the rubber increased, the continuous rubber phase became elongated more and more and then broke up into EPDM droplets. As the rubber droplets continued to form, the polypropylene phase grew to become the continuous phase (Abdou-Sabet & Patel, 1991).

Karger-Kocsis et al. investigated the effect of viscosity ratio on dispersion of EPDM particles in PP matrix. They observed that the average particle size and polydispersity of EPDM particles decreased with viscosity ratio (Karger-Kocsis, Kallo, & Kuleznev, 1984). The decrease of the rubber particle size with decreasing viscosity difference between the elastomer and the plastic was reported by Goharpey et al. for TPV blends of PP/EPDM (40/60 wt%) with different viscosity ratios (Goharpey, Katbab, & Nazockdast, 2003). These observations could probably be explained by the long breakup time and capillary number.

The origin of this non-dimensional parameter comes from simple emulsions. Droplet or thread deformation is governed by capillary number ( $Ca$ ) which represents the ratio of viscous forces to interfacial tension force:

$$Ca = \frac{\eta_m \gamma_p R_0}{\sigma} \quad (2-1)$$

where  $\eta_m$  is the matrix viscosity,  $\gamma_p$  is the shear rate,  $R_0$  is starting sphere radius and  $\sigma$  is the interfacial tension. Considering the capillary number, the mixing process can be divided into two regimes: when the capillary number  $Ca \gg 1$ , it implies distributive mixing leading to rearrangement and deformation of the phases. The second regime is dispersive mixing with  $Ca < 1$ . In this condition, breakup happens and leads to a reduction in phase size (Willemse, de Boer, van Dam, & Gotsis, 1998). Furthermore, in polymer blending, two main breakup mechanisms have been observed. The first one involves the breakup process of the droplets into (mostly) two droplets above a critical  $Ca_{crit}$  value, where the shear stress exceeds the interfacial stress. The second mechanism, that seems to be more realistic, is the breakup of highly elongated threads via capillary instabilities. Consequently, a line of smaller droplets would be formed Figure 2.4 shows the mentioned mechanisms schematically. (Janssen & Meijer, 1993; Potschke & Paul, 2003).

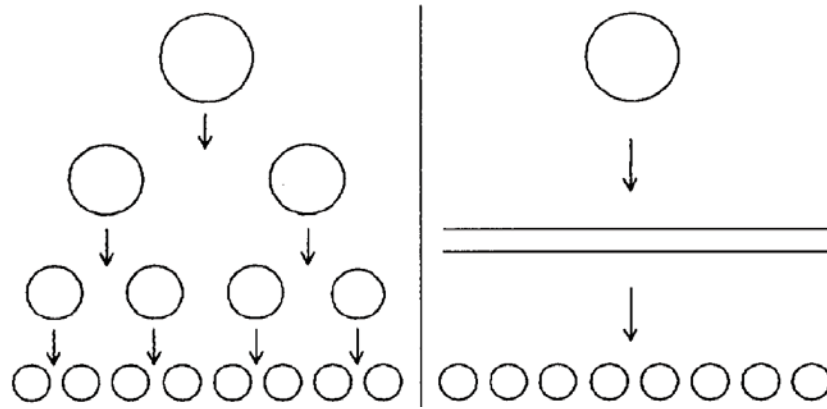


Figure 2-4. Schematic representation of the two dispersion mechanisms: Left, the stepwise equilibrium mechanism of repeated breakup at  $Ca_{critical}$ ; right, the transient mechanism of thread breakup during extension (Janssen & Meijer, 1993).

The diameter of the elongated thread  $B$  is a function of the total amount of strain imposed. Assuming affine deformation, it is determined as follows:

$$B = 2R_0(1 + \gamma^2)^{-\frac{1}{4}} \quad (2-2)$$

where  $\gamma$  is  $\gamma_{pt}$  and  $t$  is time.

During the mixing process when the stretching increases, the local capillary number decreases. The stability of the filament is expected as long as the local capillary number of the thread is greater than one. In this condition, the filament does not break up. Therefore, high matrix viscosity, high shear rate, large starting droplet sizes and low interfacial tensions favor the generation of co-continuous structure, which is made by the stable threads. After a certain thread diameter that leads to  $Ca$  less than one, breakup occurs, if the residence time during the mixing process is higher than their breakup time (Potschke & Paul, 2003). The breakup time is obtained by:

$$t_b = \left( \frac{\eta_m B}{\Omega(l, \lambda) \sigma} \right) \ln \left( \frac{0.8B}{2\alpha_0} \right) \quad (2-3)$$

where  $\alpha_0$  is the amplitude of the initial distortion and  $\Omega(l, \lambda)$  is the Tomokita function which is a dimensionless distortion growth rate, depending on the distortion wavelength  $l$  and the viscosity ratio  $\lambda$  (See Figure 2.5). The factors influencing the breakup process are indicated by this equation. Breakup is less likely at low interfacial tension and high thread diameters. High matrix

viscosity should lead to long breakup times, but this term is already included in  $\Omega(l,\lambda)$ , which increases with decreasing viscosity ratio. To get a low value of  $\Omega(l,\lambda)$ , thread viscosity should be high and the matrix viscosity has to be low.

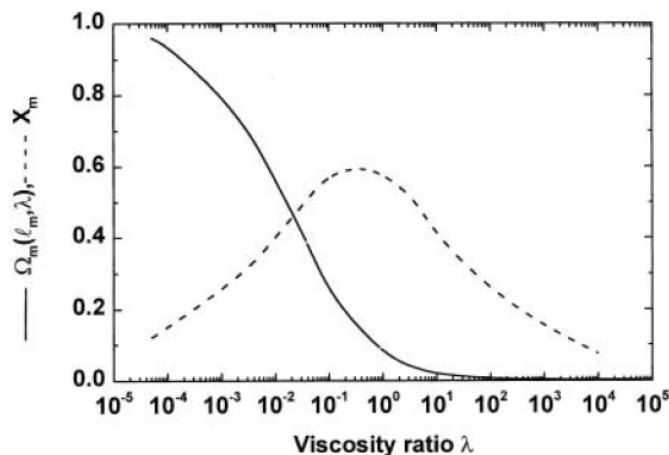


Figure 2-5. Distortion growth rate at dominant wavelength and dominant wave length vs  $\lambda$   
(Potschke & Paul, 2003)

It is noteworthy to mention that the critical capillary number also depends on the type of flow; as seen in figure 2.6, the elongational flow field is much more effective for droplet breakup in a dispersive mixing regime (Grace 1982).

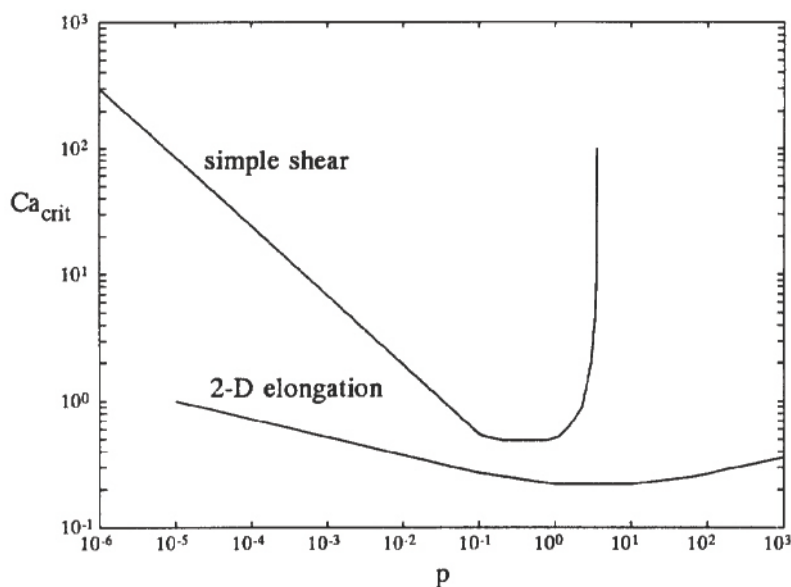


Figure 2-6. Comparison of effect of viscosity ratio on critical shear in rotational and irrotational shear fields (Grace 1982).

### **2.1.2.2 Interfacial Tension**

Interfacial tension is an important factor that could be considered as a driving force for the transformation of a co-continuous structure into a dispersed one (Li, Ma, & Favis, 2002). It is known that low interfacial tension reduces the rate of breakup and facilitates the formation of co-continuous structure. The effect of interfacial tension on the range of co-continuity has been studied by Willemse et al. They chose different pairs of polymers having different interfacial tension but the same viscosity ratio. They found that in systems with higher interfacial tension, the onset volume fraction of co-continuity (percolation onset) was higher, the co-continuity range was narrower, the stability of morphology was lower and the phase dimensions were larger, compared to systems with low interfacial tension. This behavior was similar for both high viscosity ratio and low viscosity ratio systems (Willemse, de Boer, van Dam, & Gotsis, 1998). For blends with compatibilizers at the same viscosity ratio, the broadness of the co-continuity was directly related to the interfacial tension, but the same phase inversion as uncompatibilized blends was observed (Bourry & Favis, 1998). On the other hand, the effect of elasticity is considered as an apparent increase in interfacial tension, where a droplet of higher elasticity than the matrix is stabilized against deformation and breakup during flow (Potschke & Paul, 2003).

### **2.1.2.3 Processing Conditions and Other Parameters**

The co-continuous structure as intermediate structure could be formed during the initial stages of morphology development. Even at low volume fractions of one component, stable co-continuous morphologies can be observed using suitable processing conditions. Goharpey et al. studied the morphology development of PP/EPDM (40/60, wt. %) during mixing. Samples were taken from a hot running mixer and rapidly quenched in liquid nitrogen, before and after the onset of rubber vulcanization. They demonstrated that the rubber domains were dispersed throughout the polypropylene matrix for the unvulcanized but frozen samples. However, the unfrozen blends showed a co-continuous morphology. For the dynamically vulcanized blends, they also showed that the rubber phase that finally formed the dispersed phase was the one that had formed the matrix in early mixing stages. (Goharpey, Nazockdast, & Katbab, 2005).

There are two different mechanisms for co-continuity development. The first is thread-thread coalescence for low-interfacial tension systems, while the second is droplet-droplet coalescence for high interfacial tension systems. It has been mentioned that the possibility of

coalescence of dispersed phase and dispersed phase percolation rate determine the co-continuity broadness. Therefore, the shift of co-continuity is not only related to rheological properties of both components, but also to the degree of mobility of the interface. Willis et al. suggested that factors, that limited coalescence phenomenon in a polymer blend decreased the co-continuity range of the blend (Willis & Favis, 1988).

Finally, any parameter, that affects the viscosity ratio or elasticity ratio of a particular blend, would be expected to produce a change in both the co-continuity interval and the final morphology. For instance, plasticizers can affect dramatically the rheological properties of polymers. Shabbikian et al. (Shant Shabbikian et al., 2011a) covered the relationship between rheology of immiscible blends based on ethylene-propylene-diene-terpolymer and polypropylene, in the presence and absence of a paraffinic plasticizer. In the morphological part of their research, based on a solvent extraction method, they showed that the plasticization led to the better interconnectivity of the elastomeric phase and consequently a more rapid percolation of the rubber component at low EPDM content compared to the corresponding blends without plasticizer (Figure 2.7).

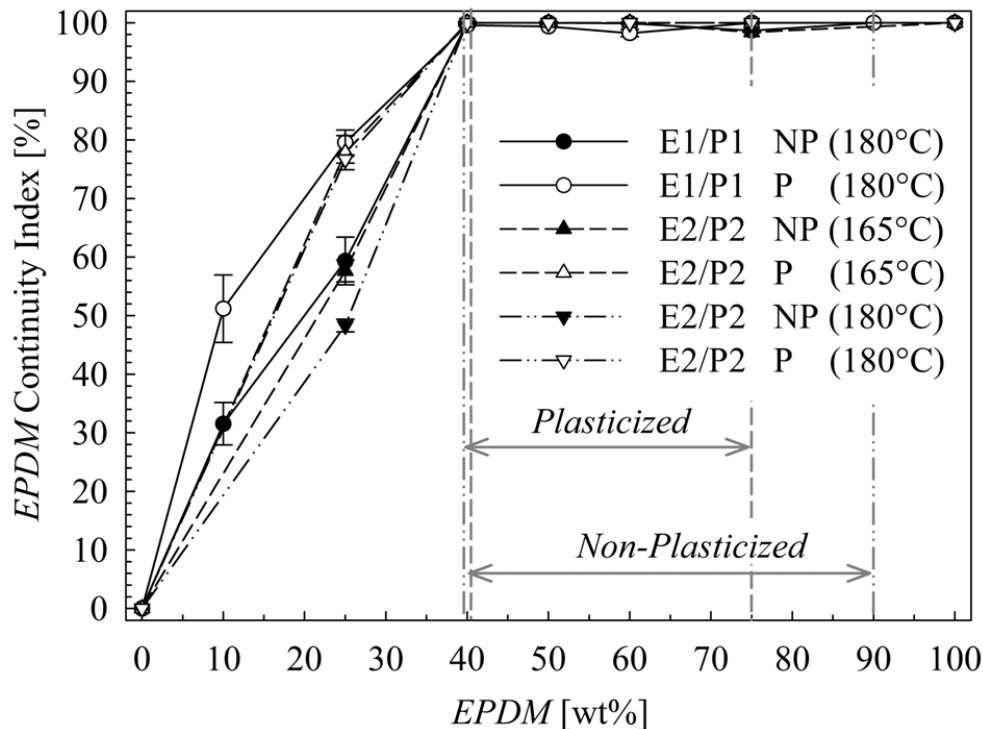


Figure 2-7. Continuity index of EPDM in non-plasticized and plasticized PP/EPDM blends (Shant. Shabbikian, 2010).

Furthermore, a comparative study on the morphology development of reactive and nonreactive EPDM/PP blends, using an internal mixer and a twin-screw extrusion showed that the intensive flow field inside the twin screw extruder resulted in a finer morphology in comparison to the internal mixer. The interconnectivity of the EPDM domains to some extent was observed even for dynamically cross-linked blends (TPVs) due to the plasticizer presence (Shant. Shahbikian, 2010; Shant Shahbikian et al., 2011b).

### 2.1.3 Equations for the Phase Inversion and Co-continuous Composition

It is of interest to determine which phase will form the matrix and at which composition co-continuity can be formed. A number of studies have been carried out over the last 30 years to estimate the phase inversion composition ( $\phi_{PI}$ ) and to compare these estimates with experimental results. Generally, phase inversion compositions are given in the literature, and co-continuous composition range can be expected within a composition region about  $\phi_{PI}$ . The breadth of co-continuity depends not only on material and processing parameters but also on the experimental concentration step size used. The following simple equation, suggested first by Avgeropoulos et al., relates the phase inversion composition to volume fractions and viscosities:

$$\frac{\phi_{1,PI}}{\phi_{2,PI}} \times \frac{\eta_2}{\eta_1} \cong 1 \quad (2-4)$$

where  $\phi_{i,PI}$  is a volume fraction at phase inversion and  $\eta_i$  is the viscosity of the component  $i$ . This equation can be simplified using  $\lambda = \eta_1/\eta_2$  and  $\phi_{1,PI} = 1 - \phi_{2,PI}$  (Avgeropoulos, Weissert, Biddison, & Boehm, 1976) :

$$\phi_{1,PI} = 1/(1 + \lambda) \quad (2-5)$$

The viscosity ratio of the non-Newtonian blends should be evaluated at the shear stress used for preparation of the blends. Avgeropoulos used the torque ratio rather than the viscosity ratio. Because the basic equation was proposed for systems with almost the same viscosity, there is considerable deviation for the polymer blends in which the viscosity ratio of the components is very different from unity. Therefore a number of researchers have developed the relations, to obtain a good representation of the experimental data. These modified relations have the following general form:

$$\phi_{1,PI} / \phi_{2,PI} = A(\tau_1 / \tau_2)^B \quad (2-6)$$

Where A and B are fitting parameters. For example, according to Ho et al. A and B are 1.22 and 0.29, respectively, where the subscript 1 represents EPR and subscript 2 represents PP (Ho, Wu, & Su, 1990). Utracki obtained better fits by an approach based on “intrinsic viscosities”  $[\eta]$  and maximum packing volume fraction  $\phi_m$ . The equation involves the viscosity concentration dependence. His assumption was based on equal blend viscosities resulting from addition of polymer 2 into polymer 1 and vice versa at the phase inversion composition. Using this assumption the following equations were proposed (L. A. Utracki, 1991) :

$$\lambda = \left[ \frac{(\phi_m - \phi_{2,PI})}{(\phi_m - \phi_{1,PI})} \right]^{[\eta]\phi_m} \quad (2-7)$$

$$\phi_{2,PI} = \frac{(1 - \log \lambda / [\eta])}{2} \quad (\text{for } 0.1 < \lambda < 10) \quad (2-8)$$

where  $[\eta]$  was assumed to be 1.9 for spherical domains and  $\phi_m = 0.84$ . It has been mentioned that interfacial tension effects can also be taken into account using proper expressions for  $[\eta]$ . In another attempt Metelkin and Blekht assumed that the breakup times of one material in the other are equal at the phase inversion composition. They derived a relation for the phase inversion volume fraction in terms of the viscosity ratio and a function of viscosity ratio  $F(\lambda)$  (Metelkin & Blekht, 1984).

$$\phi_{2,PI} = (1 + F(\lambda) \times \lambda)^{-1} \quad (2-9)$$

$F(\lambda)$  could be determined theoretically from consideration of stability of individual layers or by following function proposed by Utracki :

$$F(\lambda) = 1 + 2.2g \log(\lambda) + 1.8[\log(\lambda)]^2 \quad (2-10)$$

Luciani and Jarrin considered that co-continuous morphology is governed by the stability of fibrillar structures in three dimensions. They assumed that stability for both fibrillar structure networks is equal. the instability coefficient (q) or growth rate is defined as (Luciani & Jarrin, 1996).

$$q = \left( \frac{\sigma}{2\eta_m R_0} \right) \Omega(l, \lambda) \quad (2-11)$$

where  $\sigma$  is interfacial tension,  $\eta_m$  is matrix viscosity,  $R_0$  is initial thread radius, and  $\Omega(l, \lambda)$  is the Tomokita function. In addition, they assumed that the two networks are made from the same number of fibers of the same length but these structures differ only in the diameters of their fibers. Therefore, they equated the instability coefficients ( $q$ ) for both phases and set  $R_0$  (in equation 2.11) proportional to the square root of volume fraction. By combining both assumptions, they developed the following relation for the concentration of maximum co-continuity;

$$\phi_{2,PI} = \frac{1 - (\lambda^2 \Omega^2(\lambda))}{[\lambda^2 \Omega^2(\lambda) + \Omega^2(1/\lambda)]} \quad (2-12)$$

It has been stated that the validity of this equation is limited to viscosity ratio between 0.25 and 4 (Luciani & Jarrin, 1996).

Shahbikian et al. (Shant Shahbikian et al., 2011b) presented experimental mid-composition of phase inversion for non-plasticized and plasticized TPEs based on PP/EPDM as a function of their corresponding viscosity ratios as well as phase inversion predictions for different semi-empirical viscosity based-models (Figure 2.9). They pointed out that the model of Metelkin and Blekht (Metelkin & Blekht, 1984) overestimates the phase inversion composition but the best agreement for their case observed with the model presented by Utracki (L. A. Utracki, 1991). On the other hand, it was also mentioned that the optimization procedure in which the Utracki model parameters should be modified to obtain the best fit, resulted in a curve with a weak dependency on the viscosity ratio. Furthermore, the experimental data obtained from different studies about the influence of viscosity ratios on the phase inversion concentration (P. A. Bhadane, M. F. Champagne, M. A. Huneault, F. Tofan, & B. D. Favis, 2006; Steinmann, Gronski, & Friedrich, 2001; L. A. Utracki, 1991) disagree with most theories based on viscosity ratio.

Since these models do not always completely agree with phase inversion compositions found experimentally, the observed differences could be attributed to melt elasticity effects. The higher elasticity may be stated as an apparent increase in interfacial tension:

$$\sigma = \sigma_0 + (R/6)(N_{2,d} - N_{2,m}) \quad (2-13)$$

Where  $\sigma_0$  is the interfacial tension in the absence of flow, R is droplet radius, and  $N_{2,i}$  is the second normal stress difference (Potschke & Paul, 2003).

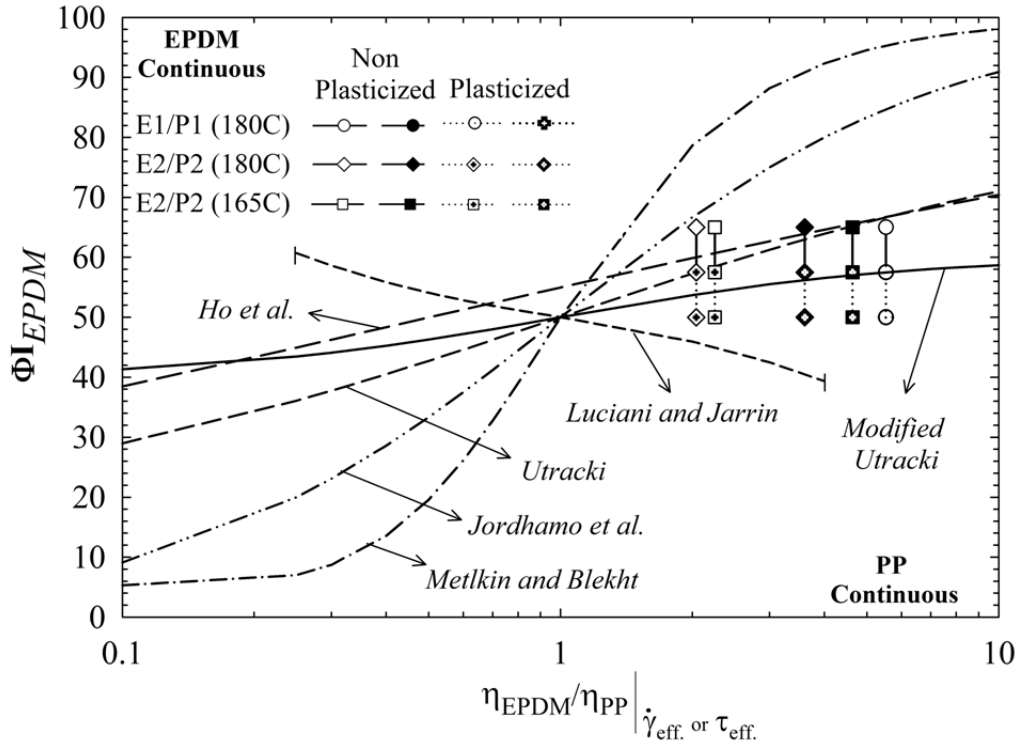


Figure 2-8. Phase inversion predictions for different viscosity based-models as well as the experimental mid-composition of phase inversion for non-plasticized and plasticized TPOs: Open symbols: at constant apparent shear rate, i.e. 50s-1; Filled symbols: at constant matrix shear stress evaluated at 50s-1.

Bourry and Favis introduced the storage modulus  $G'$  or  $\tan\delta$  to represent the elasticity of components in phase inversion (Bourry & Favis, 1998):

$$\frac{\phi_{1,PI}}{\phi_{2,PI}} = \frac{G'_2(\omega)}{G'_1(\omega)} \quad (2-14)$$

$$\frac{\phi_{1,PI}}{\phi_{2,PI}} = \frac{\tan \delta_2(\omega)}{\tan \delta_1(\omega)} \quad (2-15)$$

This means that the more elastic component tends to encapsulate the less elastic one. The validity of Cox-Merz rule ( $\eta^*(\omega) = \eta(\gamma_p)$ ) should be verified to measure  $G'$  and  $\tan \delta$  at frequency  $\omega$  corresponding to the shear rate  $\gamma_p$ . The use of the former equation (2.14) for the experimental data evaluated at a constant matrix shear stress (Sarazin & Favis, 2003; Shant Shahbikian et al., 2011b) and the second relation (2.15) for the data obtained at a constant shear rate (Shant Shahbikian et al., 2011b; Steinmann, Gronski, & Friedrich, 2001) provides a better agreement with the prediction of the Bourry and Favis model.

Phase inversion prediction models focus on only a single composition range, where as in reality, co-continuous structures are observed over a composition range. Considering the definition of co-continuous structure and equations based on the percolation theory, Lyngaae-Jorgensen et al. proposed the following relation for the continuity index (Lyngaae-Jorgensen, Lunde Rasmussen, Chtcherbakova, & Utracki, 1999):

$$\Phi_I = k(\phi - \phi_{cr})^x \quad (2-16)$$

where  $\phi_{cr}$  is the volume fraction at onset of co-continuity and  $k$  is an empirical coefficient. Numerical simulation predicted  $x$  to be 0.45 and  $\phi_{cr}$  to be about 0.2 for classical percolation in three-dimensional systems (Dietrich & Amnon, 1994). The values of  $\phi_{cr}$  depend on shearing history and thermal treatment in the molten state, and  $\phi_I$  depends on the solvent used for the extraction of the component (Potschke & Paul, 2003).

## 2.2 Crosslinking Systems

In principle, any curing agent could be employed for the crosslinking of the elastomer phase. Three major curing systems are sulfur systems, peroxide systems and resole type phenolic resin systems. Sulfur systems are usually used for thermoset elastomers. TPVs prepared with these systems show unstable melt morphology (C. Nakason, P. Wannavilai, & A. Kaesaman, 2006; Kinsuk Naskar, 2004).

The general advantages of peroxide-based crosslinks are good elastic behavior in particular compression set, high temperature resistance and no discoloration of the final products. It has been shown that the rate at which peroxide crosslinking takes place is dependent on the decomposition temperature of the selected peroxide (Thitithammawong, Nakason, Sahakaro, & Noordermeer, 2007). Therefore, the proper peroxide should be selected, on the basis of its decomposition rate at the processing temperature. Other criteria for the selection of the peroxide relate to their tendency to show a blooming effect and to decompose into smelly by-products. However, the most important problem in selecting the peroxide systems in TPV production is related to their low ability to crosslink the elastomer phase selectively (Charoen Nakason, Puripong Wannavilai, & Azizon Kaesaman, 2006; Thitithammawong, Nakason, Sahakaro, & Noordermeer, 2007).

Although resole cross-linking is rarely used for curing thermoset elastomer with the exception of butyl rubber, it is the “workhorse” for TPVs based on PP/EPDM, since it crosslinks the unsaturated elastomer phase selectively, it is effective at extrusion temperatures and it yields thermally-stable crosslinks. Moreover, the corresponding TPVs exhibit excellent properties and good processability (Machado & Van Duin, 2005; M. Van Duin & Machado, 2005). Machado et al studied the chemistry of resole crosslinking of EPDM. They showed that the resole, a phenol/formaldehyde oligomer, is degraded into mono-phenolic units, which finally link two EPDM chains via chroman and/or methylene-bridged structures (Figure 2.9). After the scission of the dimethylol ether linkage of the resole by  $\text{SnCl}_2$  as an activator, cationic intermediates add to the EPDM unsaturation. For EPDM with 5-ethylidene-2-norbornene (ENB) as diene, only methylene/chroman crosslinks are formed (Lattimer, Kinsey, Layer, & Rhee, 1989; Winters, 2002). The experiments with EPDMs with various diene monomers have demonstrated that EPDM with ethylidene norbornene (ENB) as diene monomer is more reactive towards resole cross-linking than EPDM with dicyclopentadiene (DCPD), 1,4-hexadiene (HD) or vinylidene norbornene (VNB), because of the relatively high stability of the benzyl cations (Winters, 2002). It has been suggested that most probably, the resole does not react with PP, because of the absence of unsaturation (M. Van Duin & Machado, 2005).

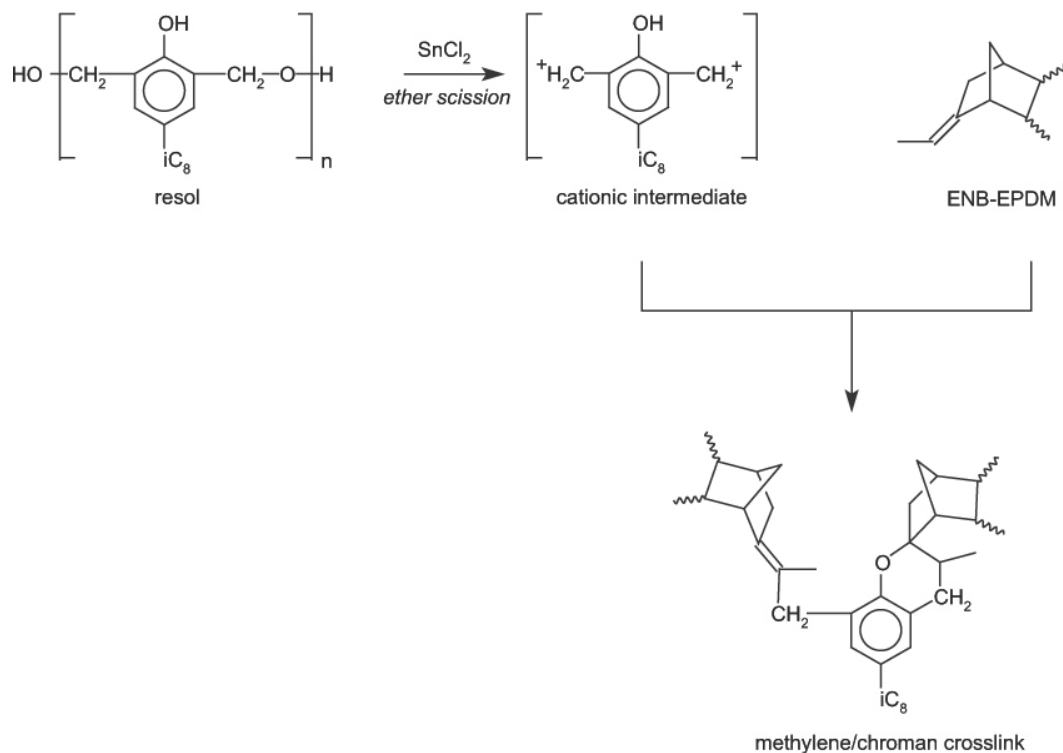


Figure 2-9. Simplified mechanism of  $\text{SnCl}_2$ -activated resol crosslinking of ENB-EPDM (M. Van Duin & Machado, 2005)

Besides the chemical crosslinking systems, gamma irradiation of EPDM has been investigated extensively (Özdemir, 2008; Rivaton, Cambon, & Gardette, 2004; Zaharescu, Setnescu, Jipa, & Setnescu, 2000). Ozdemir investigated the effect of high and low dose rate irradiation by tensile, compression set, DSC, DMA, TGA, FTIR, TGA-FTIR tests. They conclude that the extent of crosslinking reaction is lower for the high dose rate irradiation compared with that of low dose rate irradiation. It is shown that the degradation occurs for the high dose rate irradiation through the chain scission. It is also mentioned that higher ENB content increases the rate of crosslinking reaction (Özdemir, 2008). In another attempt, radiation crosslinking of polymer blends containing the ethylene propylene terpolymer and polypropylene at different compositions was studied (Zaharescu, Setnescu, Jipa, & Setnescu, 2000). Zaharescu et al. found that the optimal dose for maximum crosslinking was in the range of 40 to 180 kGy depending on PP concentration.

However, the radiation crosslinking of PP/EPDM blends should be considered as an interesting unconventional procedure of polymer product manufacture, it is already useful to investigate the continuity development in thermoplastic elastomer blends in order to fix the

rubber morphology for the thermoplastic matrix dissolution and its continuity experiments (P. Bhadane, M. Champagne, M. Huneault, F. Tofan, & B. Favis, 2006).

## 2.2.1 Extent of Crosslinking Reaction

The extent of crosslinking in the rubber phase has profound effects on its viscosity and elasticity and the final TPVs properties. In order to find the correlation between the evolution of the two-phase blend morphology and the extent of the crosslinking reaction, the level of crosslinking can be investigated by different criteria such as solvent swelling, gel content, viscosity, NMR signal line width, bound curative content, residual diene concentration and domain hardness measurements.

### 2.2.1.1 Solvent Swelling

The equilibrium solvent-swelling method in cyclohexane at room temperature, by the application of the Flory–Huggins equation, could be used to determine the crosslink density of EPDM (Maiti, Patel, Naskar, & Bhowmick, 2006; K. Naskar & Noordermeer, 2004):

$$\ln(1 - v_2) + v_2 + \chi v_2^2 + \rho \frac{V_1}{M_c} v_2^{1/3} = 0 \quad (2-17)$$

where  $v_2$  is the volume fraction of the rubber in the swollen gel,  $\rho$  is the density of the material,  $V_1$  is the molar volume of the solvent,  $M_c$  is the molecular weight between two crosslinks and the parameter  $\chi$  is the Flory-Huggins interaction parameter between the elastomer network and the solvent, which can be calculated as follows:

$$\chi = \frac{(\delta_s - \delta_r)^2 V_0}{RT} \quad (2-18)$$

where  $\delta_s$  and  $\delta_r$  are the solubility parameters of solvent and elastomer network, respectively;  $R$  is the universal gas constant and  $T$  is the absolute temperature (Bhadane, 2005). The mentioned parameter, in this case was estimated to be 0.315 (Dikland, 1992). However, in case of TPVs where EPDM is surrounded by a relatively less swellable matrix like PP, rubber phase swells against the compressive force exerted by the PP. Therefore, one can assume that the limited swelling of the rubber takes place under a hydrostatic pressure  $p'$  (Maiti, Patel, Naskar, & Bhowmick, 2006). Consequently, the extent of the swelling can be evaluated by

$$\ln(1 - v'_2) + v'_2 + \chi v'^2_2 + \rho \frac{V_1}{M_c} v'^{1/3}_2 + p' \frac{V_1}{RT} = 0 \quad (2-19)$$

Here,  $v'_2$  is the volume fraction of the rubber in the swollen vulcanizates under the forced swelling condition. If we replace  $p'$  by an equivalent quantity  $G$ , the shear modulus of PP, equation (2.19) gives an approximate value of the crosslink density ( $\mu$ ) of the EPDM rubber in a EPDM/PP TPV from the following equation:

$$\mu = \frac{\rho}{2M_c} \quad (2-20)$$

### 2.2.1.2 Gel Content

The EPDM gel content is used as a measure for the extent of crosslinking. Machado et al. concluded that in other conventional techniques, the composition of the TPVs, i.e. the EPDM/PP ratio, influences the experimental results. Consequently, those techniques do not provide a fair comparison of the extent of crosslinking of the rubber phase of the various TPVs, but the EPDM gel content does (Machado & Van Duin, 2005). In order to follow the extent of the crosslinking reaction of the TPVs based on PP/EVA, the gel content variation ( $\tau'_i$ ) and volume swelling rate ( $G_v$ ) were measured for different sampling times by Verbois and coworkers (Agnès Verbois, 2004). Gel content and morphology analysis, showed that the gel content increased and the swelling rate decreased between the beginning of the torque measurement and the maximum of the torque, as shown in Figure 2.10. After the maximum of the torque, the values of these two parameters remained constant. They reported that the phase inversion (from matrix -dispersed particles to co-continuous structure) along the screw axis of the twin screw extruder occurred at the same gel content ( $\tau'_i=59\%$ ) of the phase inversion in the internal mixer (Verbois, Cassagnau, Michel, Guillet, & Raveyre, 2004).

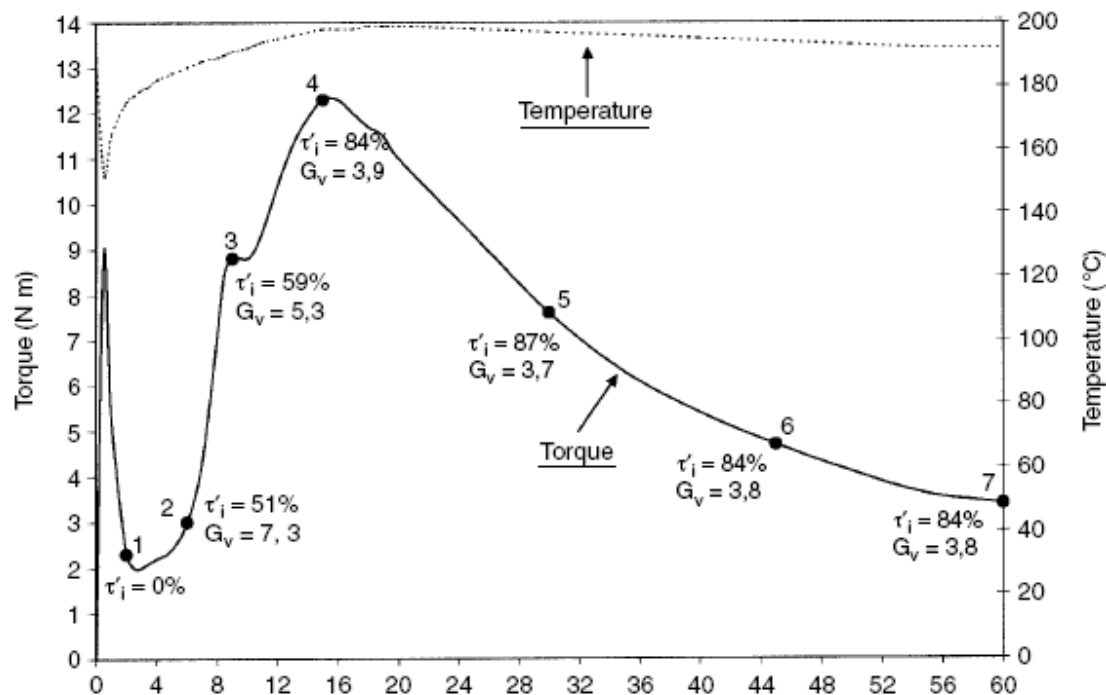


Figure 2-10. Change of the extent of EVA crosslinking in the internal mixer (Agnès Verbois, 2004)

### 2.2.1.3 Solid State NMR

solid state NMR have been extensively used to study the crosslinking extents in rubbers (Leisen, 1999; V. Litvinov, 1998; Winters, 2002). It has been shown that solid state NMR spectra can be also used to determine the crosslink extent in TPVs based on PP/EPDM, which are prepared using different curatives such as phenolic resin (V. M. Litvinov, 2006). A representative spectrum is shown in Figure 2.11. Signals at 1.0, 1.4, 5.1–5.3, and 7.0 ppm are assigned to methyl, methylene, residual diene, and aromatic components, respectively (Ellul, Tsou, & Hu, 2004). Each spectrum contains three different parts that can be used to determine the curing extent in a TPV:

#### A) Backbone peak base width

The mobility of a polymer segment is directly related to its signal width. An increase in segmental mobility narrows the observed segment signal. In cured systems, segments, which are away from a crosslink, are more mobile than segments that are close. Since away-from-crosslink segments have lower signal line width as compared to that obtained from close-to-crosslink

segments. In other words, the contribution of the away-from-crosslink segments, or non-crosslinked linear segments is more in the narrower part of the peak. Usually, the line width at peak base (<1% of maximum) is used as a measure of the crosslink density.

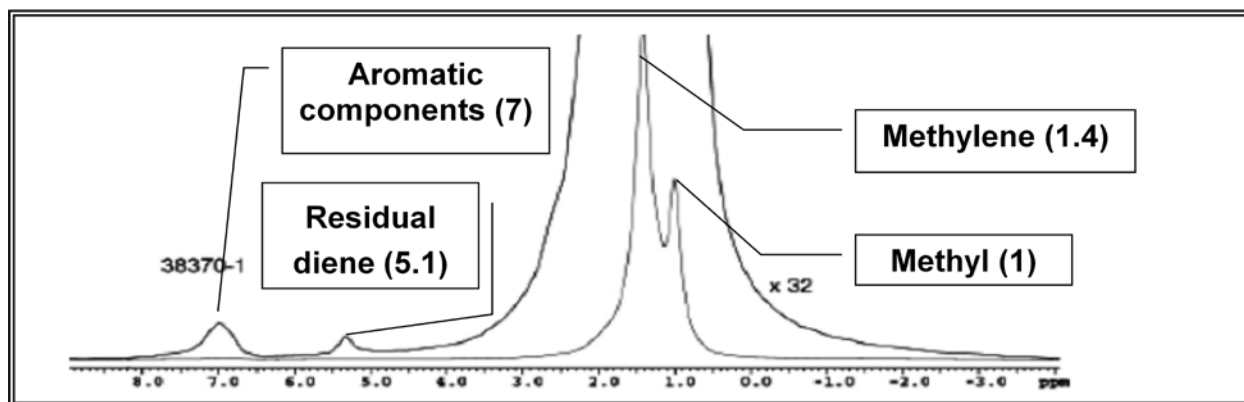


Figure 2-11  $^1\text{H}$  MAS NMR spectrum of thermoset rubber (before extraction) (Ellul, Tsou, & Hu, 2004).

However, one should consider that the  $^1\text{H}$  NMR line width can be affected by other factors. For example, the presence of polypropylene and strong interactions between polymer and fillers, could broaden the peak base width. Also to have a fair comparison between two systems, spectrometer conditions must be kept the same (Ellul, Tsou, & Hu, 2004).

## B) Aromatic content

The resonance of the aromatic protons in the curative about 7 ppm can be clearly seen in the  $^1\text{H}$  spectra (Figure 2.12). These aromatic protons could have come from two possible sources; phenolic molecules that are not part of the crosslinks and reacted phenolic. After extraction process to remove unreacted curative, the signal at 7 ppm in extracted TPV samples could be only on bound phenolic molecules. The ratio of aromatic area ( $\sim 7$  ppm) to the total area under the backbone peaks can be used as a measure of the extent of crosslinking (Ellul, Tsou, & Hu, 2004).

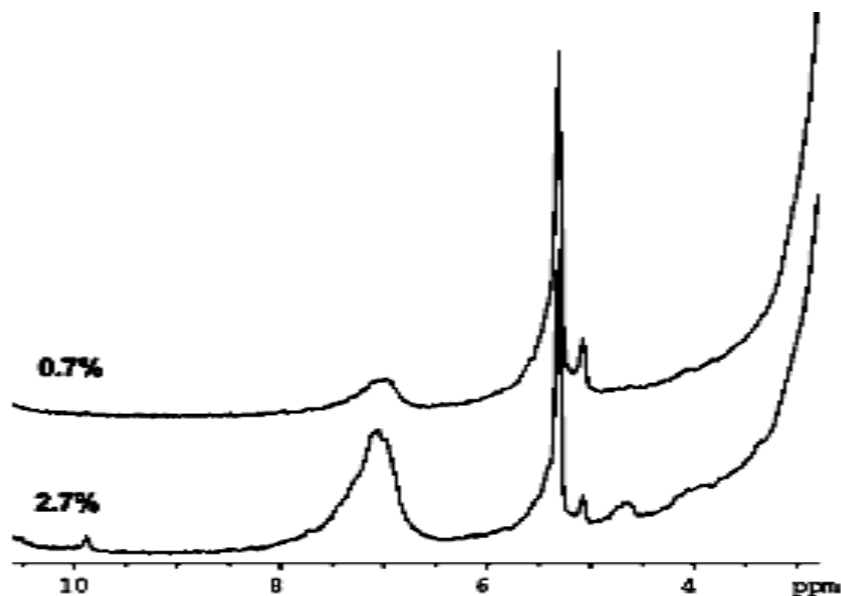


Figure 2-12.  $^1\text{H}$  MAS spectra of EPDM samples (after extraction), with Different phenolic resin content (Ellul, Tsou, & Hu, 2004)

### C) Diene content

Based on different approaches, several mechanisms have been proposed for phenolic resin vulcanization of unsaturated elastomers (Lattimer, Kinsey, Layer, & Rhee, 1989; M. van Duin, 1995). Due to the 1,4-cyclic addition mechanism, dienes are consumed during cure and consequently the backbone will be saturated. The peaks at 5.1 and 5.3 ppm are related to the two isomers of ENB, ethylene norbornene, unsaturated protons, respectively. It has been indicated that, with increasing curative content, the diene content will be reduced. This suggests the consumption of diene during vulcanization cure. Therefore, one can calculate residual ENB weight fraction as a measure of crosslinking extent.

However, according to one of the other proposed mechanisms (M. van Duin, 1995), the diene that has reacted with curative could have preserved the unsaturation. In that case, residual dienes in a cured EPDM could be on either the unreacted diene or the reacted one. According to Ellul et al, based on the different dynamic behavior, these two types of unsaturation can be distinguished from each other; the unreacted diene would have much more motions in comparison to the reacted diene, therefore, the former would have most probably a longer  $^1\text{H}$   $T_2$  than that of reacted diene. They mentioned that the mechanism of retaining unsaturation during

cure is ruled out because all diene signals have a slightly longer  $^1\text{H T}_2$  than that of the backbone. (Ellul, Tsou, & Hu, 2004; V. M. Litvinov, 2006).

#### **2.2.1.4 AFM Force Modulation Amplitude**

Despite the complicated relationship between the force modulation amplitude and modulus, the mechanical stiffness of the rubber phase could be estimated by the force modulation amplitude. The application of the force modulation amplitude for the evaluation of the crosslink density has been demonstrated in NR (Galuska, Poulter, & McElrath, 1997), SBR (Mareanukroh, 2000) and more recently in EPDM in a dynamically vulcanized TPV (Ellul, Tsou, & Hu, 2004).

### **2.3 Mechanical and Viscoelastic Properties**

According to Coran and Patel, a few characteristics of the pure rubber and thermoplastic components should be considered in the material selection to increase the probability of success for producing a TPV with good mechanical properties and elastic recovery. They suggest that the best compositions are prepared with following characteristics: (A. Coran, 1982):

- A) The surface energies of the plastic and elastomer should be matched, which is satisfied in the case of TPVs based on PP/EPDM. (The surface energies of PP and EPDM are both about 28 mN/m)
- B) The entanglement molecular length of the elastomer should be low (high entanglement density)
- C) The plastic phase should be at least 15% crystalline.

Additionally it is essential to have stable rubber and plastic as well as an appropriate curing system under desired processing conditions.

For the TPVs based on PP/EPDM, as the crosslink density of the rubber phase and plastic content increased the tensile strength improved continuously (A. Y. Coran, Patel, & William, 1981b). It was shown that complete vulcanization improved the mechanical properties of the blend. For instance, the tensile strength increased from 300-500% after complete vulcanization. The ultimate tensile strength and the ultimate elongation increased with the degree of vulcanization and PP content in the blend. The ultimate elongation increased from 180-200% to 460-560% after vulcanization. Young's modulus decreased slightly as a result of vulcanization and increased with PP content in the blend (Bhadane, 2005; A. Coran, 1982). The TPVs also had

better resistance to high temperatures and oils in comparison to their uncured blends. Only a small amount of vulcanization was required to improve fatigue resistance and tension set. The latter increased with the PP content in the blend. A composition with higher shear modulus was obtained as a result of an increase in the viscosity of the elastomer phase, crystallization in the thermoplastic or hard phase or dissimilarity between the polarity and wetting characteristics of the two phases. The ultimate mechanical properties and elastic recovery increased with the similarity of the rubber and plastic, as measured by the surface tension (Bhadane, 2005; A. Coran, 1982).

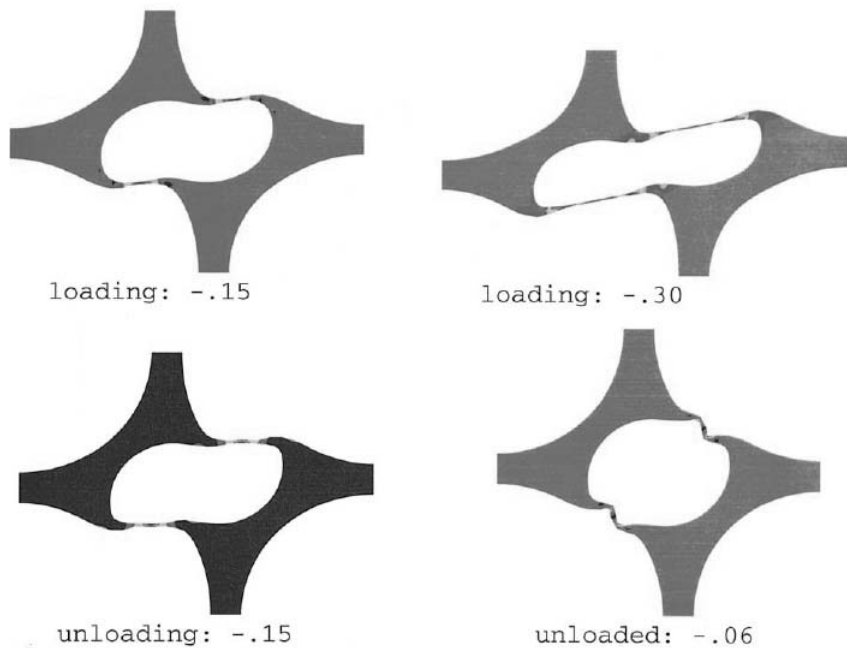


Figure 2-13. Schematic representation of deformation mechanism in TPVs (C. Boyce, Socrate, Kear, Yeh, & Shaw, 2001).

The morphology of the TPV plays a key role in the mechanical properties, but its effect is still not well understood. As mentioned earlier, TPVs show rubber-like properties, although the stiffer PP phase is still continuous. This phase is present as thin films between the elastomer particles. The deformation of these PP films is the base of the deformation mechanism models. During deformation in the solid state, the PP phase only yields partially in the equatorial region of the elastomer particles and the rest of the PP phase remains unaffected (Sengers, 2005). As seen in Figure 2.13, upon unloading, the retraction of the elastomer phase results in buckling of the stiff PP lamellae that cannot deform elastically (C. Boyce, Socrate, Kear, Yeh, & Shaw, 2001;

Martin Van Duin, 2006). This buckling mechanism has been confirmed by AFM studies during deformation of TPVs (Groeninckx, Oderkerk, De Schaetzen, Goderis, & Hellemans, 2002).

### **2.3.1 Elastomeric Properties Characterization**

Compression set measurement is the well known method to characterize elastomeric property. It was designed originally to characterize a thermoset rubber. Compression set value obtained from a single-phase rubber material is mainly associated to the crosslink density and does not vary significantly between two different laboratories. However, in a two-phase TPV material, the compression set would not be a proper criterion because it is not only related to the crosslink density and the network tightness, but also strongly depends on the sample preparation method, which could change the orientation of the two phases. (Cai, Reid, Srinivasan, & Vennemann, 2004). It seems that the recoverable strain using a modified hysteresis test and the stress relaxation behavior using a temperature scanning stress relaxation test (TSSR) can characterize TPV products better than the compression set test (Barbe et al., 2005; Cai, Reid, Srinivasan, & Vennemann, 2004; Vennemann, Bökamp, & Bröker, 2006).

#### **2.3.1.1 Modified Hysteresis Tensile Analysis**

This test is one of the recent developments for characterization of the thermoplastic elastomers. Unlike in a traditional hysteresis tensile test, the determination of the permanent set  $\epsilon_p$  (the irreversible part of the strain) is carried out using various strain amplitudes (2-20%) and testing speeds (5-50 mm/min). As seen in Figure 2.14, the modified hysteresis tensile test gives critical strain ( $\epsilon_{crit}$ ) identifying a limit of the strain amplitude, to avoid high plastic deformation. TPVs behave like a thermoset rubber below and act more like a plastic above  $\epsilon_{crit}$ . The elastomeric slope ( $m_E$ ) and plastic slope ( $m_p$ ), obtained from low and high strain regions, provide more information on behavior of a TPV in real application under various conditions. In other words, the degree of reversibility of deformation is related to the elastomeric slope; a lower value of  $m_E$  indicates improved rubber-like behavior (Cai, Reid, Srinivasan, & Vennemann, 2004).

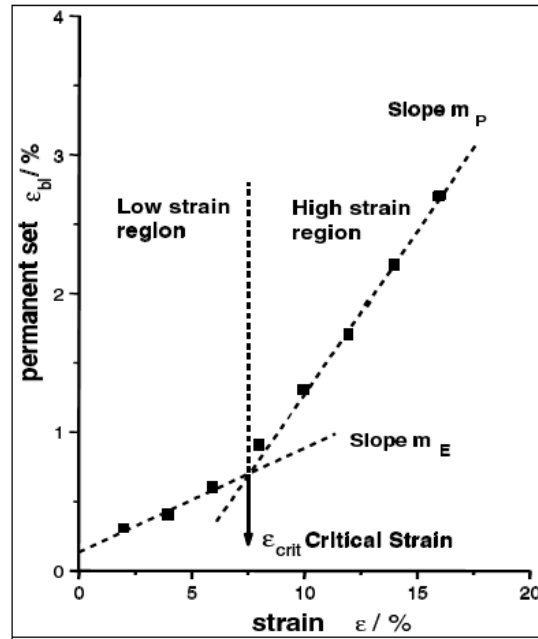


Figure 2-14. Strain-permanent set curve generated from the modified hysteresis tensile test (Cai, Reid, Srinivasan, & Vennemann, 2004).

### 2.3.1.2 Temperature Scanning Stress Relaxation Test (TSSR)

Mechanical stress relaxation is one of the most important phenomena regarding to the final TPVs application. Due to the presence of thermoplastic phase as the continuous phase in TPVs, the high temperature relaxation is more significant than what is observed with thermoset rubbers. To characterize this behavior precisely, the thermal scanning stress relaxation test method (TSSR) could be used (Barbe et al., 2005; Cai, Reid, Srinivasan, & Vennemann, 2004; Vennemann, Bökamp, & Bröker, 2006). Unlike in a conventional stress relaxation test, in which the relaxation occurs in isothermal condition, here the sample is heated. Therefore, the TSSR test is significantly faster. The temperatures to reduce the tensile stress by 10% (T10), 50% (T50) and 90% (T90) and the integral of the curve (rubber index) are evaluated by the obtained normalized force-temperature curve (Figure 2.15) to characterize the thermal–mechanical behavior of the sample. It was shown that the integral value increased with increase of crosslink density (Cai, Reid, Srinivasan, & Vennemann, 2004).

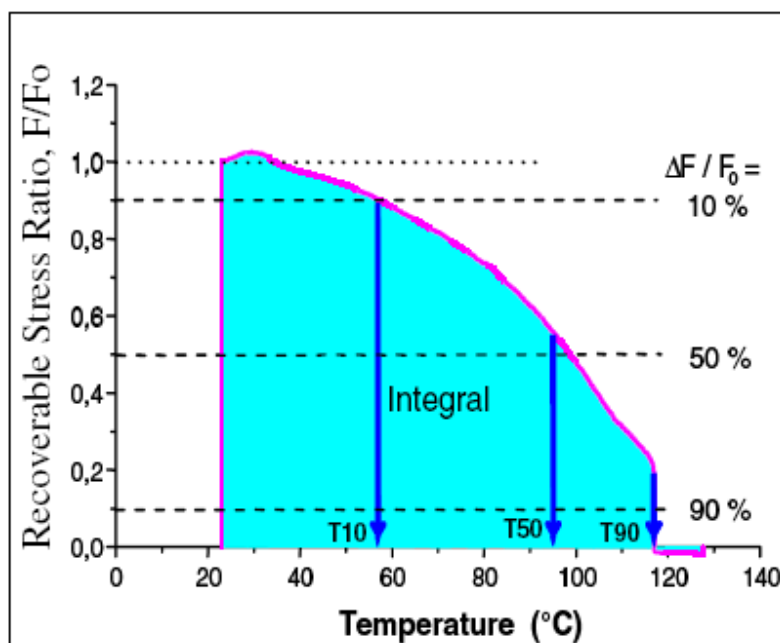


Figure 2-15. Temperature-recoverable stress ratio curve from a TSSR test (Cai, Reid, Srinivasan, & Vennemann, 2004)

## 2.4 Rheological Properties

The rheological properties of TPVs can be classified with those of highly filled polymers. Due to the elastomeric network structure, TPVs have a yield stress as proven by melt creep measurements (Araki & White, 1998). The value of the yield stress increases with increasing elastomer content (Sengers, 2005). Once the network-like structure is broken, a shear thinning behavior with the power-law exponent close to the one of the thermoplastic phase is observed. Therefore, this would mean that steady shear flow properties are dominated by this phase. The shear viscosity is lower than the dynamic viscosity. The flow behavior is stronger function of the applied stress and strain than on the temperature (Goettler, Richwine, & Wille, 1982; Han & White, 1995; Jain, Gupta, & Nagpal, 2000; Radhesh Kumar, Nair, George, Oommen, & Thomas, 2003). Unlike the common blends in which the storage modulus decreases with a logarithmic slope of 2 at the terminal flow regime (Tucker & Moldenaers, 2002), the storage modulus of TPVs tends to show a plateau as the frequency goes to zero. This indicates that these materials have a rest state structure (Han & White, 1995). By crosslinking the rubber phase, the loss modulus becomes always lower than the storage modulus. On the other hand, rheological and morphological investigation of the plasticized thermoplastic elastomer blends shows that the

presence of a low molecular weight plasticizer has a significant coarsening effect on the morphology development (Shant Shahbikian et al., 2011a). It has been shown that, in the non-reactive blends, during the single step stress growth test, the magnitude of the normalized overshoot increases with the elastomer content. In contrast to the non-reactive blends, no clear overshoot is observed for the reactive blends without plasticizer (Shant. Shahbikian, 2010).

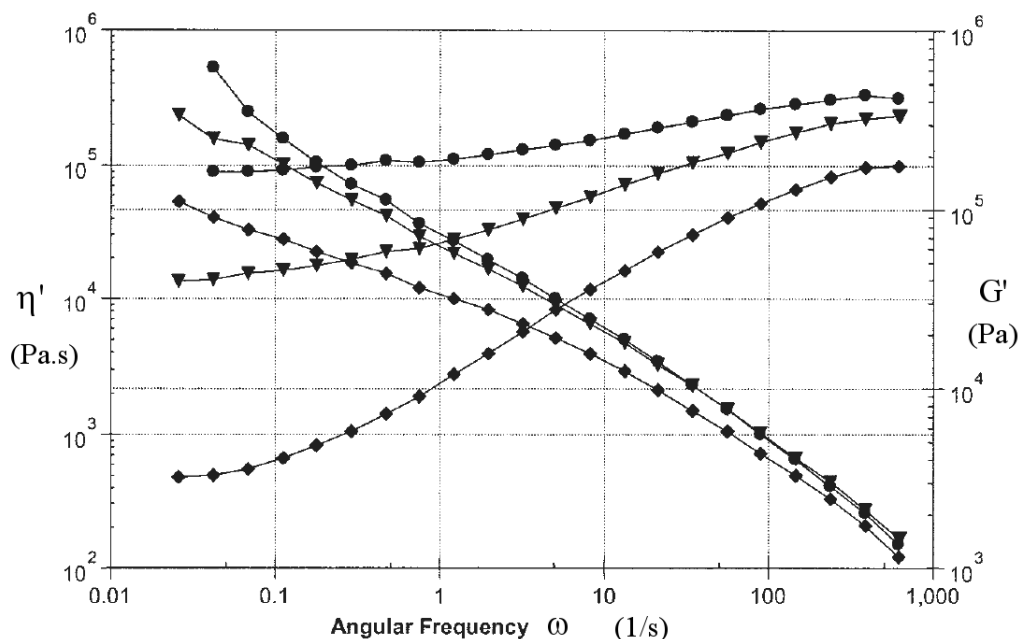


Figure 2-16. Storage modulus and dynamic viscosity of *EPDM/PP TPVs* of different compositions at 220°C: 20/80 ◆; 40/60 ▼; 60/40 ●, (w/w) (Goharpey, Nazockdast, & Katbab, 2005)

Goettler et al. (Goettler, Richwine, & Wille, 1982) studied the processing properties of PP, and EPDM/PP based TPEs and corresponding TPVs at different shear rates. They observed that the die swell of dynamically vulcanized blends was much lower than for PP and non-vulcanized blends at a constant temperature. They also concluded that processing temperatures were not critical in post processing of TPVs and melt viscosity was slightly affected by moisture. The relation between observed rheological and viscoelastic properties and TPV morphology is a challenging topic in this field.

## 2.5 Reactive Extrusion of TPVs

The term “reactive processing” stands for a polymer processing procedure that involves chemical reactions. However, usually the term denotes to reactive extrusion, and especially, to the reactive compatibilization of immiscible polymer blends (In situ immobilization of one phase (dynamic vulcanization)), usually conducted in a twin screw extruder (L. A. Utracki, 2002; Xanthos, 1992).

In spite of some difficulties, due to reactions in which the high residence time is required and the lack of satisfactory mathematical models of the reactive extrusion, some of the most important features of reactive extrusion are (L. A. Utracki, 2002):

- A) The possibility of dividing the reactive mass into small melt pools, bounded by the screw flights and barrel walls, with short mass and heat transfer distances.
- B) The ability to manage a series of operations in a logical well controlled sequence along the length of the extruder (melting, mixing, reacting, homogenization and forming).
- C) The ability to create rapidly renewed interfaces that control the overall reaction rate.
- D) The possibility of introducing reactants and catalysts at the desired locations.
- E) Self cleaning system that allows narrow and adjustable distribution of residence time.

The residence time distribution depends on the screw configuration, the amount of material passing through the extruder (the degree of fill) and the screw speed. The residence time distribution is narrower for counter-rotating twin screw extruders than for co-rotating twin screw extruders.

Reactive extrusion is controlled by selection of equipment, screw configuration, and ingredients, as well as by the control of process conditions. In the present case, preparation of TPVs using twin the screw extruder combines crosslinking chemistry with polymer processing. Thus, its development involves following steps:

### **A) Studies of chemical kinetics in internal batch mixers**

Pesneau et al. investigated TPVs based on PP/EMA by twin screw extrusion (Pesneau, Champagne, & Huneault, 2002). Using pentanediol as the curative agent and dibutyltin oxide as the catalyst, they first studied the crosslinking kinetic of the EMA in the internal mixer. They

showed that, when the catalyst or temperature increased, the reaction started sooner; the torque peak was reached faster after curative agent addition. However, the same insoluble fraction and torque-time curve was obtained, as shown in Figure 2.17. According to the torque-time curves, they concluded that the cross-linking reaction could be fast enough to allow for scale-up in twin screw extruders, because typical residence times in twin screw extruders range from 30 s to a few minutes, depending on operating conditions and machine geometry. In addition, they commented that the high mixing efficiency of twin-screw extruders increased reaction rates, which improved the scalability of EMA cross-linking by diols.

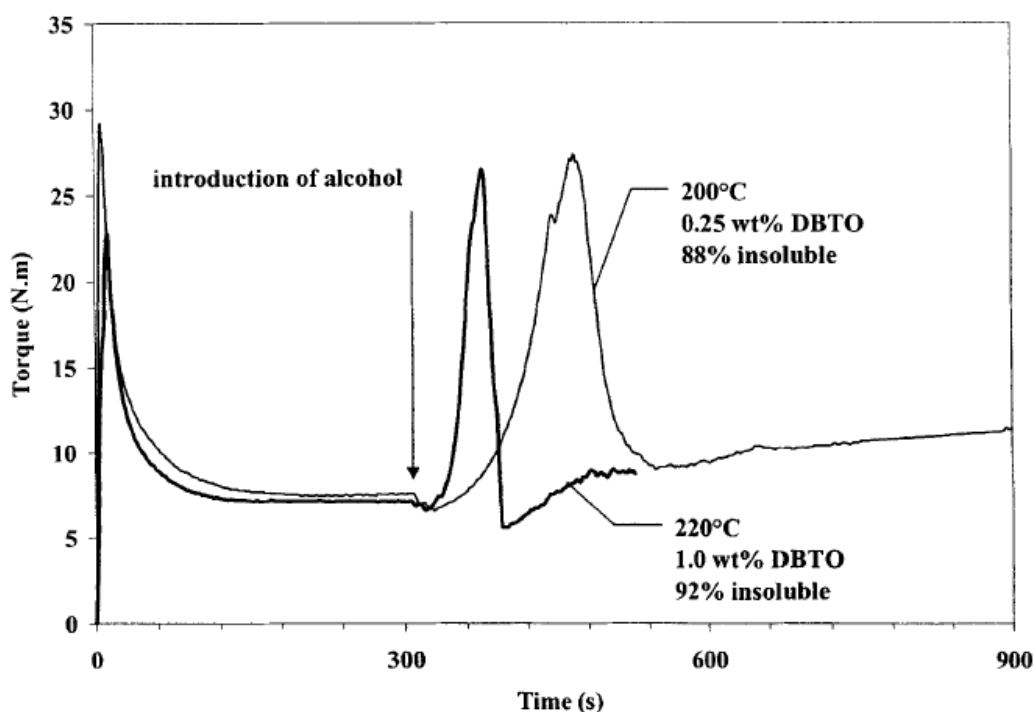


Figure 2-17. Torque evolution during the reaction between EMA and pentanediol at different temperatures and DBTO contents (Pesneau, Champagne, & Huneault, 2002).

In addition, they reported that the extent of EMA cross-linking was enhanced significantly at higher curative concentrations.

The same trend was observed by Verbois et al. (Verbois, Cassagnau, Michel, Guillet, & Raveyre, 2004). They investigated the evolution of EVA/PP TPV morphology, with respect to the crosslinking reaction conversion. They prepared different reactive blends in the internal mixer, and the influence of different parameters (temperature, TPOS and DBTO concentrations) on the rheological behavior of the various EVA reactive systems was studied. As shown in Figure

2.18, gel time, which was defined as the time corresponding to the crossover between storage modulus and loss modulus, decreased by increasing the temperature or catalyst content. The main conclusion of interest was that the use of catalyst was necessary to render the crosslinking kinetics of EVA, compatible with the residence times in the extruder.

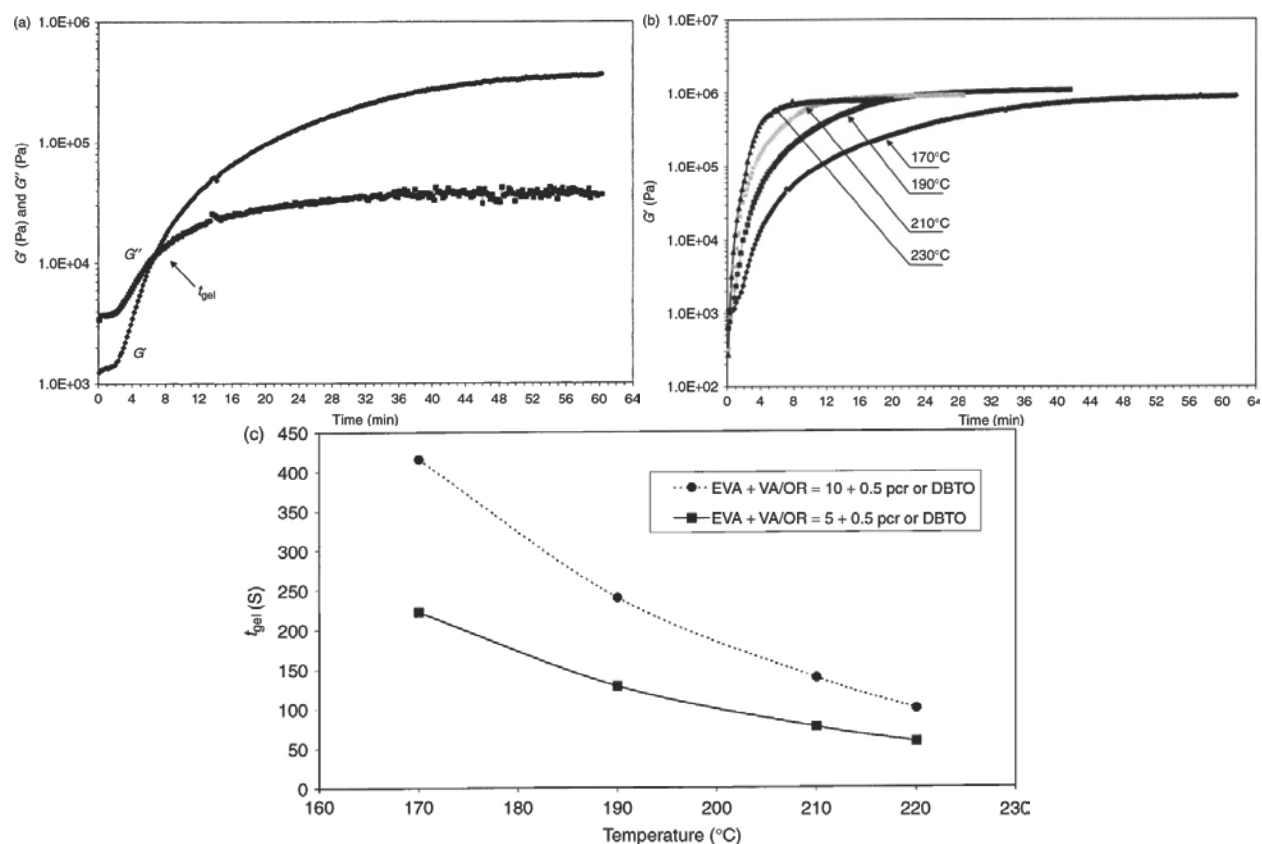


Figure 2-18. Different rheological results on the bulk EVA cross-linking at different temperatures and catalyst concentration (Verbois, Cassagnau, Michel, Guillet, & Raveyre, 2004).

## B) Determination of the rheological and thermal characteristics

The thermal stability of the dynamically crosslinked TPV should be evaluated by rheology. In the case of dynamic vulcanization, the reaction can continue, as the three components of the reaction are still present: the catalyst, the rubber, and the curative agent. Therefore, the influence of the extent of post-extrusion reaction on the processability and final properties should be considered. Figure 2.19 presents the viscosity evolution for a nonreactive system as compared to a cross-linked system with 78% insoluble content (Pesneau, Champagne, & Huneault, 2002). Such data gives an indication of the system stability. Thus, crosslink density

of the material leaving the extruder must be within a specified range. Otherwise the processability and the final morphology would change in post processing steps.

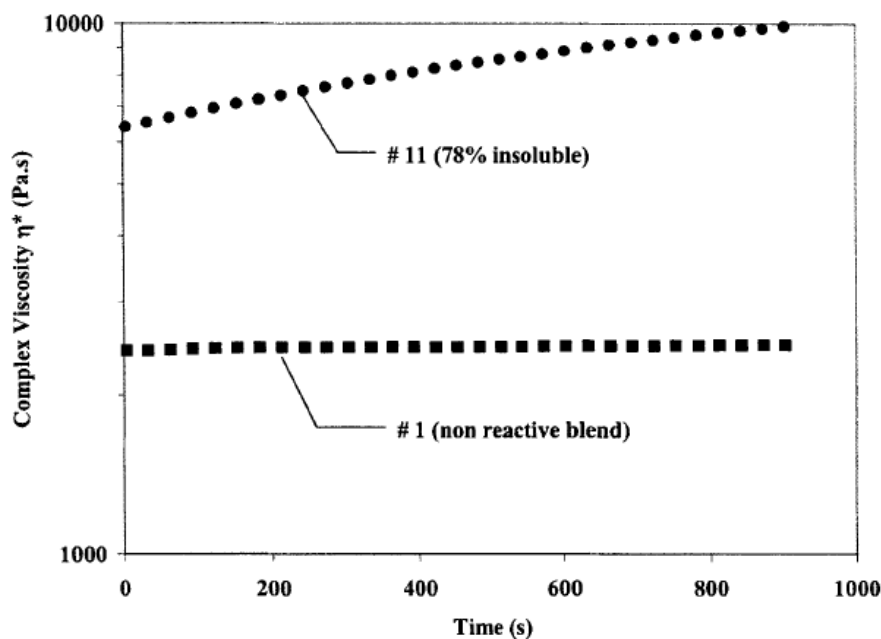


Figure 2-19. Evolution of dynamic viscosity with time for non reactive blend as compared to the same system, dynamically cross-linked at 78% insoluble (Pesneau, Champagne, & Huneault, 2002).

### C) Reactive extrusion trials

For a comprehensive approach, during the development stage, it is essential that samples are frequently taken from the extruder and analyzed for the extent of reaction as well as for the morphology and the key properties. The kinetic, structure and key properties should be determined within the full range of the expected extrusion process parameters, such as composition, temperature, screw speed and feeding order (L. A. Utracki, 2002).

As pointed out by Coran et al., vulcanization must be slow enough to permit the dispersion of the curatives (A. Y. Coran, Patel, & William, 1981a, , 1981b). On the other hand, it has been shown that decreasing the temperature lowers the reaction rate. Therefore, more time is provided for generating fine curative agent dispersion in the medium, before the reaction takes place (Pesneau, Champagne, & Huneault, 2002). If the crosslinking reaction rate is too high, another strategy would be to add the catalyst through the side feeder, just after proper dispersion of curatives.

Pesneau et al. demonstrated that the insoluble EMA fraction increased, when the screw speed increased, at constant DBTO catalyst and pentanediol content curative agent. Increasing the screw speed lowers the residence time in the extruder and consequently the time available for reaction reduces. However, higher screw speed also generates larger shear stresses and higher viscous shear heating that favor the dispersion processes and exothermic crosslinking reaction. In their case, the gel content appeared more dependent on the dispersion of pentanediol than on the residence time in the extruder (Pesneau, Champagne, & Huneault, 2002).

Machado et al. showed that dynamic vulcanization in extruders was quite different from that in batch mixers, where melting, mixing and crosslinking were separated in time (Machado & Van Duin, 2005). They studied the crosslinking chemistry, the dispersion and the crosslinking of HDPE/EPDM blends along the axis of an extruder during dynamic vulcanization with resole. They fed all of the ingredients to the extruder via the first hopper and investigated morphological characteristics of the samples taken along the screw axis. They found that dynamic vulcanization of the EPDM phase had already occurred, when the PE phase was not yet fully molten. Just after complete melting of the PE phase, the blend very quickly reached its final morphology. Only for the (50/50 wt%) blend, an evolution from co-continuous structure to fully dispersed EPDM was observed, which was driven by crosslinking (Figure 2.20).

In another attempt, Verbois et al. followed morphology development in reactive extrusion and, more particularly, in TPV production. From the gel content and morphology analysis, they concluded that the correlation between the evolution of the two-phase blend morphology and the crosslinking reaction conversion was almost the same for the elaboration of the TPV in the internal mixer and in the twin-screw extruder. The phase inversion took place at a gel content of around 60% in both methods (Verbois, Cassagnau, Michel, Guillet, & Raveyre, 2004).

Finally, detailed evaluation of the properties of reaction products and optimization of the reactive extrusion parameters, including blend composition and processing condition are the next steps of reactive extrusion development.

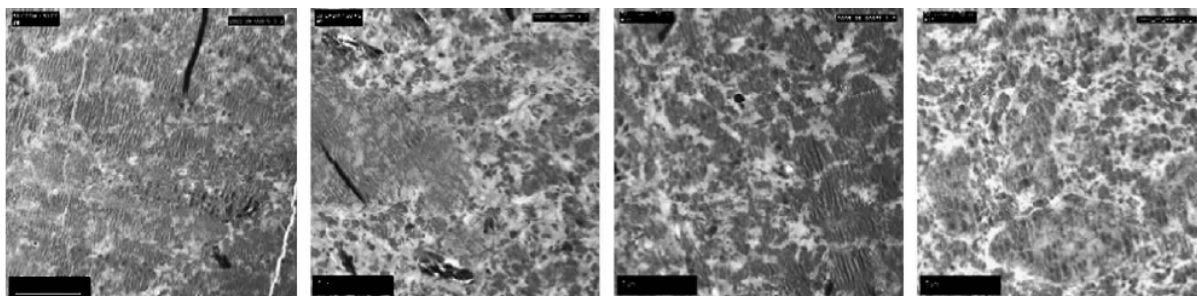


Figure 2-20. TEM micrographs of samples taken at  $L/D=8, 9, 10$  and  $15$  upon dynamic vulcanization of PE/EPDM blend (50/50; w/w) (M. Van Duin & Machado, 2005).

## 2.6 Polymer Layered Silicate Nanocomposites

In recent years, a new class of polymeric composites, so-called nanocomposites, has received considerable interest in polymer science research and technology (Biswas & Ray, 2001; E. P. Giannelis, 1996, , 1998; Singh & Balazs, 2000; Yano, Usuki, Okada, Kurauchi, & Kamigaito, 1993). In these materials, dispersed particles have at least one dimension in the nanometer scale. In particular, polymer layered silicate (PLS) nanocomposites, in which silicate layers are dispersed in a polymer matrix in nanometer sizes, belong to this category (Sinha Ray & Okamoto, 2003). PLS nanocomposites, because of their nanometric size and the large interfacial interaction between matrix and silicate layered surface, exhibit remarkable improvements in performance, including mechanical properties (E. Giannelis et al., 1999), thermal stability (Gilman et al., 2000) and barrier properties (Bharadwaj, 2001). In comparison to conventional filled polymer systems with loading levels from 10 to 40 wt%, usually it is possible to achieve improved properties in PLS nanocomposites at low levels of silicate loading (<5 wt %). The light weight of PLS nanocomposites compared to conventional composites make them competitive with other materials for particular applications. Polymer-clay composites may be divided into three general types (Leszek A. Utracki, Sepehr, & Boccaleri, 2007): conventional composites, where the clay acts as a conventional filler, intercalated nanocomposite consisting of a regular insertion of the polymer in between the clay layers, and delaminated nanocomposite or exfoliated nanocomposite where 1 nm-thick layers are dispersed in the matrix. The latter structure is of special interest, because it causes the maximum polymer-clay interactions and makes the entire surface of the layers available for the polymer. This should lead to most dramatic changes in physical and mechanical properties.

## 2.6.1 Nano-clay

Montmorillonite is a special type of the smectite family of clays, in which the layered structure consists of two silica ( $\text{SiO}_4^{4-}$ ) tetrahedral sheets bonded to an alumina ( $\text{AlO}_6^{9-}$ ) octahedral sheet. As shown in Figure 2.21, in Montmorillonite (MMT), oxygen atoms from the silica tetrahedral sheets also belong to alumina octahedral sheet. The three sheets form 1 nm thin layer. These layers are, in turn, connected together by Van der Waals bonds and organized in stacks with regular gaps between them called “gallery” or “interlayer” spaces. Within the layers, an excess of negative charge is generated because of isomorphous substitution of atoms as  $\text{Al}^{3+}$  with  $\text{Mg}^{2+}$  or  $\text{Fe}^{2+}$ . The amount this charge is defined through the charge exchange capacity (CEC) and characterizes each clay type. The CEC value for MMT depends on its mineral origin; it is typically 90-120 meq/100g. Usually ions such as  $\text{Na}^+$ ,  $\text{Li}^+$  or  $\text{Ca}^{2+}$  balance this excess negative charge in natural clays. This means that natural MMT is only miscible with a few number of hydrophilic polymers, like polyethylene oxide and polyvinyl alcohol (Sinha Ray & Okamoto, 2003).

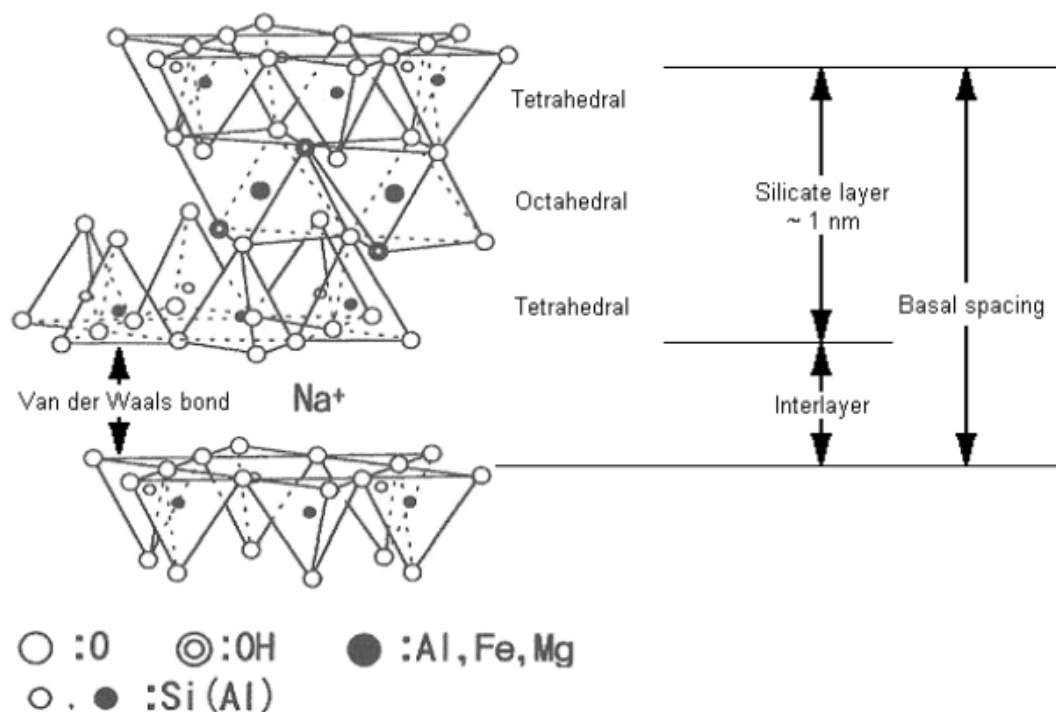


Figure 2-21. Schematic illustration of atoms arrangement in a typical MMT layer(Sinha Ray & Okamoto, 2003)

Although different types of clay can be used for nanocomposite formation, depending on the various properties demanded by the product, Montmorillonite is the most common one. In order to enhance miscibility between Montmorillonite and other kinds of polymers, it is an essential requirement to exchange the alkali ions with cationic-organic surfactants, such as alkyl-ammonium ion. This is called the surface treatment. In this way, the natural clay can become ‘organophilic’ and then named “nano-clay” or “organo-clay”. Several other surface treatments can be applied to the clays in order to make them organophilic and more likely to disperse in the polymer matrix (Dell'Anno, 2004).

### 2.6.2 Surface Treatment

The modification of clay to provide the ‘organophilic’ character to the clay is essential for successful formation of nanocomposites.

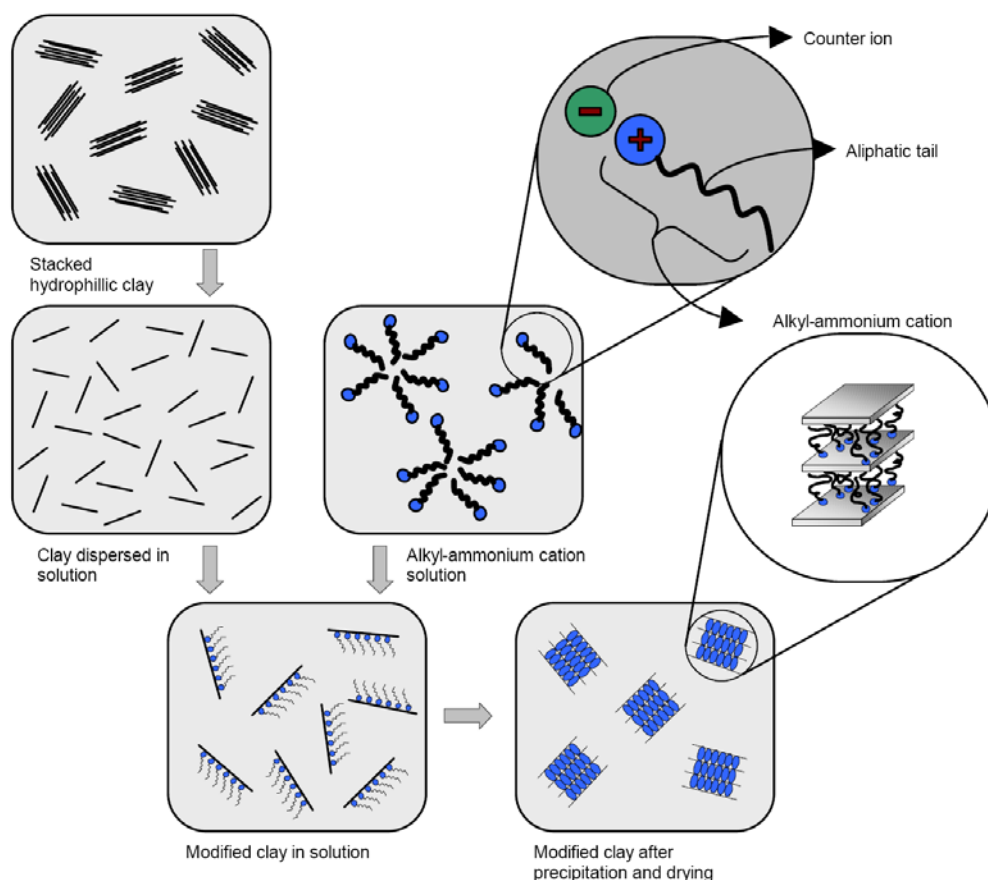


Figure 2-22. Schematic representation of clay surface treatment (Dell'Anno, 2004)

Organophilic clay can be formed by use of an ion exchange with an organic cation, such as the above mentioned alkylammonium ion. The way in which the substitution is carried out and the chemical product used as treating agent have an effect on the formation of different nanocomposite products. However, an ion exchange reaction (as shown schematically in Figure 2.22) is commonly used method to introduce alkyl-ammonium ions in the interlayer space. From economical point of view, obviously, this treatment adds to the final price of the clay. On the other hand, the alkyl-ammonium ions are relatively cheap as raw materials. It is important to note that by the surface modification, not only the clay becomes an organo-clay, but also this treatment increases the interlayer distance. Indeed, surface treated clay is used, even in the case of polar polymers, in which the modification of clay polarity is not fundamental for the nanocomposite formation. Clearly, as the amount of carbon atoms in the tail of the ammonium ion increases, the interlayer distance increases and the clay becomes more organophilic (Sinha Ray & Okamoto, 2003)

### **2.6.3 Preparation Methods of Nanocomposites**

Generally, there are three main ways to incorporate silicate layers in the polymer matrix, including the in situ polymerization method, the solution mixing method and the melt mixing method.

#### **2.6.3.1 In-situ Polymerization**

In this method, polymerization occurs between the intercalated sheets after swelling of the layered silicate with the liquid monomer or a monomer solution. Polymerization is initiated either by radiation or heat, by the diffusion of a suitable initiator, or by an organic initiator or catalyst fixed inside the interlayer before the swelling step (Sinha Ray & Okamoto, 2003). One advantage of this method is possibility of grafting the polymer onto the particle surface. Many different types of nanocomposites, such as PMMA and PS nanocomposites, have been processed by in-situ polymerization (Okamoto, Morita, & Kotaka, 2001; Okamoto et al., 2000).

#### **2.6.3.2 Solution Mixing**

This method is based on a solvent system, in which the polymer is soluble and the silicate layers are swellable. Initially, the silicate layers are swollen in a solvent, such as water, toluene,

or chloroform. Then, the resultant layered silicate and the polymer are mixed. In this step, the polymer chains intercalate and displace the solvent within the interlayer of the silicate. The resultant solution can then be cast into a solid, resulting in a polymer-layered silicate nanocomposite(Sinha Ray & Okamoto, 2003). This method is particularly attractive for water soluble polymers, such as polyethylene oxide(Aranda & Ruiz-Hitzky, 1992) and polyvinyl alcohol(de Bussetti & Ferreiro, 2004).

### **2.6.3.3 Melt Mixing**

In the third strategy, instead of passing through the monomer mixing, the silicates are directly dispersed in the polymer melt. Here, the silicates need to be modified, through the surface treatment, before mixing with the polymer. Melt intercalation is more flexible and “green” than the previous two routes, due to the absence of solvent and chemical reaction(Kornmann, 1999; Sinha Ray & Okamoto, 2003). However, in this method, it is necessary to add a third component, such as PP-g-MA when non-polar matrices are involved, even if the clay was already organically modified (Hasegawa, Kawasumi, Kato, Usuki, & Okada, 1998; Kawasumi, Hasegawa, Kato, Usuki, & Okada, 1997). The purpose of this new constituent is to improve the matrix filler interactions by reducing the interfacial tension between them.

## **2.6.4 Nanocomposites Characterization**

There are mainly two techniques to investigate the polymer-clay nanocomposite structure. The most straightforward is X-ray diffraction, which is a proper method to estimate the spacing between the clay layers. Sample preparation is simple and the X-ray analysis can be completed within a few minutes. However, the results should be interpreted carefully. Restrictions of the equipment and low sensitivity of the analysis can lead to wrong conclusions about nanocomposite structure (Kornmann, 1999). Therefore, micrographs obtained by transmission electron microscopy are necessary complement to X-ray diffraction results. However, TEM is time-intensive and requires experience in sample preparation. This technique provides a direct qualitative understanding of the nanocomposite structure and a measure of the distribution of the layers through direct visualization.

### 2.6.4.1 Wide angle X-ray Scattering Analysis

Figure 2.23 shows the diffraction from two consecutive clay layers or other scattering planes and intercept X-rays of wavelength  $\lambda_1$  at the incident angle  $\theta$ . By definition, interlamellar spacing or d-spacing is the separation distance between two layers ( $d$ ) and the experimental  $2\theta$  value is the angle between the incoming and diffracted X-ray waves. Using the wave normals connecting points of identical phase for incident and diffracted waves, the distance ( $A+B$ ) could be defined. Because the direction of  $d$  is normal to the planes, and the wave normals are normal to the wavelets, so the angles opposite  $A$  and  $B$  are also  $\theta$ . Thus,  $\sin\theta$  equals  $A/d$  (or  $B/d$ ) so that the distance  $(A+B) = 2 \times d \times \sin\theta$ . On the other hand, this distance must equal a whole number of wavelengths (i.e.  $n \times \lambda_1$ , where  $n$  is integer). Thus, a constructive interference occurs when:

$$n \cdot \lambda = 2 \cdot d \cdot \sin \theta \quad (2-21)$$

This equation is known as the Bragg Law. The integer  $n$  refers to the degree of the diffraction. It means, for instance, that if  $d_{001} = 90 \text{ \AA}$ , then  $d_{002} = 45 \text{ \AA}$ ,  $d_{003} = 30 \text{ \AA}$  etc (Kornmann, 1999).

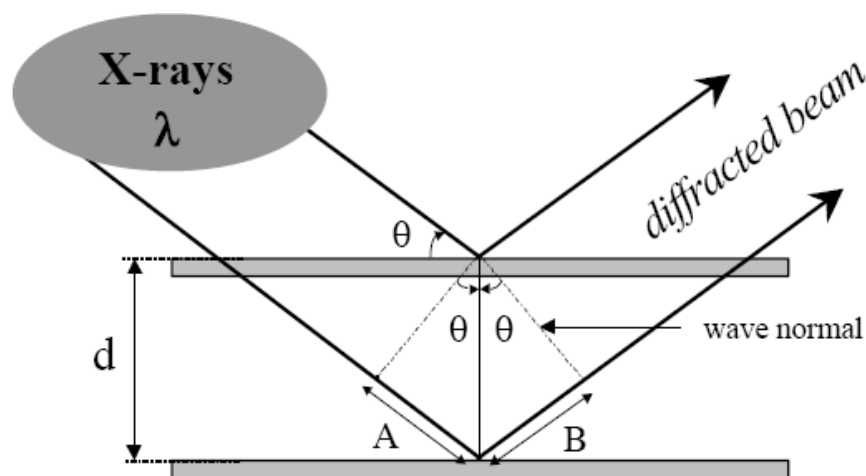


Figure 2-23. Principle of X-ray diffraction (Kornmann, 1999).

Since, nanocomposites generally contain a quite small amount of clay (usually less than 10 wt %), the XRD analysis should be sensitive enough to detect the small portion of the crystalline clay in the polymer. Otherwise, no peaks appear in the diffraction pattern and it might lead to a false interpretation, that a delaminated nanocomposite has been synthesized (Sinha Ray & Okamoto, 2003). It is shown that the XRD patterns of polypropylene nanocomposites can be divided into three main ranges:  $1^\circ$  to  $15^\circ$ ,  $15^\circ$  to  $30^\circ$  and  $30^\circ$  to  $70^\circ$ . No significant diffraction peak is present in the range from  $30^\circ$  to  $70^\circ$  and above. The peaks in the range from  $15^\circ$  to  $30^\circ$

are related to PP and PP-g-MA. The peaks corresponding to the range from  $1^\circ$  to  $15^\circ$  depend on the nano-clay presence in the materials. So, the tests can be performed only in the range from  $1^\circ$  to  $15^\circ$  (Dell'Anno, 2004; Mirzadeh & Kokabi, 2007).

#### **2.6.4.2 Transmission Electron Microscopy**

Transmission electron microscopy as a powerful technique is widely used to study structures at and below the nanometer scale and to confirm results obtained by XRD about the organization of the clay layers in the nanocomposite. Sample preparation is a time consuming step in transmission electron microscopy analysis. To prepare TEM specimens from polymer samples ultramicrotomy is used. Here, a thermally advanced arm moves the sample block toward a diamond knife. The ultrathin specimens are collected on grids and transferred to the TEM column. The intensity of the electron beam should be minimised in order to prevent degradation of the sample. It is known that more electrons are transmitted through the thinner regions or the domains with lower density. Therefore, the clay layers scatter the electron beam more strongly than the polymer and appear darker in the image. This effect is known as the “mass-thickness contrast”(Kornmann, 1999). TEM specimens must be enough thin and in the order of 100 nm, otherwise the contrast between polymer and clay reduces.

#### **2.6.5 Properties of Nanocomposites**

As indicated earlier, nanocomposites consisting of a polymer and layered silicate exhibited improved structural, mechanical, thermal and barrier properties without substantial increase in the density or decrement in the optical properties of the polymer, due to the high aspect ratio of the filler and enough interfacial adhesion between filler and polymer, in comparison to those of neat polymers. The thickness of layered silicate is of the order of 1 nm, whereas their aspect ratios can be very high, typically 100-1500. A proper dispersion of the high modulus nanoparticles into the polymer increases the modulus of nanocomposites (Hambir, Bulakh, & Jog, 2002). Sometimes higher reinforcement effects can be obtained even for the poor separation of the stacked structures. This idea has been supported by Svoboda et al. as well. They suggest that better dispersion does not mean necessarily improved mechanical properties (Peltola, Välipakka, Vuorinen, Syrjälä, & Hanhi, 2006; Svoboda, Zeng, Wang, Lee, & Tomasko, 2002). The co-existence of both colloidal sized aggregates of phyllosilicate clay particles

(tactoids) and well dispersed single layers of clay can be a positive characteristic. In fact, the tactoids act as a nucleating agent in PP. The number of spherulites in a given volume increases and their size decreases, consequently, impact strength increases (Avella, Cosco, della Volpe, & Errico, 2005; D.-Q. Wang, Ma, & Liang, 2005). The mechanical properties of PP nanocomposites increases, when the molecular weight of PP-g-MA, as a compatibilizer, increases (Reichert et al., 2000). No significant improvement in mechanical properties was observed, when the maleic content of PP-g-MA as compatibilizer was lower than 0.7 wt%. Increasing the maleic content above this level, had no more significant effect on the nanoclay dispersion level and on increasing the interlayer spacing of the layered silicates (Hambir, Bulakh, & Jog, 2002; Lertwimolnun & Vergnes, 2005; Y. Wang, Wu, & Wang, 2007). It was shown that polypropylene nanocomposites, prepared using a master-batch, exhibited higher degrees of exfoliation, tensile strength and modulus, in comparison with the direct mixing process (Zhang et al., 2007).

There are many other reports in the literature that confirm such improvements in PP nanocomposites. For the sake of brevity, they are not presented here.

## **2.7 TPV Nanocomposites**

Polymer layered silicate nanocomposites have been extensively investigated and received wide acceptance due to their high performance. Thermoplastic vulcanizates (TPVs) of various types have also gained much attention as promising rubber-like properties and thermoplastic processability. The use of these two complementary technologies together and preparing a TPV nanocomposite generates interesting properties that significantly depend on their nanocomposite structure and their final blend morphology.

Lee and Goettler studied TPV nanocomposites prepared by a commercial TPV with different kinds of clay, without any compatibilizer. They showed that the interlayer distance and the dispersion of the clay in the TPV materials were controlled by the miscibility of the clay and the polymer matrix, as already mentioned in single polymer system (Lee & Goettler, 2004).

Recently, Naderi et al. (Naderi, 2006; Naderi, Lafleur, & Dubois, 2005, , 2007) studied the effects of the nanoclay concentration, the viscosity ratio of PP/EPDM and the dynamic vulcanization on the microstructure and mechanical and thermal properties of the resulting

PP/EPDM TPEs. They prepared several nanocomposites using three polypropylene resins of different melt flow index at several loadings of nanoclay. The prepared nanocomposites were melt-mixed with EPDM in the presence of a sulfuric curing agent to obtain thermoplastic vulcanized nanocomposites (TPV nanocomposites). It was mentioned that partial exfoliation was finally achieved by the shear stress developed during the vulcanization of EPDM, due to the increased viscosity. It was demonstrated that the microstructure of the TPV nanocomposites was sensitive to the viscosity ratio of PP/EPDM and clay content. Almost complete exfoliation and random distribution of clay in the thermoplastic phase was observed. In the TPV nanocomposites prepared with low viscosity polypropylene, they showed that the rubber particles size increased with the introduction of clay. On the other hand, a reduction of the degree of crystallinity and an increase of the polymer crystallization temperature was observed in the exfoliated samples, because the dispersed clay layers acted as nucleating agents (Naderi, Lafleur, & Dubois, 2007). Without compatibilizer, the PP chains were not able to penetrate efficiently between the silicate layers of the clay. However, the degree of exfoliation of the clay increased with introduction of PP-g-MA for both the PP and TPV nanocomposites. The same results were reported by Katbab et al. (Katbab & Mirzazadeh, 2006). In another attempt, they showed that the yield stress of the prepared TPV nanocomposite, based on low viscosity PP, increased more than that for the TPV hybrid prepared by high viscosity PP. TPV nanocomposites containing 20, 40 and 60 % EPDM exhibited strong elastic modulus that tended to reach a plateau at low shear rates.

The effect of phase location of the silicate nanoclay reinforcement, whether it lay in the dispersed rubber phase or in the continuous plastic matrix, was considered by Lee and Goettler (Thakkar, Lee, & Goettler, 2003). Silicate nanoclay was incorporated in the plastic phase and in the rubber phase, selectively. It was found that clay reinforcement in either phase of a TPV tended to make it less deformable. Also, the increase in storage modulus of a reinforced TPV over that of a virgin TPV was quite similar, regardless of whether the clay resided in the plastic phase or the rubber phase. Finally, when the silicate nanoclay was added to the plastic phase, there was an increase in the  $\tan \delta$  value (compared to reinforced-rubber TPVs), indicating a TPV that was more dissipative, more viscous and less elastic. However, when the clay was added to the rubber phase, there was a reduction in the  $\tan \delta$  values, as compared to those of the unfilled TPV, indicating that reinforcement of the rubber phase made the TPV less deformable and less dissipative (Thakkar, Lee, & Goettler, 2003). Using the dynamic mechanical analysis, it was

shown that the glass transition temperature of the thermoplastic phase of TPV nanocomposite increases in comparison to its pristine counterpart, while for the EPDM phase remains constant (Joy K Mishra, 2005). Lee and Goettler (Lee & Goettler, 2004) also showed that the tensile modulus of TPV nanocomposites increased up to 170% while tensile strength gradually decreased with increase of nanoclay loading level.

## **2.8 Summary and Limitations of the Previous Works**

The main highlights of the literature review can be summarized as follows:

1. The TPEs based on PP/EPDM shows the co-continuous structure over a wide composition range. However, there is an argument about the partial miscibility in these blends.
2. The co-continuous composition range is controlled by viscosity ratio, interfacial tension, processing condition and whatever hinders coalescence in polymer blends.
3. It seems that the existing equations for the phase inversion point and the model for the co-continuous range only provide hints about how to produce co-continuous structures in a given blend system.
4. Dynamic vulcanization can be considered as the driving force for phase inversion, i.e., when the morphology changes from a co-continuous type to a dispersed-matrix type or vice versa
5. The realistic breakup mechanism in our case would be the breakup of highly elongated threads to a line of smaller droplets via capillary instabilities.
6. Resole type phenolic crosslinking system is the proper choice to prepare TPVs based on PP/EPDM, because it shows more selectivity, effectiveness and thermally-stable crosslinks in comparison to sulfur or peroxide systems.
7. EPDM with ethylidene norbornene (ENB) as diene monomer is more reactive towards resole cross-linking than EPDM with dicyclopentadiene (DCPD), 1,4-hexadiene (HD) or vinylidene norbornene (VNB)
8. The gamma irradiation crosslinking of PP/EPDM blends is used successfully to fix the rubber morphology for the thermoplastic matrix dissolution during continuity experiments.

9. Different criteria such as solvent swelling, gel content, viscosity, NMR signal line width, bound curative content, residual diene concentration and domain hardness measurements can be used to determine the extent of crosslinking in TPVs.
10. The buckling of the stiff PP lamellae in the equatorial region of the EPDM droplets is the base of the deformation mechanism models in TPVs.
11. It seems that conventional methods used to characterize the elastomeric properties of the single phase rubber are not proper techniques to investigate rubber like behavior in two-phase TPVs. Recoverable strain using a modified hysteresis test and the stress relaxation behavior using a temperature scanning stress relaxation test (TSSR) are more reliable for TPV products.
12. The rheological properties of TPVs can be classified with those of highly filled polymers.
13. Spherical dispersed phase morphology could be expected for the TPEs and TPVs based on EPDM/PP. The presence of a low molecular weight plasticizer has a significant coarsening effect on the morphology development.
14. To make the crosslinking kinetics compatible with the residence times in reactive extrusion process, different strategies such as adjusting the amount of the catalyst and temperature profile should be used, otherwise the processability and the final morphology would change in post processing steps.
15. Dynamic vulcanization in extruders is completely different from that in batch mixers, where melting, mixing and crosslinking are separated in time but the phase inversion takes place at the same gel content in both methods.
16. There is a controversy about the key parameter that controls the compatibilizer (PP-g-MA) effectiveness.
17. The use of PP-g-MA affects the viscosity ratio, interfacial tension, mobility of the interface and the degree of exfoliation. Consequently, the co-continuous composition range changes.
18. PP nanocomposites present a greater shear thinning tendency than pristine polypropylene at high shear rates, as a result of the orientation of the silicate layers.
19. The microstructure of TPV nanocomposites is sensitive to the viscosity ratio of PP and EPDM.

20. The TPV nanocomposites show higher elastic modulus compared with similar but unfilled TPV sample despite the lower degree of crystallization.
21. The mechanical properties of TPV nanocomposites strongly depend on the structure and morphology, which can be tailored by phase partitioning of the nanoclay.

According to the available literature, in spite of a number of valuable studies, in the field of TPV nanocomposites, one can categorize the limitations of the previous works to the three main groups;

The first one is related to the unanswered questions about the compatibilizer's efficiency to form a nanocomposite.

On the other hand, how do the presence of nanoclay and its dispersion level affect the co-continuity in nonreactive blends?

And since most of the studies in this field investigate the effect of the nanoclay on non reactive TPVs (adding the nanoclay to the commercially available grades of TPVs) or in reactive blends inside the internal batch mixer and not in a reactive extrusion process, the effect of nanoclay presence and different dispersion level on crosslinking reaction in a continuous production and consequently their rubber like behaviour is still unclear.

### Chapter 3 ORGANIZATION OF THE ARTICLES

To tackle the interesting and worthwhile subject of the present dissertation, the first article presented in chapter 4 provides scientific and technical information regarding the compatibilizer optimization, the formation of the nanocomposite, the morphology and co-continuity of nonreactive blends in the presence of nanoclay with different dispersion levels. It is entitled “The effect of compatibilizer on the co-continuity and nanoclay dispersion level of TPE nanocomposites based on PP/EPDM”. In this study, four different PP-g-MA as compatibilizers were first studied and used to prepare PP nanocomposite with different dispersion level. The prepared nanocomposites were used as the thermoplastic phase in the PP/EPDM based TPE nanocomposites. For a comprehensive approach towards the aforementioned objectives, different techniques such as thermogravimetric analysis, differential scanning calorimetry, X-ray diffraction, transmission electron microscopy, gamma irradiation, solvent extraction and gravimetry, scanning electron microscopy and rheological characterization were used. This paper was published in Polymer Engineering & Science.

To have a better insight about the reactive extrusion of TPV nanocomposites, in light of theoretical, quantitative principles and the previous part, “The effects of nanoclay dispersion levels and processing parameters on the dynamic vulcanization of TPV nanocomposites based on PP/EPDM prepared by reactive extrusion” are investigated in the second article, which is presented in chapter 5. In this part, the rubber phase was dynamically vulcanized using both the reactive extrusion process and in internal batch mixer by dimethylol phenolic resin along with stannous chloride dihydrate as the catalyst. The resulting TPVs were characterized to evaluate the extent of the crosslinking reaction using different criteria such as gel content, viscosity and storage modulus, NMR signal line width, bound curative content and residual diene concentration. In the second article, we attempt to find if the extent of crosslinking correlates with the continuity index of the EPDM in precursor TPEs or not. This work has been accepted for publication in Polymer Engineering & Science and is now in press.

“Morphology evolution and thermo mechanical characteristics of TPV nanocomposites based on PP/EPDM prepared by reactive extrusion” is the title of the third and the last paper which is presented in chapter 6. This paper deals with the morphology development along the screw axis and its correlation with the rubber like behaviour of the prepared blends. For this

purpose, to observe the morphology of the prepared TPVs and TPV nanocomposites, samples taken along the screw axis were quenched in liquid nitrogen and then embedded, microtomed and etched using the vapor of boiling xylene. On the other hand, a recently developed method named temperature scanning stress relaxation (TSSR) as one of the most important analysis techniques with respect to the TPVs applications especially at elevated temperatures, was employed. Furthermore, tensile properties of the TPVs and TPV nanocomposites were compared. In this paper we attempt to realize whether it is worth adding the nanoclay to these reactive blends. This paper has been submitted to Rubber Chemistry & Technology and is currently under review.

Chapter 4 **THE EFFECT OF COMPATIBILIZER ON THE CO-  
CONTINUITY AND NANOCLAY DISPERSION LEVEL OF TPE  
NANOCOMPOSITES BASED ON PP/EPDM**

Amin Mirzadeh, Pierre G. Lafleur, Musa R. Kamal\* and Charles Dubois

Chemical Engineering Department, Ecole Polytechnique, PO Box 6079, Stn Centre- Ville,  
Montreal, QC H3C 3A7, Canada

\* Chemical Engineering Department, McGill University, 3610 University, Montreal, QC H3A  
2B2

## 4.1 Abstract

The effects of different polypropylene-g-maleic anhydride (PP-g-MA) polymers, used as compatibilizers, on the degree of exfoliation and co-continuity of polypropylene (PP)/ethylene-propylene-diene terpolymer (EPDM) thermoplastic elastomer (TPE) nanocomposites were investigated. X-ray diffraction and transmission electron microscopic micrographs showed that nanocomposites ranged from intercalated structure to a coexistence of intercalated tactoids and exfoliated layers. The observed significant increase in crystallization temperature ( $\sim 20^{\circ}\text{C}$ ) could be beneficial for molding applications, because it means faster solidification and shorter cycle time. The rheological characteristic relaxation time of the compatibilizer correlated with the dispersion level in the nanocomposites. Solvent extraction and gravimetry measurements of continuity showed that compatibilizer affects the co-continuity composition range through its effect on the dispersion level of nanoclays. At high EPDM concentration, the continuity of the thermoplastic phase for semi-exfoliated TPE nanocomposites was higher than in the corresponding TPEs. Considering that TPE formation is the first step for thermoplastic vulcanizate production, where the thermoplastic phase should have a certain level of continuity, these results suggest that higher levels of EPDM could be incorporated into the semi-exfoliated system before losing matrix continuity. It was also observed that there is a direct relation between the magnitude of the normalized stress growth viscosity overshoot and the continuity of TPE nanocomposites.

**Keywords:** Thermoplastic elastomer, Nanocomposites, co-continuity, morphology, rheology.

## 4.2 Introduction

Polypropylene (PP) layered silicate nanocomposites have received much attention due to their high performance [1–3]. The use of a compatibilizer has made it easier to produce such nanocomposites by melt intercalation [4–8]. Maleic anhydride-grafted PP (PP-g-MA) has been used extensively as a compatibilizer in the preparation of PP/clay nanocomposites, with significant improvements in structure and mechanical properties. However, there is still need to identify one or more compatibilizer properties that could serve as good predictor(s) of the compatibilizer effectiveness. For example, studies showed that intercalation of the polymer did not occur, when the content of MA in the PP-g-MA polymer was low (acid value = 7 mg KOH/g for  $M_w = 12,000$ ) [3, 7]. It was also shown that intercalation was enhanced, when the PP-g-MA content was increased until it reached an intermediate level (acid value = 26 mg KOH/g,  $M_w = 40,000$ ). Further increase in the acid value (e.g., acid value = 52 mg KOH/g) had no further influence on the increase of d-spacing of the layered silicate. The evaluation of the effects of three levels of molecular weight (low, medium, and high) of PP-g-MA on the morphology and the mechanical properties of PP nanocomposites revealed that the nanocomposites incorporating the highest PP-g-MA molecular weight ( $M_w = 330,000$ , MA = 0.5 wt%) yielded the best overall mechanical properties [9]. In another study, it was reported that the degree of the intercalation and the uniformity of clay dispersion were affected by both molecular weight and the MA content [10]. The present work investigates the effects of different PP-g-MA compatibilizers on the degree of exfoliation and co-continuity of thermoplastic elastomer (TPE) nanocomposites based on PP/ethylene-propylene-diene terpolymer (EPDM).

According to the classical point of view, an ideally co-continuous structure is defined as the coexistence of at least two continuous structures within the same volume. This implies that three-dimensional spatial continuity, at some finite scale of mixing, could be found for both components [11]. Other definitions to describe co-continuous structures refer to structures with dual-phase continuity, co-phase continuity, interpenetrating polymer networks (IPNs), IPNs of phases, interpenetrating co-continuous phase structure or interpenetrating polymer blends [11–14]. Lyngaae-Jorgensen et al. [15] suggested a definition based on the percolation threshold theory that considers different structure types allowing some part of the components to be present in separate domains that are not part of the network structure. Therefore, a co-continuous

structure is described as one wherein at least a part of each phase forms a coherent continuous structure permeating the whole volume [11]. Thus, as the amount of the minor component in the blend is increased, the percolation structure is reached, suggesting a fully co-continuous structure. The percolation-based definition has been used in the present study to determine the continuity index. Thus, the continuity index, continuity fraction or the degree of co-continuity is defined as the fraction of a component that is part of the percolating structure [11, 12, 15]. The classical and percolation definitions become equivalent when the continuity index is equal to one for both phases.

One of the important mechanisms of droplet formation during blending involves the breakup of highly elongated threads via capillary instabilities, leading to a sequence of adjacent smaller droplets. The breakup occurs after the thread diameter reaches a size for which the capillary number,  $Ca$ , becomes  $<1$ , and if the residence time during the mixing process is longer than the break-up time [11]. The break-up time,  $t_b$ , is given by:

$$t_b = \left( \frac{\eta_m B}{\Omega(l, \lambda) \sigma} \right) \ln \left( \frac{0.8B}{2\alpha_0} \right) \quad (4-1)$$

where  $\alpha_0$  is the amplitude of the initial distortion, and  $\Omega(l, \lambda)$  is the Tomokita function which is a dimensionless distortion growth rate, depending on the distortion wavelength ( $l$ ) and the viscosity ratio ( $\lambda$ ). The diameter of the elongated thread  $B$  depends on the total amount of strain, as follows: (Eq. 4.2).

$$B = 2R_0(1 + \gamma^2)^{-\frac{1}{4}} \quad (4-2)$$

where  $\gamma$  is strain and  $R_0$  is the starting radius of a spherical particle. The above suggests that the viscosity ratio, interfacial tension, and processing conditions are factors that influence co-continuity.

Bhadane et al. [16] evaluated a variety of PP/EPDM blends with viscosity ratios in the range 0.2–5.0. The blends were prepared at shear stresses of 11.7–231.4 kPa. They showed that, at low blend compositions, the dispersed phase appeared as stable fibers with small diameters in the range of 50–200 nm. Continuity was established by fiber–fiber coalescence. They also reported that a sevenfold variation in the viscosity ratio had virtually no influence on the

continuity index or morphology. In fact, they obtained a single continuity master curve for PP/EPDM blends at these conditions.

Another important parameter that influences co-continuous structure is interfacial tension. The effect of interfacial tension on the co-continuity range was studied by Willemse et al. [17]. They chose different pairs of polymers having different interfacial tension values but the same viscosity ratio. They found that, in systems with higher interfacial tension, the onset volume fraction of co-continuity was higher and the co-continuity range was narrower, compared to systems with low interfacial tension. This behavior was similar for both high viscosity ratio and low viscosity ratio systems.

The present study deals with the preparation of nanocomposites based on TPE and clay. Such systems are of interest, because of their rubber-like behavior and high performance [18–21]. As nanocomposite formation usually involves the use of PP-g-MA as a compatibilizer, the molecular weight of the compatibilizer will affect the viscosity ratio and ultimately the degree of intercalation or exfoliation. Moreover, the above two parameters can affect the co-continuity composition range. The latter is quite important, because TPE formation is usually the first step of thermoplastic vulcanizates (TPV) production, and a prerequisite condition for TPV formation is thermoplastic phase continuity.

## 4.3 Experimental

### 4.3.1 Materials

“Profax” 6523 (Basell Polyolefins) general purpose PP homopolymer resin, with a melt flow index (MFI) of four (g/10 min), was used as the thermoplastic phase. “Buna” EP T 6470 (LANXESS) EPDM, with ethylidene norbornene, showing a diene of 3.9–5.1% and a Mooney viscosity of 52–62 M, was used as the rubber phase. Cloisite 15A (Southern Clay Products), which is a surface modified Montmorillonite (MMT) with di-methyl, di-hydrogenated tallow ammonium chloride, was used as the nanoclay.

Four grades of PP-g-MA with different MFI values, Orevac 18729, 18732, 18750, CA 100 (Arkema), were used as compatibilizers. Functionality of PP-g-MA for all of the above compatibilizers is in the medium range. They were sorted and designated by numbers in

ascending order of their MFI. Table 4.1 shows the information available about their properties. Irganox B 225 (Ciba) primary phenolic type was used as the antioxidant. Also, xylene and cyclohexane (Laboratoire Mat, 99% purity) were used as solvents in extraction experiments.

Table 4-1. Properties of Compatibilizers

Physical	18729 (1)	18732 (2)	CA100 (3)	18750 (4)	Test Method
Density (g/cm <sup>3</sup> )	0.900	0.890	0.900	0.920	ISO 1183
Melt Mass Flow Rate (MFR) (g/10 min)	4.5	8.0	10	35	ISO 1133
Tensile Strength @ Break (MPa)	41	20	22	21	ASTM D638
Tensile Elongation @ Break (%)	620	500	500	500	ASTM D638
Vicat softening Temperature (°C)	137	120	147	121	ISO 306
Melting Point (°C)	162	134	167	160	DSC

## 4.3.2 Blend Preparation and Nomenclature

### 4.3.2.1 Masterbatch Preparation

Four masterbatches (MBs) consisting of PP/PP-g-MA/Cloisite15A in the ratios (60/30/10 wt%) were prepared. Each MB contained one of the four PP-g-MA compatibilizers. The different MBs were designated MB<sub>*i*</sub>, where *i* = 1–4 refers to the corresponding compatibilizer used in the formulation. The MBs were melt-compounded in a laboratory scale co-rotating, closely intermeshing, twin-screw extruder (Leistritz ZSE-18HP). The temperature distribution in the extruder was maintained at 185, 190, 190, 190, 195, 195, 195, and 190°C from the hopper to the die, and the screw rotation speed was fixed at 200 rpm Cloisite was fed to the extruder through the side feeder, at a location where the granules were already partially melted.

### 4.3.2.2 Nanocomposite Preparation

To prepare PP nanocomposites with 5 wt% of Cloisite 15A, the pellets of the MB were mixed with the PP, using the twin screw extruder. For this operation, the temperature profile in the extruder was 175, 180, 185, 190, 190, and 185°C from the hopper to the die. The screw speed was held at 600 rpm. A small amount (0.5 wt%) of Irganox B 225 antioxidant was added to the mixture to reduce the oxidative degradation of PP. PP nanocomposites were designated as Nx, where x refers to the compatibilizer used in the nanocomposite.

### 4.3.2.3 TPE Nanocomposites Preparation

TPE nanocomposites were prepared using a Brabender (internal mixer) at 100 rpm and 200°C. The mixing volume was 30 ml. The compositions of the blends and related nomenclature are given in Table 4.2. TPE nanocomposites were designated as TPENx.yy, where x and yy indicate the corresponding compatibilizer and EPDM weight percent, respectively.

Table 4-2. Nomenclature of TPE nanocomposites based on their compositions.

Chapter 5 EPDM/N1 (wt%)	50/50	TPEN1.50
	60/40	TPEN1.60
	70/30	TPEN1.70
EPDM/N2 (wt%)	50/50	TPEN2.50
	60/40	TPEN2.60
	70/30	TPEN2.70
EPDM/N3 (wt%)	50/50	TPEN3.50
	60/40	TPEN3.60
	70/30	TPEN3.70
EPDM/N4 (wt%)	50/50	TPEN4.50
	60/40	TPEN4.60
	70/30	TPEN4.70

## 5.1.1 Characterization Steps

### 5.1.1.1 Thermogravimetric Analysis

Thermogravimetric analysis (TGA Q500 V6.5 Build 196, TA instruments) was performed to determine the amount of di-methyl, di-hydrogenated tallow ammonium chloride in Cloisite 15A and the level of nanoclay in MBs and nanocomposites, as well as decomposition temperatures. The samples were heated from 30°C to 600°C at a rate of 15°C/min.

### 5.1.1.2 Differential Scanning Calorimetry

Differential scanning calorimetry (DSC Q1000 V9.6 Build 290, TA instruments) tests were carried out to study the crystallinity and the possible nucleating effect of nanoclays. The samples were first heated from 30°C to 210°C at a rate of 10°C/min and were kept at 210°C for 5 min to erase prior thermal and mechanical history. The samples were then cooled from 210°C to 30°C at a rate of 10°C/min. The peak and onset crystallization temperatures were determined from the cooling scans. All measurements were performed in nitrogen atmosphere.

### 5.1.1.3 X-ray Diffraction

To evaluate the dispersion of nanoclay in the MBs, nanocomposites and TPE nanocomposites, X-ray diffraction (XRD) was carried out at room temperature using an X-ray diffractometer (Philips model X'PER) in the low angle range of  $2\theta$ . The X-ray source was Cu- $K_{\alpha}$  radiation ( $\lambda = 1.540598 \text{ \AA}$ ), using a 50 kV voltage generator and a 40 mA current. The basal spacing of silicates was estimated from the position of the plane peak in the Wide Angle X-ray Diffraction (WAXD) intensity profile using Bragg's law. The angular step size was  $0.005^{\circ}$  with a step time equal to 1 s from  $2^{\circ}$  to  $10^{\circ}$  and  $0.5^{\circ}$  to  $4^{\circ}$ .

### 5.1.1.4 Electron Microscopy

Nanoclay dispersion in the thermoplastic phase and morphology of the TPEs were studied using scanning electron microscopy (SEM) and transmission electron microscopy (TEM). For SEM, irradiated samples were first microtomed using a glass knife under liquid nitrogen. The instrument was a Leica-Jung RM 2065 equipped with a cryochamber. Subsequently, the samples were etched with xylene vapor for 10 (s) and coated with gold-palladium alloy. SEM micrographs were obtained using a scanning electron microscope (JSM 840, Jeol) operated at a

voltage of 15 kV. To calculate the number average diameter ( $D_n$ ) and the volume average diameter ( $D_v$ ), the SEM micrographs were analyzed using a digitizing table and user-defined transformer file [22]. To observe nanoclay dispersion, the amorphous phase of PP was removed. Further details regarding this technique have been explained elsewhere [23].

For TEM, PP nanocomposites were first trimmed to obtain a truncated pyramid section with a razor blade, to avoid the high pressure on the diamond knife. Then, they were ultramicrotomed at  $-130^\circ\text{C}$  using a diamond knife to prepare samples with thickness of 50 nm. A water bath was used to transfer the micro-thin sections to 200-mesh copper grids. Micrographs were taken with a TEM (JEM-2100F, Jeol) and recorded with a digital camera.

#### 5.1.1.5 Solvent Extraction and Gravimetry for Continuity

This technique was used to estimate the continuity of EPDM in TPE nanocomposite samples. Because surface area to volume ratio could affect the results, three samples of approximately  $8 \times 8 \times 1.4 \text{ mm}^3$  were prepared from each of the noncrosslinked blends.

The specimens were immersed in 35 ml of fresh cyclohexane solvent in a centrifuge tube for 3 days at room temperature, while they were shaken constantly. Then, the sample was dried in a vacuum oven at  $60^\circ\text{C}$ . This process was repeated consecutively at least three times, until the sample weight remained unchanged.

To estimate the continuity index of PP in the various systems, gamma irradiation was carried out in air with  $^{27}\text{Co}$  source, to fix the EPDM morphology. In this regard, TPE blends, together with the pure materials were irradiated with a dose rate of 20 kGy/h for 8 h, using commercial carrier-type 8900 irradiator. Further details regarding this technique have been described elsewhere [16, 24]. The irradiated blends were cut into the same size. These samples were immersed in 100 ml of boiling xylene for an hour and dried. The well-dried samples were subjected to the same procedure till the complete phase removal was confirmed by comparing the sample weight after consecutive drying steps. The ratio between the extracted mass of a specific phase and its total content, based on a defined cube, is the continuity index,  $i$ , calculated as follows:

$$\phi_i = \frac{W_{1i} - W_{2i}}{W_{1i}}$$

(4-3)

where  $W_{1i}$  and  $W_{2i}$  represent the weights of component  $i$  before and after extraction, respectively.

### 5.1.1.6 Rheological Measurements

Rheological measurements were carried out using a parallel plate rheometer, ARES (Rheometrics Scientific) with 25-mm diameter parallel disc geometry at 200°C. In all cases, the linearity of the sample response with respect to stress amplitude was verified. Nitrogen gas was used to prevent thermal oxidation of the materials.

## 5.2 Results and Discussion

### 5.2.1 Thermogravimetry

TGA was used to estimate the actual amounts of Cloisite 15A in the MBs and in PP nanocomposites, and to evaluate the thermal degradation characteristics of the modifier. Figure 4.1 shows that the modifier started to decompose at about 240°C, which is higher than the maximum processing temperature. Since about 43 wt% of Cloisite 15A is attributable to the modifier, the average nanoclay content was calculated based on the TGA analysis of the prepared MBs (Table 4.3). The observed differences are reasonable, considering the use of the side feeder in the extrusion process. These averages were used to calculate the PP weight that should be added to each MB to prepare PP nanocomposites with 5 wt% Cloisite 15A. Table 4.3 shows that the amount of nanoclay in these samples is in the acceptable range.

Table 4-3. Nanoclay content for the masterbatches and nanocomposites obtained by TGA

Sample name	MB1	N1	MB2	N2	MB3	N3	MB4	N4
Cloisite 15A content (wt%)	10.3	4.8	10.1	4.9	9.5	4.7	9.7	4.7
STDV	2.4	0.1	0.7	0.1	1.5	0.1	0.4	0.1

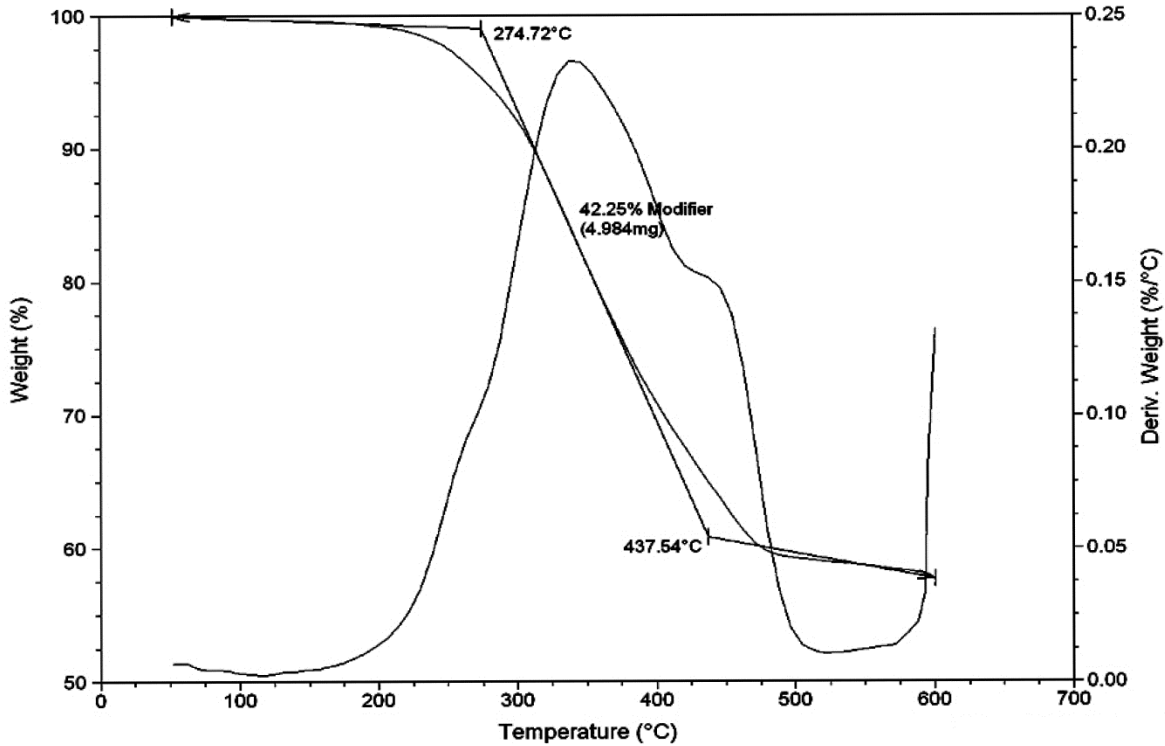


Figure 4-1. Thermo-gravimetric analysis of Cloisite 15A.

## 5.2.2 Differential Scanning Calorimetry and Crystallinity.

Differential scanning calorimetry was used to evaluate the thermal behavior of PP and PP/clay nanocomposite specimens and to estimate the percentage of crystalline phase in the samples. It has been reported that the clay particles act as nucleating agents for the crystallization of PP and that they cause an increase of PP crystallinity [25].

The percent of crystallinity was determined as follows (Eq. 4.4):

$$\chi = \frac{\Delta H_m}{f_p \Delta H_f^\circ} \quad (4-4)$$

where  $\Delta H_m$  (J/g) is the latent heat of fusion of the nanocomposite measured by DSC,  $f_p$  is the PP weight fraction in the nanocomposite, and  $\Delta H_f^\circ$  is the theoretical latent heat of fusion of a pure crystalline PP, namely 207 J/g [26]. Table 4.4 shows that nanocomposite crystallinity increased about 10% compared to pure polypropylene. On the other hand, the significant increase in

crystallization temperature ( $\sim 20$  °C) could be beneficial for molding applications, because of the faster solidification and shorter cycle time.

Table 4-4. Percent of crystallinity and crystallization temperature

Material name	Crystallinity (%)	Crystallization. Temp.
PP	34	112 (°C)
N1	41	130 (°C)
N2	42	132 (°C)
N3	41	117 (°C)
N4	44	118 (°C)

### 5.2.3 Clay Dispersion in PP and TPE Nanocomposite.

X-ray diffraction analysis was performed on Cloisite 15A, PP nanocomposites, and TPE nanocomposites. Figure 4.2a shows the results for Cloisite 15A. There are three peaks in the range of  $2^\circ$  to  $10^\circ$ . The first peak is related to the basal spacing ( $d_{001}$ ) of Cloisite 15A which appears at  $2\theta = 2.85^\circ$  (corresponding d-spacing is 3.1 nm). The second characteristic peak of the clay is observed as a shoulder in the vicinity of the first one at  $2\theta = 4.6^\circ$  (corresponding d-spacing is 1.9 nm) and the last peak for Cloisite 15A appears at  $2\theta = 7.17^\circ$  (corresponding d-spacing is 1.1 nm) which can be attributed to the portion of the clay that is not properly modified.

The results shown in Fig. 4.2 demonstrate that the degree of intercalation depends on the compatibilizer. The XRD pattern for N4 shows that the three peaks of Cloisite 15A (Fig. 4.2b), are shifted to lower angles corresponding to a change in d-spacing from 3.1 to 3.8 nm. The higher basal spacing of clay in comparison with the virgin Cloisite 15A suggests intercalation by the polymer chains.

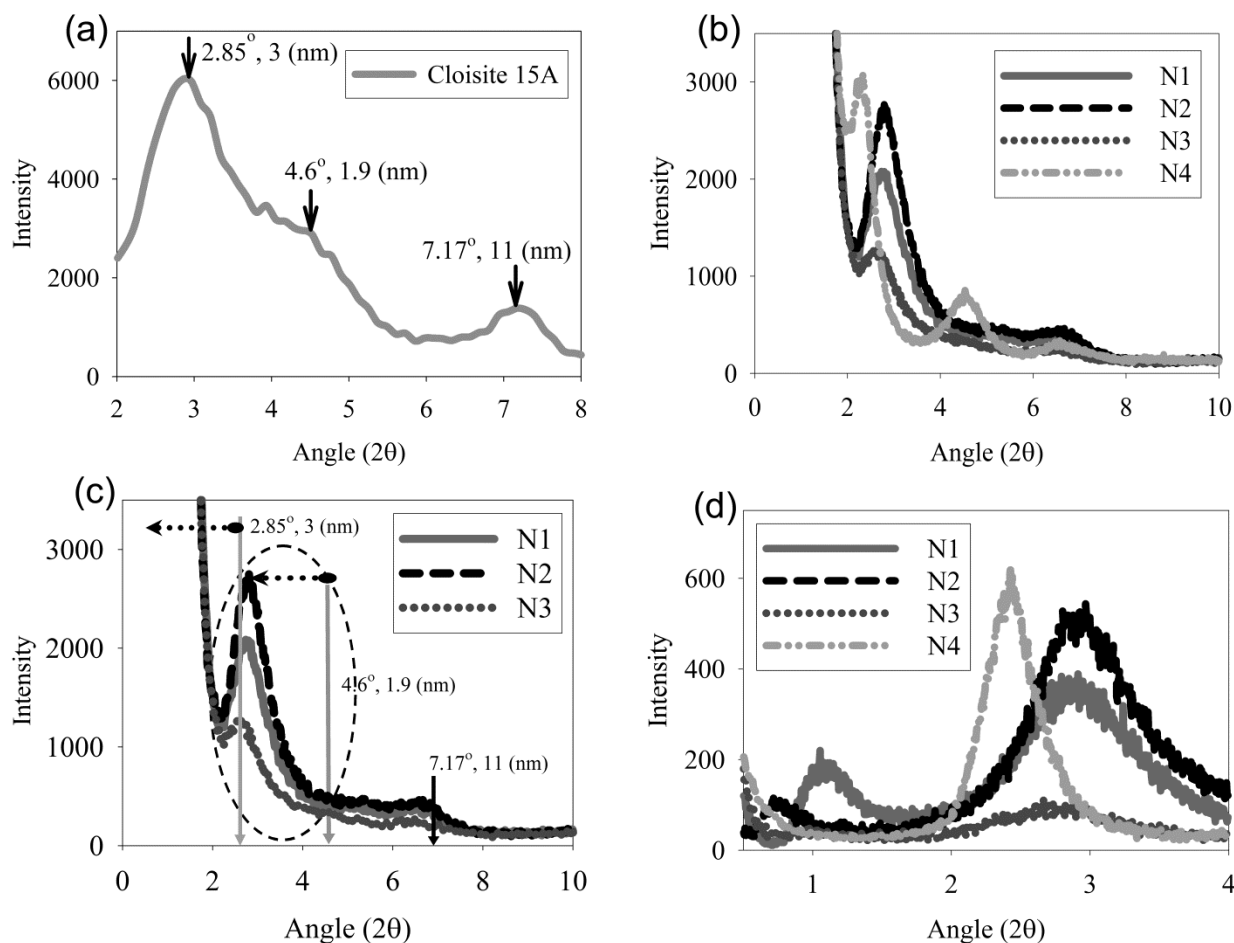


Figure 4-2. XRD patterns of Cloisite 15A and nanocomposites at different scan range.

The XRD patterns of N1, N2, and N3 nanocomposites show only two peaks in the range of  $2^\circ$  to  $10^\circ$  (Fig. 4.2c). The first observed peak at  $2\theta \cong 2.64^\circ$  corresponds to d-spacing of about 3.3 nm and the second peak is at  $2\theta \cong 6.5^\circ$ . It is likely that these two peaks are related to the second and third peaks of Cloisite 15A at  $2\theta \cong 4.6^\circ$  and  $2\theta \cong 7^\circ$ , respectively. All of the peaks of Cloisite 15A, with positions indicated by arrows in Fig. 4.2c, were shifted to lower angles. The first characteristic peak of Cloisite 15A at  $2\theta = 2.85^\circ$ , was shifted to angles below  $2\theta \cong 2^\circ$ . However, because of the high intensity of the X-ray beam in this range, the detector could not detect this small portion of montmorillonite (MMT) layers.

To overcome the above problem and reduce the X-ray beam intensity in the range of  $2\theta \cong 0.5^\circ$  to  $2^\circ$ , a thin steel knife and cylindrical base were used as a sample holder to prevent edge effect. The setup adjusted in a manner that the upper surface of the sample touched the edge of

the knife entirely. Also, great care was taken to align the edge of the knife with the X-ray generator and detector. This setup is a simplified model of the system used by Dell'Anno [26] to obtain data at smaller angles using the WAXD technique. After optimization of sample thickness, slit size, frame size, starting angle and scan rate to obtain reproducible data, X-ray scans were performed in the range of  $2\theta = 0.5^\circ$  to  $2\theta = 4^\circ$ .

It is suggested that the peaks observed in Fig. 4.2d in the range of  $2\theta = 0.5^\circ$  to  $2\theta = 2^\circ$  are attributed to the intercalation of polymer chains in Cloisite 15A, into galleries with the original d-spacing of about 3.1 nm (at  $2\theta \cong 2.8^\circ$ ). This peak is absent in pure PP and N4 nanocomposite. The above XRD analyses suggest a coexistence of intercalated MMT tactoids and exfoliated MMT layers in N1, N2, and N3 nanocomposites.

TEM images shown in Fig. 4.3 confirm the existence of intercalated dispersed tactoids containing small numbers of clay layers. These tactoids are well dispersed and separated from each other. The observed “semi-exfoliated” structure tends to confirm the XRD results.

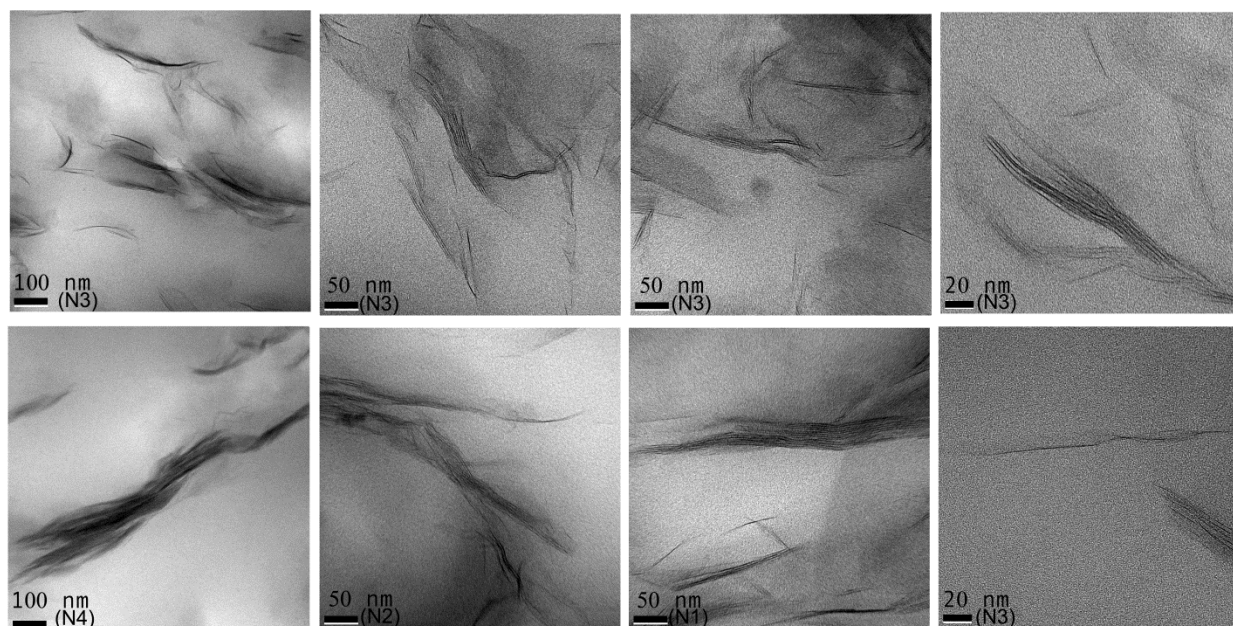


Figure 4-3. TEM micrographs of PP nanocomposites.

The quality and uniformity of dispersion of nanoclay were investigated by SEM. The amorphous phase of PP was removed chemically from the microtomed surface. Thus, the nanoclays could be observed by SEM. Figure 4.4 shows that the agglomerates were uniformly

dispersed in the matrix with no large particles, reflecting good mixing quality. Examination of micrographs at higher magnification suggested that nanoclay dispersion quality in N3 nanocomposite was better than that in N2 and N1. Tactoids observed in N2 and N1 were longer than those in N4, possibly due to slippage of MMT layers over each other, due to the higher intercalation of polymer chains.

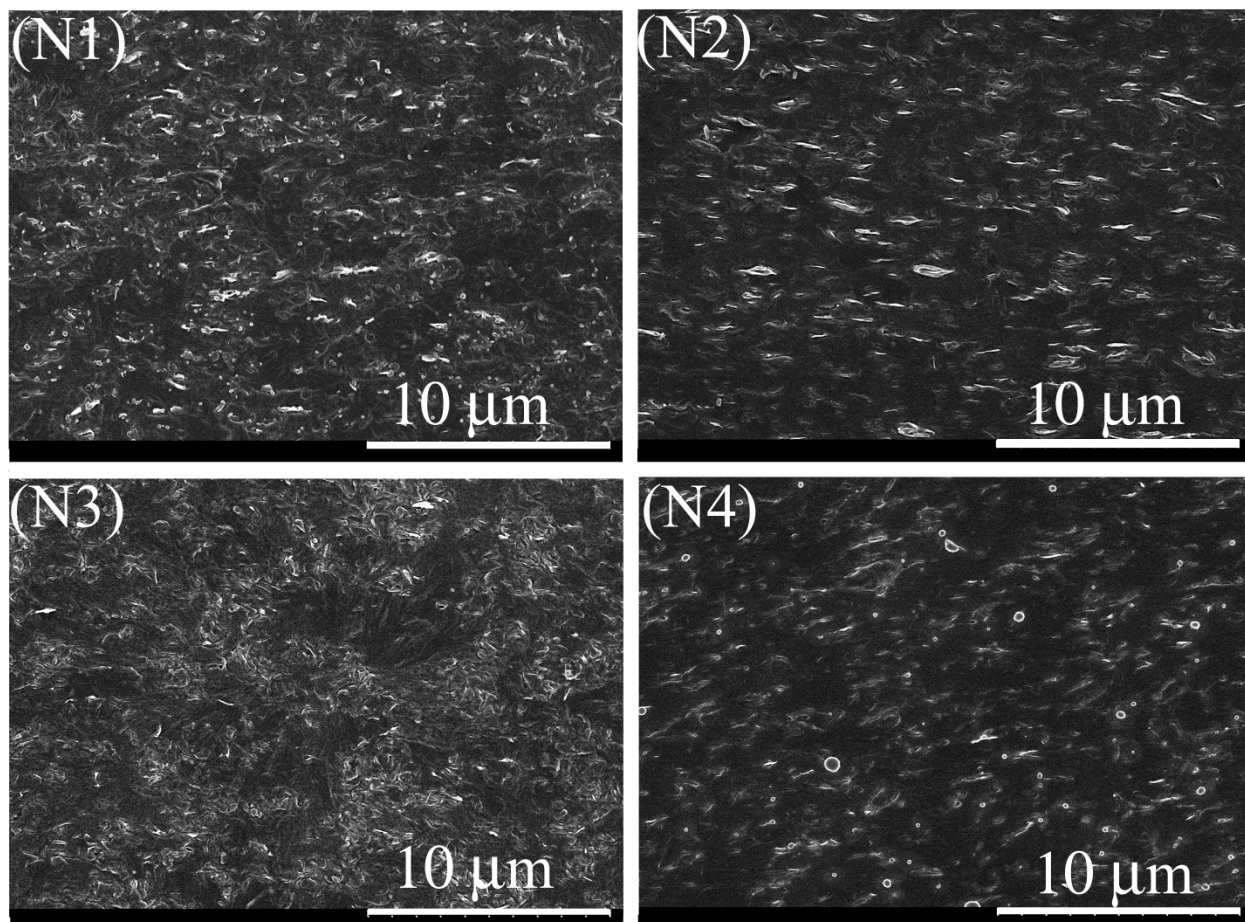


Figure 4-4. SEM images of PP Nanocomposites after removing the amorphous phase.

According to the XRD analysis of TPEs (see Fig. 4.5), it seems that the higher shear stress, as a result of the incorporation of EPDM into the system, did not enhance polymer intercalation significantly.

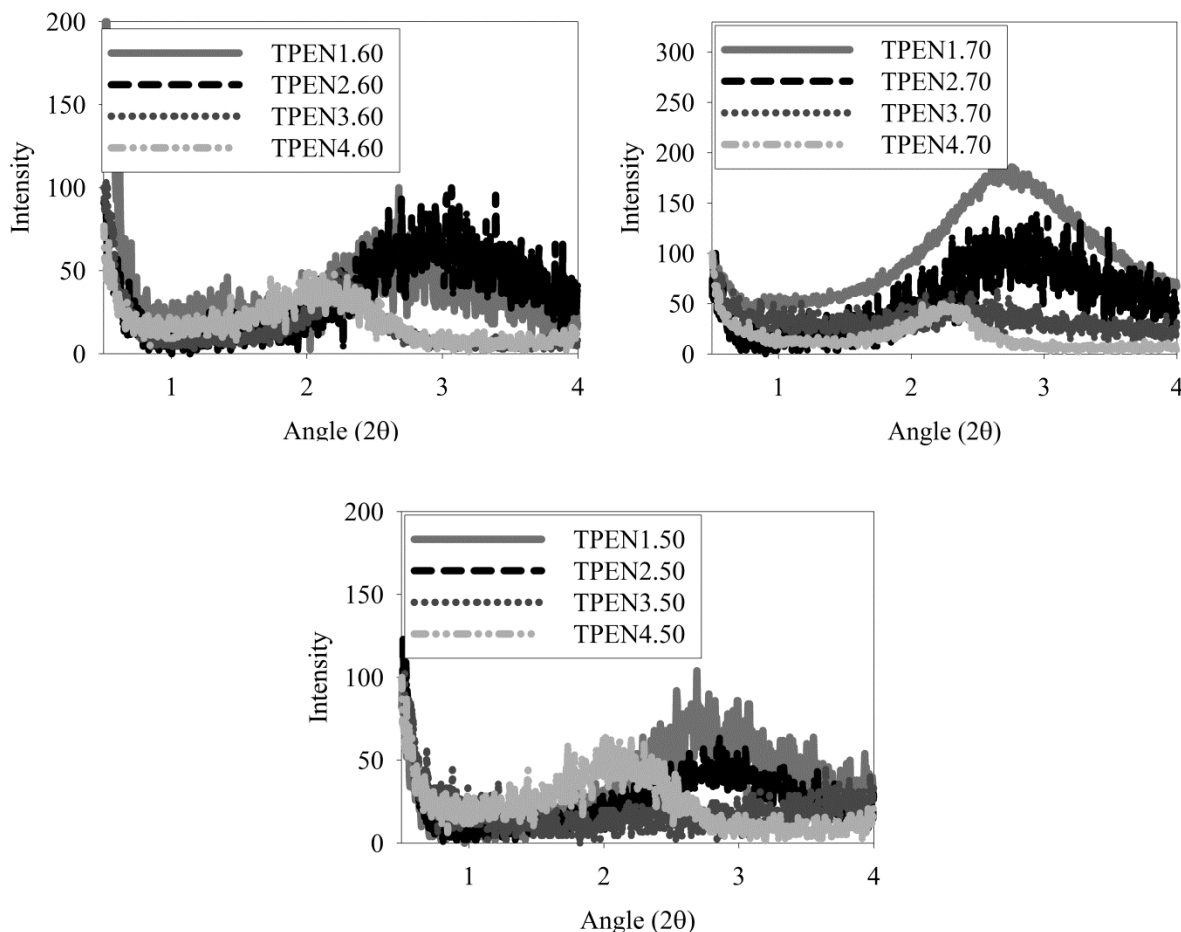


Figure 4-5. XRD patterns of TPE nanocomposites at different EPDM content.

## 5.2.4 Correlation between Rheological Behavior of PP-g-MA and Nanoclay Dispersion

### 5.2.4.1 Thermal Stability of PP-g-MA During Rheological Tests.

To assess the thermal stability of the samples, a time sweep was carried out in the ARES device at 6.285 rad/s over 1 h at 200°C (processing temperature). Measurements were made under nitrogen atmosphere to reduce degradation risk. Table 4.5 shows the maximum changes in complex viscosity and storage modulus of the neat polymers. The change in the above properties of the compatibilizers was more pronounced than for PP and EPDM. This may be attributed to residual chemicals from MA grafting reaction. As all rheological measurements in this study were completed in <1 h, it is safe to assume that no degradation occurred during processing.

Table 4-5 . Change in storage modulus and complex viscosity after one hour at 200 °C.

Materials	Variation in storage modulus	Variation in Complex viscosity
PP	5%	4%
EPDM	5%	3%
Compatibilizer # (1)	7%	5%
Compatibilizer # (2)	7%	5%
Compatibilizer # (3)	10%	7%
Compatibilizer # (4)	8%	7%

#### 5.2.4.2 Determination of Linear Zones in Rheological Tests

To ensure that oscillatory shear measurements are conducted within the linear regime, stress sweep experiments were performed, using a parallel plate rheometer (ARES from Rheometrics Scientific) with parallel disc geometry of 25 mm diameter and 1.1 mm gap. Experiments were repeated at three frequencies. Theoretically, the stress limit at low frequency should also apply at high frequency. However, sometimes, as in the present case, this value is so small in the high frequency range that it limits the precision of data. Therefore, frequency sweep experiments were carried out following several sequences, as shown in Table 4.6. In this way, both linearity and accuracy of measurement were taken into account.

Table 4-6. Stress values at three sequences for frequency sweep tests

Frequency (rad/s)	0.628-6.28	6.28-62.8	62.8-628
Stress (Pa) for compatibilizers	20	100	400
Stress (Pa) for nanocomposites	50	500	1000

### 5.2.4.3 Correlation between Compatibilizer Viscosity and Clay Dispersion

Dynamic measurements were performed using parallel plate geometry to determine material functions of the pure compatibilizers. At least four experiments were carried out for each material. Figure 4.6 shows the complex viscosities of the four compatibilizers. It is clear that there is no evidence of a Newtonian-plateau at low frequencies. Within the experimental window employed, the complex viscosity of the compatibilizer with 35 MFI (No. 4) is higher than the complex viscosity of the compatibilizer with 10 MFI of (No. 3).

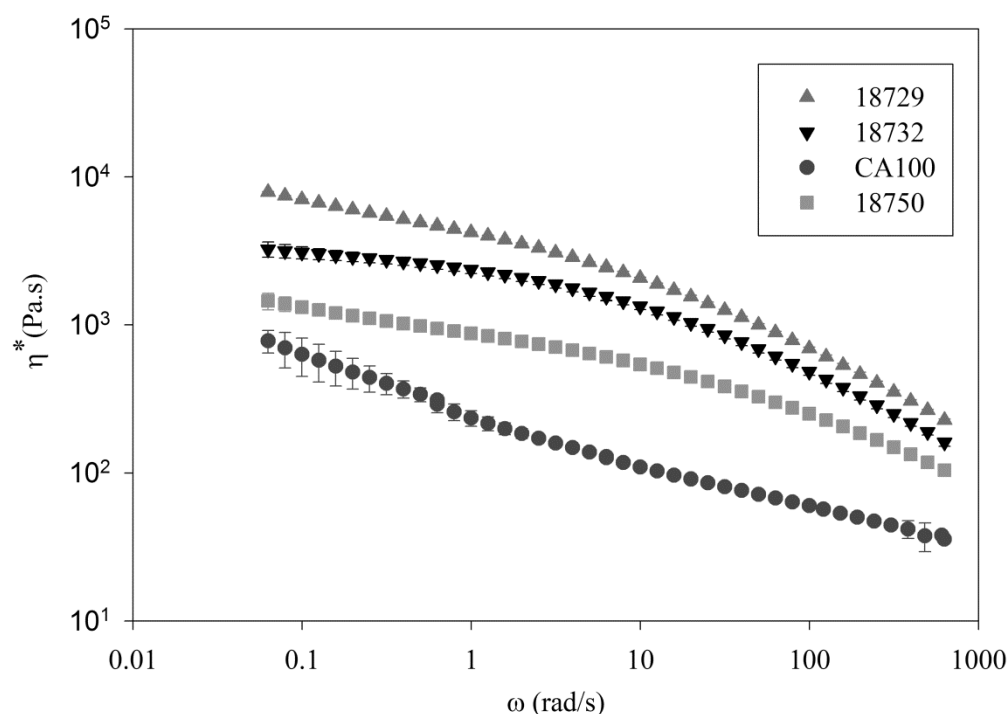


Figure 4-6. Complex viscosity as a function of angular frequency for pure compatibilizers.

XRD analysis results shown in Fig. 4.2d indicated that sample N3 exhibits a coexistence of intercalated MMT tactoids and exfoliated MMT layers. Sample N4 exhibits mainly intercalated structure, while the dispersion levels in N1 and N2 nanocomposites are between those in N3 and N4. Sample N1 appears to have better platelet dispersion than N2, based on XRD, SEM, and TEM results (Figs. 4.3 and 4.4). Thus, it is possible to rank the dispersion quality in the nanocomposites in the following descending order: N3, N1, N2, and N4.

An attempt to find a correlation between complex viscosity and XRD patterns showed that as the compatibilizer viscosity decreased, the dispersion level first decreased, then it unexpectedly increased significantly. Obviously, various factors, such as acid content (functionality), molecular weight, and processing conditions influence the contribution of the compatibilizer to dispersion and intercalation. It seems that complex viscosity behavior does not reflect the balance of the various contributions of these factors to the quality of dispersion. Therefore, another rheological parameter was sought that might show better correlation with XRD observations.

#### 5.2.4.4 Correlation between Compatibilizer Relaxation Time and Clay Dispersion

The characteristic relaxation time of each compatibilizer was calculated, using the corresponding storage and loss moduli obtained in frequency sweep experiments. The results are shown in Table 4.7.

Table 4-7. Characteristic relaxation time at 200 °C,  $\omega=1$  Hz.

Compatibilizer	G'	G''	$\lambda = G' / (G''\omega)$
(1)	8304	13200	0.62
(2)	4671	8999	0.51
(3)	748	1011	0.73
(4)	1174	2592	0.45

Moreover, stress relaxation experiments were carried out using an applied strain of 0.2 at 200°C. Figure 4.7 shows the normalized stress relaxation moduli of the pure compatibilizers versus time. Table 4.7 and Fig. 4.7 indicate that there is a direct relation between relaxation time and polymer chain intercalation in nanoclays. As the relaxation time of the compatibilizer increases, the extent of intercalation in the corresponding nanocomposite becomes higher.

It is suggested that, during the mixing process in the twin screw extruder, compatibilizer chains enter the narrow interlayer galleries of the nanoclays. When shearing stops, as the melt leaves the die, compatibilizer chains tend to recover their entropies by diffusing out and recoiling in the vicinity of MMT layers, because of the favorable interaction between MA groups and

MMT layers. If the relaxation time of the compatibilizer is higher, the recoiling and diffusion process requires longer time. This permits the PP chains to enter the enlarged galleries and to form intercalated structures. This seems to explain the good correlation between higher relaxation time of the compatibilizer and the degree of intercalation in the nanocomposite.

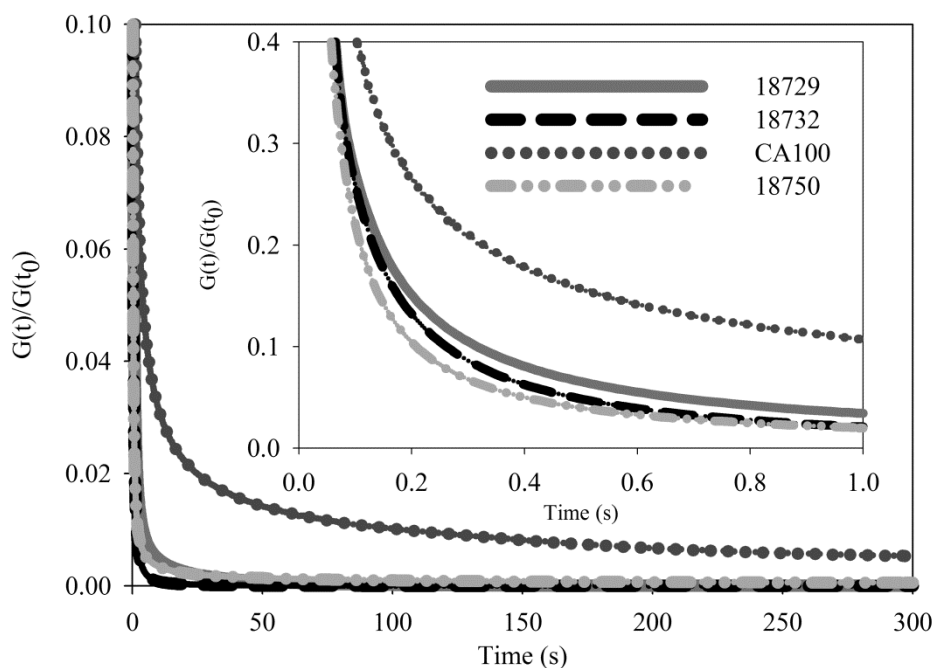


Figure 4-7. Normalized stress relaxation modulus as a function of time for pure compatibilizers.

## 5.2.5 Effect of Nanoclay Dispersion Level on Co-continuity and Morphology of TPEs

### 5.2.5.1 Rubber Phase Continuity in TPEs

Interfacial tension, viscosity ratio, and processing conditions influence the continuity index. The interfacial tension between PP and EPDM is very low ( $\sim 0.3$  mN/m at  $190^\circ\text{C}$ ) [27]. A system with such low interfacial tension should exhibit very broad regions of co-continuity [16]. Figure 4.8 shows that the differences among the nanocomposite viscosities at high frequencies were not large. A single master-curve for continuity development was observed for the TPE blends at viscosity ratios between 0.7 and 5.0. This would suggest that the observed differences in the continuity index (Fig. 4.9a) could not be the result of different viscosity ratios of the

thermoplastic and rubber phases. As the processing conditions used in nanocomposite preparation were the same, the observed differences in continuity index might be attributed to the presence of clay in the system. Figure 4.9a shows that the incorporation of clay causes a reduction of the continuity index of the EPDM phase. The effect is more pronounced in the intercalated nanocomposites than in the semi-exfoliated nanocomposites.

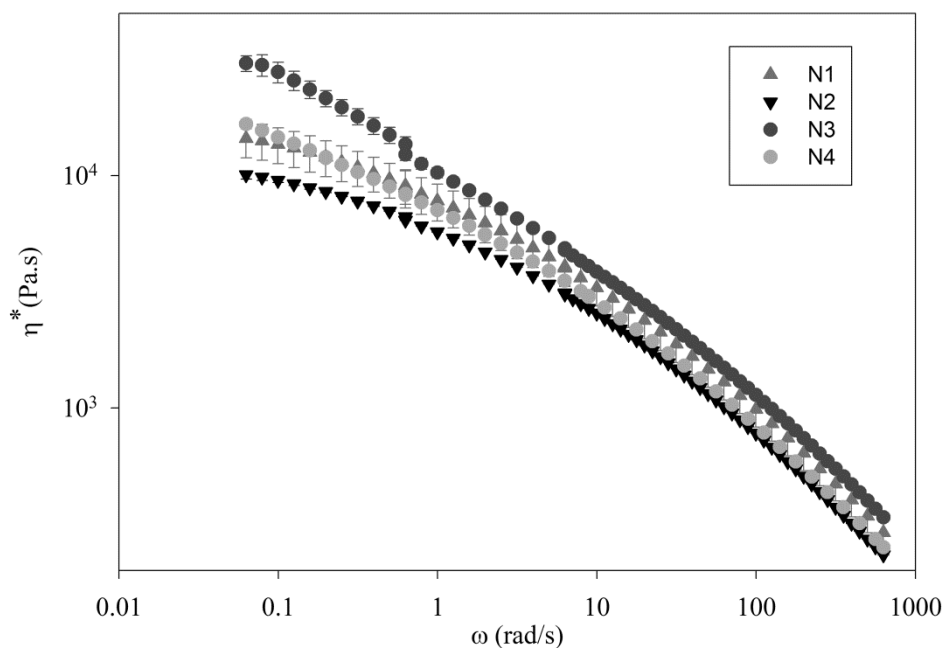


Figure 4-8. . Complex viscosity as a function of angular frequency for PP nanocomposites.

Figure 4.10 shows micrographs of the EPDM phase in intercalated and semi-exfoliated nanocomposites, at 50 wt% EPDM. These images clearly point to the higher connectivity of the EPDM phase in the TPEs prepared using “intercalated/exfoliated” PP nanocomposites as the thermoplastic phase.

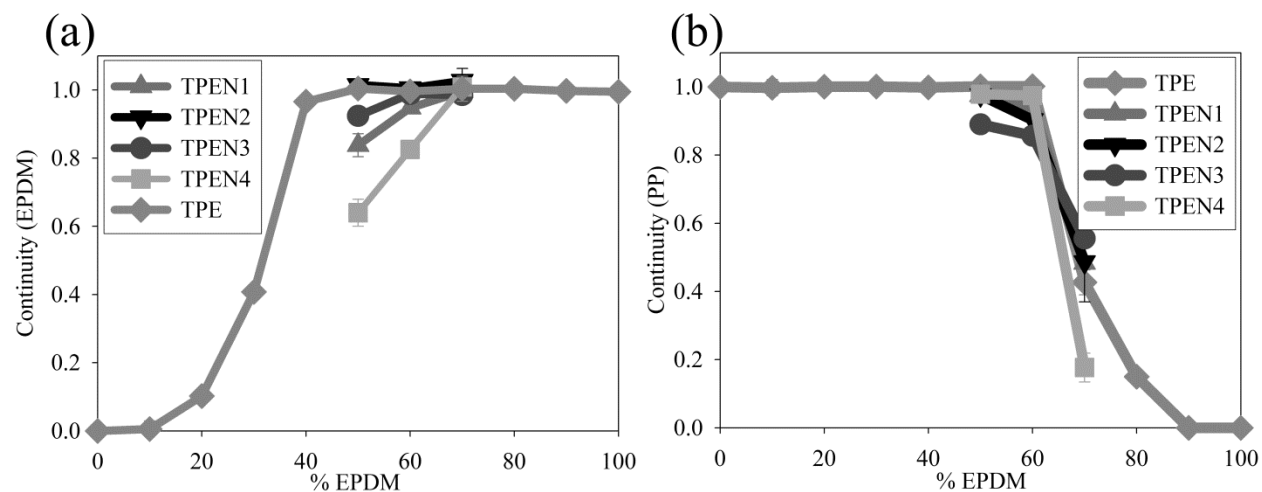


Figure 4-9. The continuity indices of EPDM (a) from non-crosslinked specimens and PP (b) from irradiated samples (corrected for thermoplastic phases solubility in cyclohexane at room temperature, and irradiated EPDM solubility in xylene).

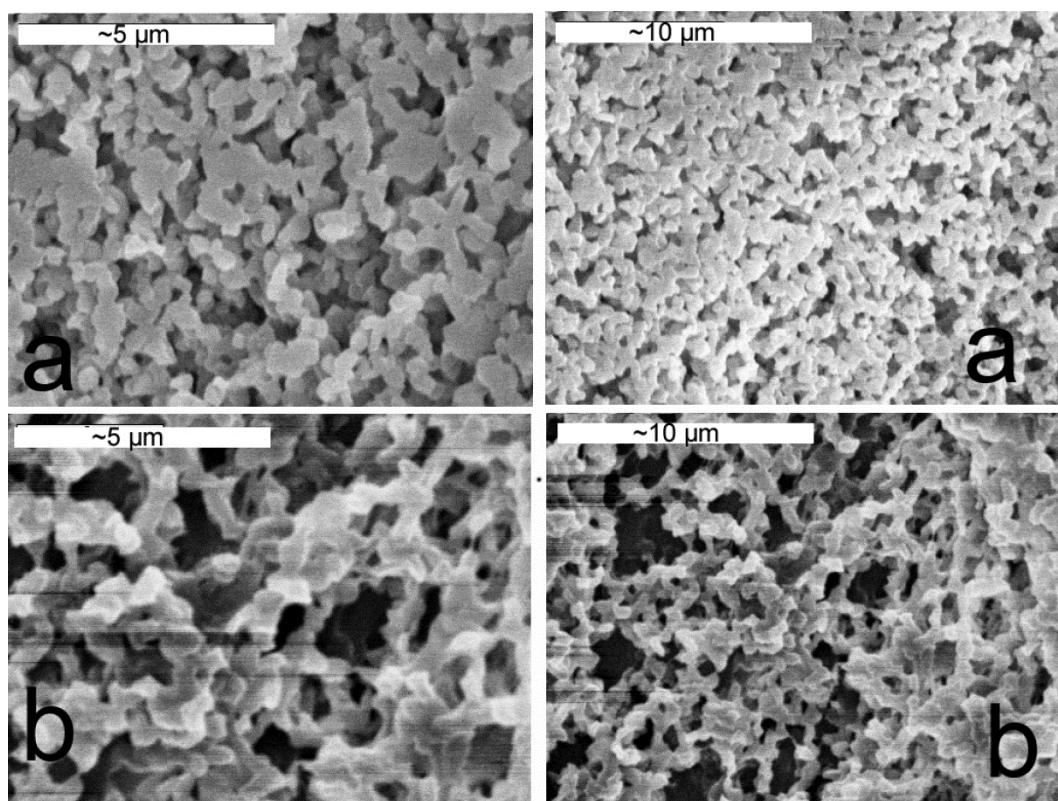


Figure 4-10. SEM micrographs of TPE nanocomposites after partial PP matrix dissolution. (a) exfoliated system TPEN3.50, (b) intercalated system TPEN4.50.

The above differences in the blend morphology influence the rheological behavior of TPE nanocomposites at the specified composition. It was found that stress growth viscosity is more sensitive to the continuity index than other material functions obtained using frequency sweep, stress relaxation, and creep experiments. The physical significance of the stress overshoot is that it indicates impending structural change [28]. Figure 4.11a reveals that a higher EPDM continuity index is associated with a lower overshoot of normalized stress growth viscosity, in cases where PP was the continuous phase.

Polymers that adapt themselves to stress can damp the applied stress or sustain uniform shear, and thus the overshoot would not be observed. When PP is the continuous phase, the stress is transferred to the EPDM phase. Because deformation of the isolated domains of EPDM would be easier than alteration of the coherent continuous structure permeating the whole volume, a higher EPDM continuity index leads to a lower overshoot of normalized stress growth viscosity (Fig. 4.11a). Thus, it is likely that the rubber phase could adapt itself to the applied stress more readily, when the rubber connectivity is more complete. These observations are potentially useful to provide qualitative information about continuity indices, especially in view of the time consuming solvent extraction and gravimetry measurements.

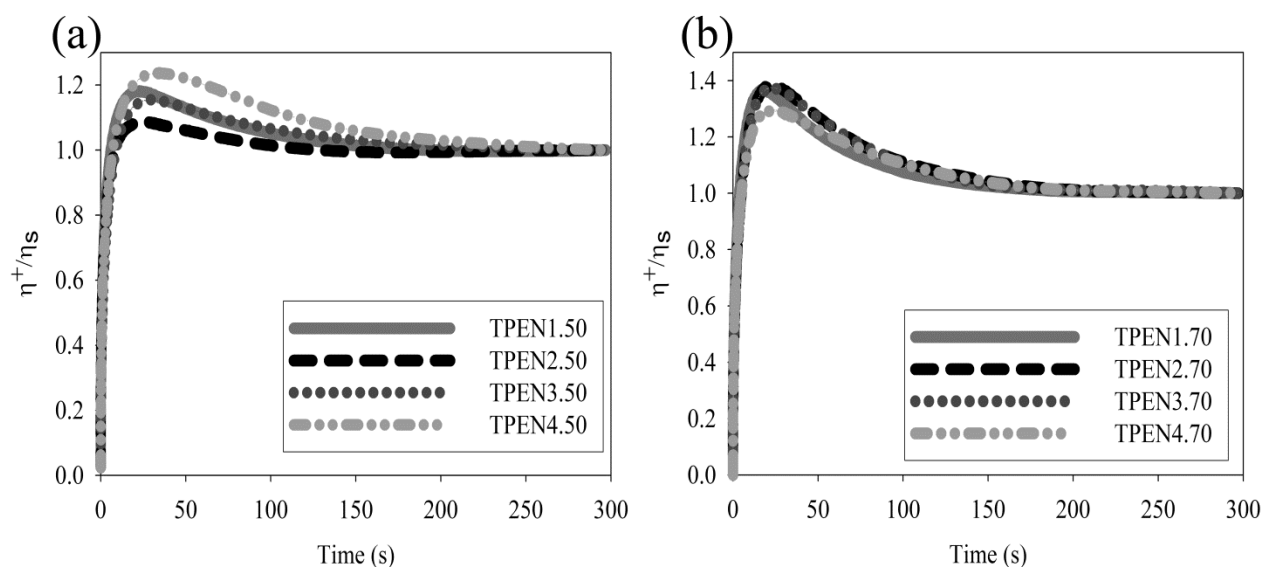


Figure 4-11. Normalized stress growth viscosity as a function of time for (a)TPENx.50 and (b) TPENx.70 .

### 5.2.5.2 Thermoplastic Phase Continuity.

Since, most PP solvents would also dissolve EPDM, it is difficult to determine PP continuity by solvent gravimetry. To overcome this difficulty the irradiation crosslinking method was used. Upon gamma irradiation, by beta decay of  $^{27}\text{Co}$ , high local concentrations of free radicals are formed in the rubber molecules. The crosslinking mechanism is similar to that obtained with peroxide crosslinking. Homogeneous crosslinking can be achieved, because of the tissue penetrating property of gamma rays [24]. A dose rate of 20 kGy/h and a total dose of 160 kGy were used to prevent the chain scission reaction. The gel content of irradiated pure EPDM was estimated with the same procedure used for PP dissolution. Because of the chain scission of EPDM to a certain extent by gamma irradiation and the presence of noncrosslinkable EPDM, the difference between the weight of the sample before and after extraction is related to the continuous portion of PP in the blend with the addition of small fraction of EPDM that should be subtracted. In the present case, the solubility of irradiated EPDM was found to be about 3.5 wt% in boiling xylene and corrections were applied appropriately to the PP continuity development curve.

Figure 4.9b shows continuity development of the thermoplastic phase for each nanocomposite. It is clear that an increase in the EPDM content leads to a reduction of the continuity index of the thermoplastic phase. However, the rate of reduction decreases when the dispersion level improves. Although intercalation leads to the low continuity of the thermoplastic phase, the continuity index of TPEN3.70 prepared using the semi-exfoliated PP nanocomposite is about 0.2 higher than that of TPE prepared using pure PP. As  $Ca \gg 1$  for this system, the mixing process involves basically distributive mixing that leads to rearrangement and deformation of the phases. The main break-up mechanism is due to the breakup of highly elongated threads via capillary instabilities that produce a line of smaller droplets. Breakup occurs when a thread diameter for which  $Ca < 1$  is reached, if the residence time during the mixing process is longer than their break-up time. Thus, the higher continuity of PP in semi-exfoliated systems may be attributed to the higher melt strength of the thermoplastic threads of semi-exfoliated system. Larger tactoids act as defects that reduce break-up times. Figure 4.12 shows SEM images of TPEs based on intercalated and semi-exfoliated systems at 70% of EPDM.

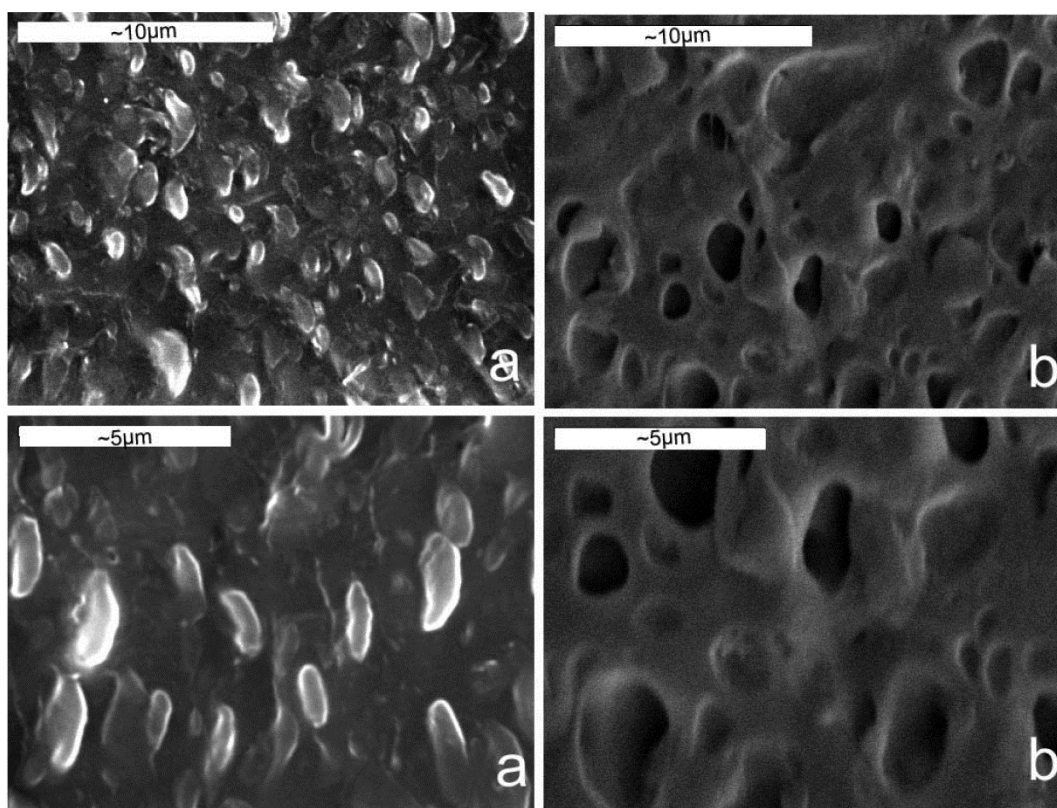


Figure 4-12. Micrographs of TPE nanocomposites after PP dissolution for (a) semi exfoliated system TPEN1.70, (b) intercalated system TPEN4.70 .

The thermoplastic phase droplets in the semi-exfoliated system are smaller and more elongated than droplets in intercalated TPEs. Although it is difficult to infer the real TPE morphology using two-dimensional images,  $D_n$  and  $D_v$ , the number and volume average diameters, for the semi-exfoliated system were calculated 1.3 and 1.6  $\mu\text{m}$ , respectively in comparison with  $D_n$  of 1.6  $\mu\text{m}$  and  $D_v$  of 1.8  $\mu\text{m}$  for the intercalated system. At high EPDM composition, it was found again that the significant change in morphology could influence the overshoot of normalized stress growth viscosity. Here, because the higher viscosity component is the matrix, when the continuity of the thermoplastic phase decreases, the amount of overshoot decreases (Fig. 4.11b).

It should be mentioned that there are some evidences that clay remained mainly in the PP phase. After complete extraction of thermoplastic phase, the clay particles could be observed clearly on the wall of the thimbles. However, there was no trace of clay powder in the solution or

on the wall of centrifuge tube that were used to complete extraction of EPDM phase. Moreover, Fig. 4.13 shows accumulated nanoclay agglomerates in the irradiated samples after complete thermoplastic phase dissolution (bright spots). These big agglomerates formed in the free domains that had been filled by the thermoplastic phase before PP dissolution. These bright spots were not detected in the bulk, when EPDM was extracted completely. Therefore, it may be concluded that the nanoclay remained in the thermoplastic phase. This is in agreement with reported observations that nanoclay remains mainly in the low viscosity phase or the phase which the clay was originally incorporated in [18, 29].

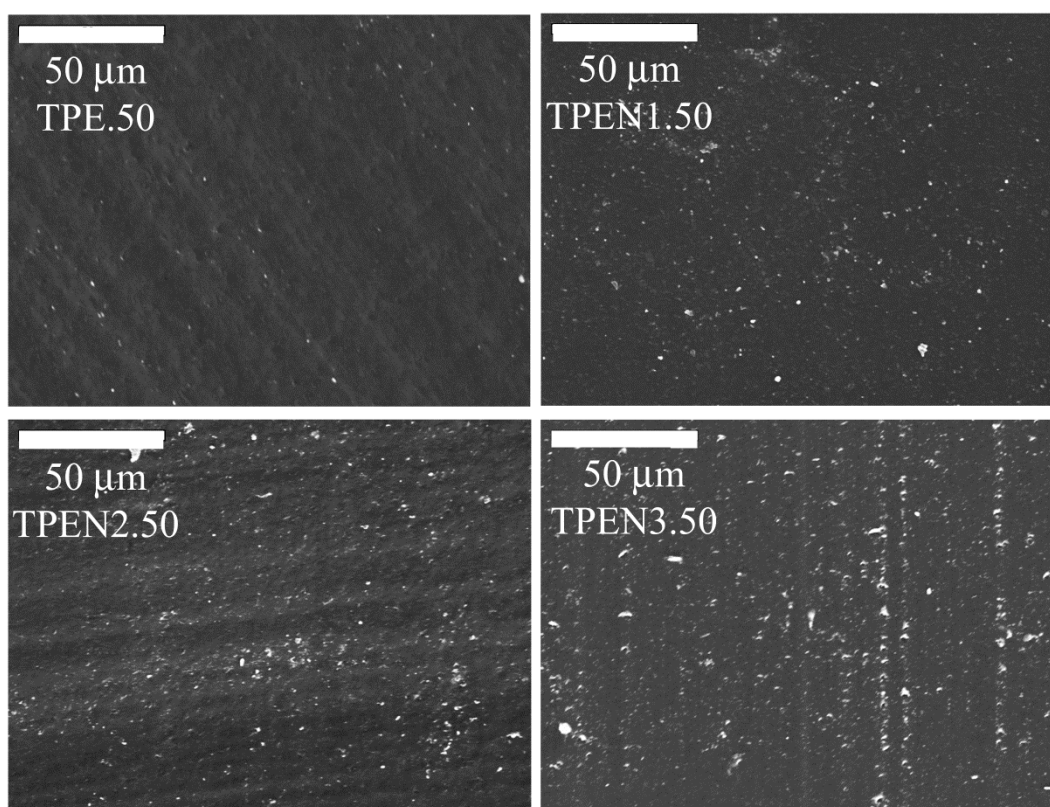


Figure 4-13. Micrographs of irradiated TPE nanocomposites after complete PP dissolution

(Bright spots show accumulated nanoclay agglomerates).

### 5.3 Conclusion

The effects of compatibilizer on the nanoclay dispersion level and co-continuity in TPE nanocomposites were investigated. The relaxation behavior of compatibilizer was found to

correlate with the extent of intercalation and nanoclay dispersion. Higher relaxation times of the compatibilizer were associated with better dispersion of nanoclay.

It was also found that the presence of nanoclay reduces the co-continuity composition range. However, better dispersion of the nanoclay limits the reduction of the thermoplastic phase continuity.

The present study suggests that the optimization of the microstructure and properties of TPV/clay nanocomposites is enhanced by the optimization of the microstructure of their precursor TPE/clay nanocomposites.

### **Acknowledgement**

The authors would like to thank Prof Monique Lacroix and Mr Guy Desroches, of the INRS-Institut Armand-Frappier, Université du Québec, for irradiating the blends. This work has been carried out with the financial support of the Natural Sciences and Engineering Research Council of Canada, to whom the authors are sincerely grateful.

## 5.4 References

1. M. Avella, S. Cosco, G. della Volpe and M. E. Errico, *Advances in Polymer Technology*, 24,2 132-144 (2005).
2. K. Y. Lee and L. A. Goettler, *Polymer Engineering and Science*, 44,6 1103-1111 (2004).
3. M. Kawasumi, N. Hasegawa, M. Kato, A. Usuki and A. Okada, *Macromolecules*, 30,20 6333-6338 (1997).
4. W. Lertwimolnun and B. Vergnes, *Polymer*, 46,10 3462-3471 (2005).
5. S. Hambir, N. Bulakh and J. P. Jog, *Polymer Engineering and Science*, 42,9 1800-1807 (2002).
6. P. Reichert, H. Nitz, S. Klinke, R. Brandsch, R. Thomann and R. Mülhaupt, *Macromolecular Materials and Engineering*, 275,1 8-17 (2000).
7. M. Kato, A. Usuki and A. Okada, *Journal of Applied Polymer Science*, 66,9 1781-1785 (1997).
8. N. Hasegawa, M. Kawasumi, M. Kato, A. Usuki and A. Okada, *Journal of Applied Polymer Science*, 67,1 87-92 (1998).
9. P. Svoboda, C. Zeng, H. Wang, L. J. Lee and D. L. Tomasko, *Journal of Applied Polymer Science*, 85,7 1562-1570 (2002).
10. M. Ton-That, F. Perrin-Sarazin, K. C. Cole, M. N. Bureau and J. Denault, *Polymer Engineering and Science*, 44,7 1212-1219 (2004).
11. P. Potschke and D. R. Paul, *Polymer Reviews*, 43,1 87-141 (2003).
12. J. Lyngaae-Jorgensen, K. Lunde Rasmussen, E. A. Chtcherbakova and L. A. Utracki, *Polymer Engineering and Science*, 39,6 1060-1071 (1999).
13. N. Mekhilef, B. D. Favis and P. J. Carreau, *Journal of Polymer Science, Part B: Polymer Physics*, 35,2 293-308 (1997).
14. J. He, W. Bu and J. Zeng, *Polymer*, 38,26 6347-6353 (1997).
15. J. Lyngaae-Jorgensen, A. Kuta, K. Sondergaard and K. V. Poulsen, *Polymer networks & blends*, 3,1 1-13 (1993).

16. P. Bhadane, M. Champagne, M. Huneault, F. Tofan and B. Favis, *Polymer*, 47,8 2760-2771 (2006).
17. R. C. Willemse, A. P. de Boer, J. van Dam and A. D. Gotsis, *Polymer*, 39,24 5879-5887 (1998).
18. G. Naderi. in Thèse de doctorat (Ecole polytechnique de Montréal); École polytechnique de Montréal. Département de génie chimique  
2006, p 203.
19. D. Hoon Kim, P. D. Fasulo, W. R. Rodgers and D. R. Paul, *Polymer*, 48,20 5960-5978 (2007).
20. H.-s. Lee, P. D. Fasulo, W. R. Rodgers and D. R. Paul, *Polymer*, 46,25 11673-11689 (2005).
21. D. H. Kim, P. D. Fasulo, W. R. Rodgers and D. R. Paul, *Polymer*, 49,10 2492-2506 (2008).
22. B. D. Favis and J. P. Chalifoux, *Polymer Engineering & Science*, 27,21 1591-1600 (1987).
23. J. Park, K. Eom, O. Kwon and S. Woo, *Microscopy and Microanalysis*, 7276-286 (2001).
24. T. Özdemir, *Radiation Physics and Chemistry*, 77,3 787-793 (2008).
25. A. Pozsgay, T. Frater, L. Papp, I. Sajo and B. Pukanszky, *Journal of Macromolecular Science, Part B*, 41,4 1249 - 1265 (2002).
26. G. Dell'Anno. University of Pisa 2004.
27. A. Y. Coran, R. P. Patel and S. William, *Rubber Chemistry and Technology*, 55,1 116-136 (1981).
28. R. Sham and W. Shi-Qing, *Journal of Rheology*, 52,3 681-695 (2008).
29. H. Thakkar, K. Y. Lee and L. A. Goettler. Nashville, TN, United States, 2003, pp 3009-3013.

**Chapter 6 THE EFFECTS OF NANOCLAY DISPERSION LEVELS AND  
PROCESSING PARAMETERS ON THE DYNAMIC VULCANIZATION  
OF TPV NANOCOMPOSITES BASED ON PP/EPDM PREPARED BY  
REACTIVE EXTRUSION**

Amin Mirzadeh, Pierre G. Lafleur, Musa R. Kamal\* and Charles Dubois

Chemical Engineering Department, Ecole Polytechnique, PO Box 6079, Stn Centre- Ville,  
Montreal, QC H3C 3A7, Canada

\* Chemical Engineering Department, McGill University, 3610 University, Montreal, QC H3A  
2B2, Canada

*“Polymer Engineering and Science”*, in press (2011)

## 6.1 Abstract

The study considers the effects of different dispersion levels of nanoclay on the crosslinking reaction of thermoplastic vulcanizate (TPV) nanocomposites based on polypropylene/ethylene propylene diene M-class rubber (PP/EPDM). Polypropylene nanocomposites, with dispersion level ranging from intercalated structures to a mixture of intercalated tactoids and exfoliated layers were used as the thermoplastic phase. Dimethylol phenolic resin or octylphenol-formaldehyde resin were used as curing agents, along with stannous chloride dihydrate as the catalyst, to vulcanize the rubber phase during the reactive extrusion process. Initially, temperature effects were investigated in internal batch mixer. Subsequently, the effects of screw speed (i.e. shear rate and residence time) were evaluated along the screw length. Different criteria such as nuclear magnetic resonance (NMR) signal line width, bound curative content, and residual diene concentration were used to evaluate the extent of crosslinking, along with normalized storage modulus and gel content. X-ray diffraction (XRD) analysis and transmission electron microscopy (TEM) micrographs showed that the dynamic vulcanization process improves the dispersion level of nanoclay in the final TPVs. It was found that the presence of nanoclay influences the crosslinking reaction, mainly through its effect on the continuity index of the EPDM phase.

## 6.2 Introduction

Among the different types of thermoplastic elastomer blends, thermoplastic vulcanizates (TPVs) are prepared by dynamic vulcanization, which was described first by Gessler et al. and Fischer [1, 2]. By definition, vulcanizing an elastomer during melt mixing with a thermoplastic polymer is called dynamic vulcanization [1, 3-5]. Coran and Patel [6] showed that various elastomers and thermoplastics can be melt-mixed to produce different TPVs. However, practically the best chemical and physical properties of these materials have been obtained with a TPV based on ethylene propylene diene M-class rubber (EPDM) and polypropylene (PP).

In theory, various curing agents could be used for the crosslinking of the elastomer phase. Three major types of curing systems are sulphur, peroxide and resole type phenolic resin systems. TPVs prepared using sulphur systems show unstable melt morphology [7]. In spite of the advantages of peroxides, the most important drawback of these curing agents in TPV production is their limited capacity to crosslink the elastomer phase selectively [8]. Although resole crosslinking is rarely used for curing thermoset elastomers, with the exception of butyl rubber, it would be a likely candidate for TPVs based on PP/EPDM. It crosslinks the unsaturated elastomer phase selectively, is effective at regular extrusion temperatures and yields thermally-stable crosslinks. Moreover, the corresponding TPVs exhibit excellent properties and good processability [9]. Machado & van Duin [10] showed that after the scission of the dimethylol ether linkage, benzyl cations eventually add to the EPDM unsaturation. For EPDM with 5-ethylidene-2-norbornene (ENB) as diene, only methylene/chroman crosslinks are formed. Experiments with EPDMs containing various diene monomers demonstrated that EPDM containing ethylidene norbornene is more reactive towards resole cross-linking than EPDM containing dicyclopentadiene (DCPD), 1,4-hexadiene (HD) or vinyl norbornene (VNB), because of the relatively high stability of the cationic intermediate. It has been suggested that, most probably, the resole does not react with PP, because of the absence of unsaturation [10]. These issues were considered in the material selection step of the present study.

Various approaches have been studied to improve the engineering properties of TPVs. Recently, the incorporation of nanoclay into the system has received much attention, in order to enhance the potential of TPVs and to expand their fields of application. However most of these studies investigated the effect of nanoclay presence on non-reactive systems or in processing

reactive systems in internal batch-mixers. For example, Lee and Goettler [11] prepared TPV nanocomposites, using a commercially available TPV with different kinds of clay, without any compatibilizer. They reported that the interlayer distance and the dispersion of the clay in the TPV materials were strongly dependent on the miscibility of the clay and the polymer matrix. Katbab and Mirzazadeh [12] showed that the degree of exfoliation of the clay increased with introduction of polypropylene grafted maleic anhydride (PP-g-MA) for both the PP and TPV nanocomposites. In another attempt, the effect of phase location of the silicate nanoclay reinforcement, whether it was located in the rubber droplets or in the continuous plastic matrix, was considered by Thakkar, Lee and Goettler [13]. They found that clay reinforcement in either phase of a TPV tends to render it less deformable. When the silicate nanoclay was added to the plastic phase, there was an increase in the  $\tan \delta$  value (as compared to reinforced-rubber TPVs), indicating a TPV that is more dissipative and more viscous. Recently, Naderi et al. [14] studied the effects of nanoclay concentration, viscosity ratio of PP/EPDM and dynamic vulcanization on the microstructure, mechanical and thermal properties of the resulting PP/EPDM TPVs that were prepared in an internal batch-mixer using a sulfuric curing system. They showed that partial exfoliation was achieved, due to the increased viscosity. Naderi [15] also reported that the size of rubber particles increased with the introduction of clay in the TPV nanocomposites prepared with low viscosity polypropylene.

The above suggests that more studies are needed to obtain better insight into the effect of nanoclay presence in reactive extrusion of these materials. Here, the term “reactive extrusion” is used to describe a polymer processing operation that is conducted in a twin screw extruder and involves chemical reactions. It is used, in particular, for in situ immobilization of one phase (dynamic vulcanization)) [16]. In the present case, preparation of TPVs using the twin screw extruder combines crosslinking chemistry with polymer processing. Thus, it requires studies of chemical kinetics in internal batch mixers to determine if the cross-linking reaction is fast enough to permit scale-up in twin screw extruders. For example, Pesneau et al. [5] first studied the crosslinking kinetics of the ethylene-methyl acrylate (EMA) in the internal mixer using pentanediol as the curing agent and dibutyltin oxide as the catalyst, to investigate TPVs based on PP/EMA by twin screw extrusion. They showed that the reaction starts sooner and the torque peaks are reached faster, when the concentration of the curing agent or catalyst is increased and when temperature increases. In addition, they suggested that the high mixing efficiency of twin-

screw extruders increases reaction rates, which improves the scalability of EMA cross-linking by diols. The same trend was observed by Verbois et al. [17] for TPVs based on EVA/PP. Ideally, the thermal stability of dynamically crosslinked TPVs should be evaluated, for example by rheology. In the case of dynamic vulcanization, since the catalyst, the rubber, and the curative agent remain in the system, the reaction may continue after the extrusion. Therefore, it is necessary to investigate the extent of reaction in the post processing steps [5].

Finally, for a comprehensive approach, reactive extrusion trials are essential. Samples should be frequently taken from the extruder and analyzed to evaluate the extent of reaction. Machado et al. [9] showed that dynamic vulcanization in extruders proceeds quite differently from that in batch mixers, where melting, mixing and crosslinking are separated in time.

In a previous publication we evaluated the effects of different PP-g-MA compatibilizers on the degree of exfoliation and co-continuity of thermoplastic elastomer (TPE) nanocomposites based on PP/EPDM [18]. It was shown that the incorporation of clay resulted in a reduction of the continuity index of the EPDM phase. The effect was more pronounced in the intercalated nanocomposites than in partially exfoliated nanocomposites. Also, the mobility of the compatibilizer was the key parameter that determines the dispersion level in PP nanocomposites.

By definition the continuity index, is the portion of a component that is part of percolating structure [19-21]. Based on the percolation threshold theory, Lyngaae-Jorgensen et al. [19, 20] described a co-continuous structure as one wherein at least a part of each phase forms a coherent continuous structure permeating the whole volume.

In the present paper, we attempt to find if the extent of crosslinking correlates with the continuity index of the EPDM in precursor TPEs. The dynamic vulcanization of the prepared TPVs and corresponding nanocomposites are characterized using different techniques, such as gel content, viscosity and storage modulus, NMR signal line width, bound curative content and residual diene concentration. It will be shown that none of these techniques alone is sufficient to provide a clear description of the systems. However, the combination of the above three techniques appears to be sufficient.

## 6.3 Experimental Procedures

### 6.3.1 Materials

The materials selected for the present study are described below. They were chosen based on our previous work [18]. General purpose polypropylene (PP) homopolymer resin, “Profax” 6523 (Basell Polyolefins), with melt flow index of 4 (g/10 min), was used as the thermoplastic phase. “Buna” EP T 6470 (LANXESS Corporation) ethylene propylene diene M-class rubber (EPDM), with ethylidene norbornene (ENB) as diene (~ 3.9 - 5.1 %) and Mooney viscosity of 52-62 M, was used as the rubber phase. Cloisite 15A (Southern Clay Products), which is surface modified montmorillonite with di-methyl, di-hydrogenated tallow ammonium chloride, was used as the nanoclay. Among different MMT commercially available, Cloisite 15A has the highest d-spacing (3.1 nm) permitting PP chains to enter the galleries more readily compared to other grades of Cloisite. Also, the decomposition temperature of its modifier is higher than our processing temperature. On the other hand, its modifier is more compatible with polyolefins compared to the modifiers used to modify other grades of Cloisite.

Two grades of maleic anhydride-grafted-polypropylene (PP-g-MA), Orevac CA 100 and Orevac 18750 (Arkema), were chosen, in view of our previous study [18], as compatibilizers to prepare polypropylene nanocomposites with different clay dispersion levels. Irganox B 225 (Ciba) primary phenolic type antioxidant was used in order to prevent oxidative degradation of thermoplastic phase. Dimethylol phenolic resin or octylphenol-formaldehyde resin (SP-1045) manufactured by Schenectady International Inc. was used as the curing agent, along with stannous chloride dihydrate ( $\text{SnCl}_2 \cdot 2\text{H}_2\text{O}$ ; Merck) as the catalyst. Also, xylene and cyclohexane (Laboratoire Mat, 99% purity) were used as solvents in extraction experiments.

### 6.3.2 Blend Preparation and Nomenclature

Initially, masterbatches consisting of PP/PP-g-MA/Cloisite15A with the same composition (60/30/10 wt %) and different compatibilizer grades were prepared in a laboratory scale co-rotating, closely intermeshing, twin-screw extruder (Liestritz ZSE-18HP). The temperature of the extruder was maintained at 185, 190, 195, 195, 195 and 195 °C from the hopper to the die and the screw was fixed at 200 rpm. The nanoclay was fed to the extruder through the side feeder, in the zone where the granules were partially melted. Then, in order to

prepare polypropylene nanocomposites with 5 wt% of Cloisite 15A, the pellets of the masterbatches were mixed with the PP, using the same twin screw extruder. The temperature profile in the extruder was 175,180,185,190,190,185°C from the hopper to the die. The screw speed was held at 600 rpm. A small amount (0.5 wt.%) of Irganox B 225 antioxidant was added to the mixture to reduce the oxidative degradation of PP. Polypropylene nanocomposites were designated as N3 and N4, where numbers 3 & 4 refer to the compatibilizer used in the composition (Orevac CA100 and Orevac 18750, respectively). The various components and processing conditions were guided by available literature and the results were analyzed in light of theoretical and quantitative principles.

Table 5-1. Processing conditions and the elements used in screw profile

Zone 1	Zone 2	Zone 3	Zone 4	Zone 5	Zone 6	Zone 7	Zone 8	Zone 9
190°C	195°C	200°C	200°C	200°C	200°C	200°C	200°C	195°C
Feeder zone , Transport Elements	Conveying and pressurizing elements	First mixing zone (first 30° , 60° then 90 ° elliptical elements)	Transport and pressurization elements	Second mixing Zone (30° elliptical elements)	Short transport, pressurization	Third mixing zone (60° elliptical elements)	Final transport Zone	Final pressurizing Zone and die

Finally TPVs and TPV nanocomposites were prepared at 50, 60 and 70 wt% of EPDM using a Brabender (internal mixer) with a mixing volume of 30 ml at 100 rpm and at 170 °C & 200 °C and also using the above mentioned twin screw extruder at screw rotation speeds of 200 and 400 rpm. The rubber phase was dynamically vulcanized using 5 phr phenolic curing agent (SP-1045,Schenectady) in combination with 1 phr Stannous Chloride.

Table 5.1 summarizes the processing conditions and describes the elements used in its screw profile, and Table 5.2 shows the compositions of the blends and related nomenclature.

Table 5-2. . Nomenclature of TPV nanocomposites and their compositions.

EPDM/PP (wt%)	50/50	TPV50
	60/40	TPV60
	70/30	TPV70
EPDM/N3 (wt%) (N3: "Partially exfoliated" PP Nanocomposite)	50/50	TPVN3.50
	60/40	TPVN3.60
	70/30	TPVN3.70
EPDM/N4 (wt%) (N4: Intercalated PP Nanocomposite)	50/50	TPVN4.50
	60/40	TPVN4.60
	70/30	TPVN4.70

### 6.3.3 Sample Preparation and Characterization Steps

#### 6.3.3.1 X-ray Diffraction

To evaluate the dispersion of nanoclay in the prepared compounds, X-ray diffraction (XRD) was performed at room temperature using an X-ray diffractometer (Philips model X'PER) in the low angle range of  $2\theta$ . The X-ray source was Cu-K<sub>a</sub> radiation ( $\lambda = 1.540598$  angstroms) using a 50 kV voltage generator and a 40 mA current. The angular step size was  $0.005^\circ$  with a step time equal to 1 second from  $2^\circ$  to  $10^\circ$  and  $0.5^\circ$  to  $4^\circ$ . A thin steel knife and cylindrical base were used as a sample holder to prevent edge effect. Great care was taken to adjust the setup in a manner that the upper surface of the sample touched the edge of the knife entirely and to align the edge of the knife with the X-ray generator and detector. This setup is a simplified model of the system used by Dell'Anno [22] to reduce the X-ray beam intensity in the range of  $0.5^\circ$  to  $4^\circ$ . More detail could be found in our previous publication [18].

### 6.3.3.2 Electron Microscopy

Scanning electron microscopy (SEM) and transmission electron microscopy (TEM) were used to study nanoclay dispersion in the thermoplastic phase. Leica-Jung RM 2065 equipped with a cryochamber was used to microtome the samples, using a glass knife under liquid nitrogen. In order to observe nanoclay dispersion, the amorphous phase of polypropylene was removed chemically. Further details regarding this technique have been explained elsewhere [23]. Subsequently, the samples were coated with gold–palladium alloy to obtain SEM micrographs using a scanning electron microscope (JSM 840, Jeol).

For TEM, trimmed polypropylene nanocomposites were ultra-microtomed at  $-130\text{ }^{\circ}\text{C}$  using a diamond knife to prepare samples with thickness of 50 nm. A water bath was used to transfer the micro-thin sections to 200-mesh cooper grids. TEM micrographs were recorded with a digital camera of the transmission electron microscope (JEM-2100F, Jeol).

### 6.3.3.3 Determination of Gel Content along the Screw Axis

To study the extent of the crosslinking reaction in reactive extrusion trials, samples were taken along the screw length, using a screw pull-out technique. After cessation of the extrusion, the screws were taken out of the barrel in about 90 seconds and immersed in liquid nitrogen to quench the materials and stop the reaction. Enough material was taken out from each zone along the screws to obtain the required samples.

Various arguments justify the use of the screw pull-out technique to determine the gel content distribution along the extruder axis. It should be pointed out that as the extrusion stops, the crosslinking regime changes from dynamic vulcanization to static vulcanization. The latter occurs at a significantly lower rate than dynamic vulcanization. In the present case, the required time to effect a significant change in gel content is longer than 90 s. Machado and Duin [9] obtained used a similar phenolic crosslinking system in conjunction with oil-extended EPDM. They reported that complete crosslinking required 25 min at  $150\text{ }^{\circ}\text{C}$  and 17 min at  $175\text{ }^{\circ}\text{C}$ . The presence of oil contributes to enhancing the crosslinking rate in this system. Furthermore, in our case, the rate of crosslinking decreases in the TPV compared to EPDM due to the presence of thermoplastic phase that limits the diffusion of the resol crosslinker. More importantly, the extruder has two accessible ports, in the first and second mixing zones, for direct sampling inline. Measurements of the gel content for samples drawn from each zone yielded the same values,

within experimental error, as the corresponding gel content values obtained by the screw pull-out technique.

For determination of gel content, the samples were immersed in boiling xylene for 45 to 60 minutes. The process was repeated consecutively to assure the complete removal of the PP and non-crosslinked EPDM phase. Considering the weight of the screen before and after extraction and drying as well as nanoclay weight percent, the gel content was calculated using the following formula:

$$\% \text{ Gel content} = \frac{(\text{Wt. of the sample after extraction} - \text{Wt. of the filler in the sample})}{\text{Wt. of EPDM in the sample}} \times 100 \quad (5-1)$$

#### 6.3.3.4 Rheological Measurements

Rheological measurements were carried out using a Physica MCR-501 rheometer from Anton Paar with 25 mm diameter parallel disc geometry at 200 °C. In all cases, the linearity of the sample response with respect to stress amplitude was verified. Nitrogen gas was used to prevent thermal oxidation of the materials.

#### 6.3.3.5 Solid State NMR

The extent of crosslinking was investigated by different criteria obtained from NMR analysis. Solid state NMR experiments were carried on pure non-crosslinked EPDM and extracted TPVs using a Bruker AVANCE-600 spectrometer (600.17 MHz <sup>1</sup>H, 150.92 MHz <sup>13</sup>C), with chemical shifts referenced to tetramethylsilane at room temperature.

## 6.4 Results and Discussion

### 6.4.1 Nanocomposite Characterization

According to Fig. 5.1a, Cloisite 15 A shows three characteristic peaks. The first one at  $2\theta = 2.85^\circ$  (corresponding d-spacing is 3.1 nm), the second one at  $2\theta = 4.6^\circ$  (corresponding d-spacing is 1.9 nm) and the third peak at  $2\theta = 7.17^\circ$  (corresponding d-spacing is 1.1 nm). The latter is attributed to the portion of the clay that remained in the pristine (unmodified) state.

The XRD pattern for N4 shows that the three peaks of Cloisite 15A are shifted to lower angles. This suggests that the peak observed in the XRD pattern of N4 at  $2\theta=2.42^\circ$  (corresponding d-spacing of 3.8 nm; original  $2\theta \cong 2.85^\circ$ , d-spacing of about 3.1 nm) is attributed to the intercalation by polymer chains into galleries of Cloisite 15A. Considering the use of the same sample thickness, slit, frame and the other test conditions to perform the experiment, the lower signal intensity shows the better intercalation of polymer chains into the galleries of Cloisite 15A in N3 compared to N4. On the other hand, N3 nanocomposites show only two peaks in the range of  $2^\circ$  to  $10^\circ$  (Fig. 5.1a).

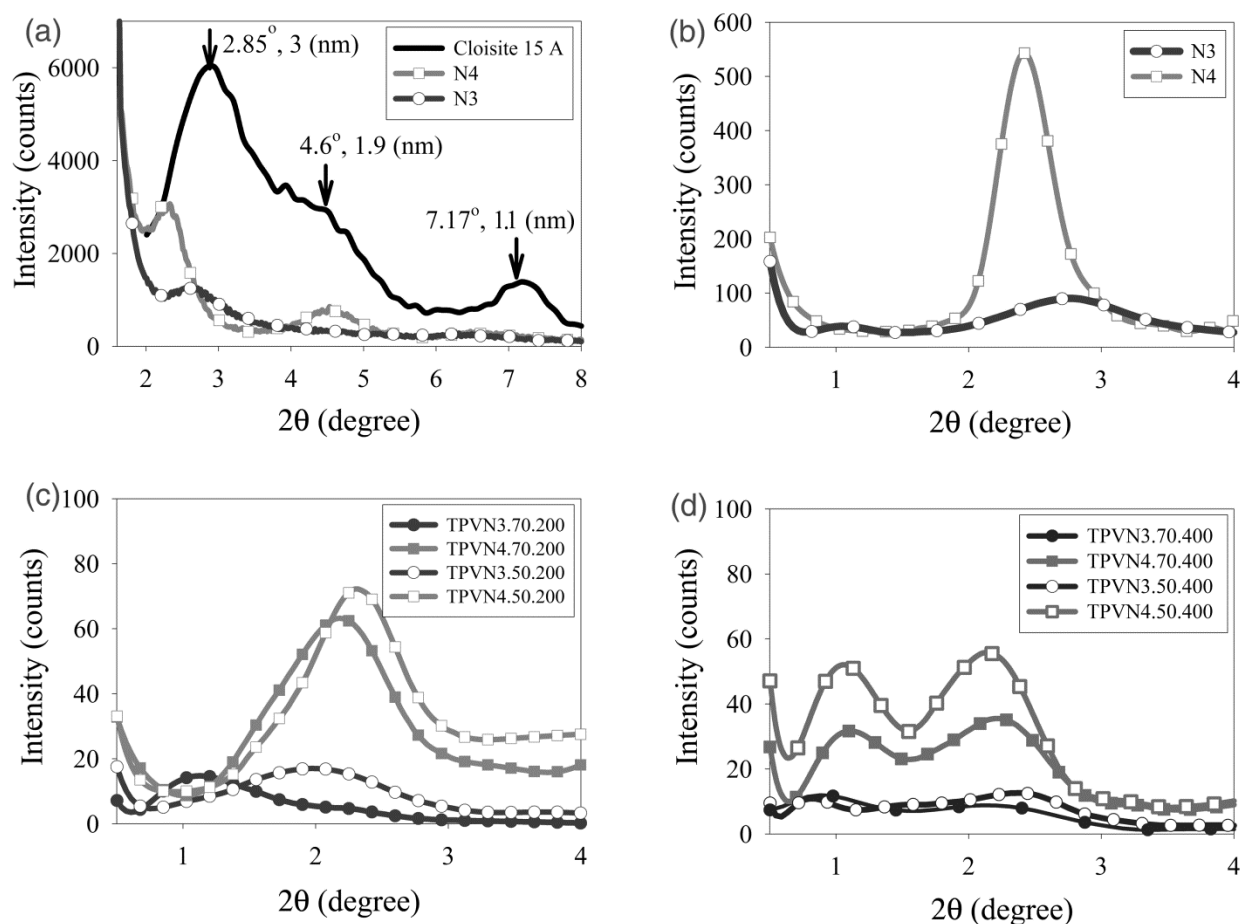


Figure 5-1. XRD patterns of Cloisite 15A and nanocomposites at different scan range.

The first observed peak at  $2\theta \cong 2.64^\circ$  corresponds to d-spacing of about 3.3 nm and the second peak is at  $2\theta \cong 6.5^\circ$ . It is likely that these two peaks are related to the second and third peaks of Cloisite 15A at  $2\theta \cong 4.6^\circ$  and  $2\theta \cong 7^\circ$ , respectively. Using the setup described in the

experimental section and after optimization of sample thickness, slit size, frame size, starting angle and scan rate to obtain reproducible data, X-ray scans were performed in the range of  $2\theta = 0.5^\circ$  to  $2\theta = 4^\circ$ . It is suggested that the peak observed in Fig. 5.1b at  $2\theta = 1.05^\circ$  corresponding to d-spacing of 8.5 nm for N3 (in the range of  $2\theta = 0.5^\circ$  to  $2\theta = 2^\circ$ ) is attributable to some exfoliation of Cloisite 15A, with the original d-spacing of about 3.1 nm (at  $2\theta \cong 2.8^\circ$ ). Therefore, the XRD analysis (Fig. 5.1b) suggests a coexistence of intercalated MMT tactoids and exfoliated MMT layers in N3 nanocomposite namely “partially exfoliated” nanocomposite.

TEM as a complementary technique was used to evaluate the nanostructure of PP nanocomposite. TEM images shown in Fig. 5.2c and Fig. 5.2d confirm the “partially exfoliated” structure of N3 suggested by XRD results.

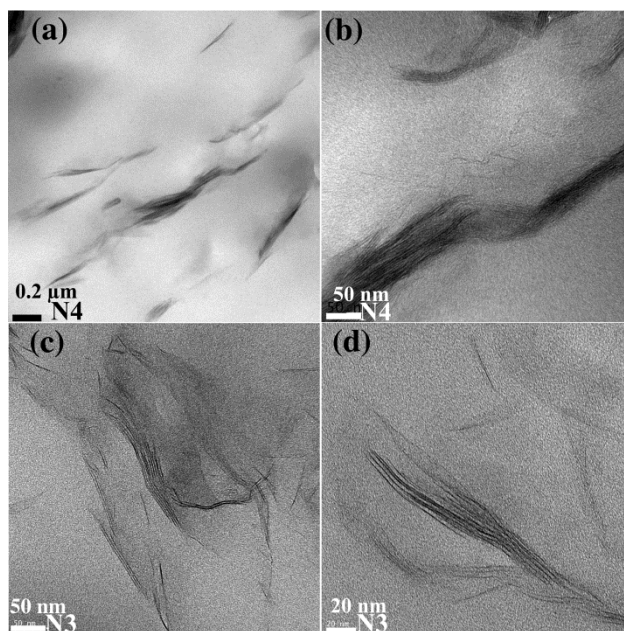


Figure 5-2. TEM micrographs of PP nanocomposites.

The quality and uniformity of dispersion of nanoclay were also investigated by SEM. The amorphous phase of polypropylene was removed chemically from the microtomed surface. Thus, the nanoclays could be observed by SEM. Fig. 5.3 shows that the agglomerates were uniformly dispersed in the matrix with no large agglomerates, reflecting good mixing quality. Examination of micrographs at higher magnification suggested that nanoclay dispersion quality in N3 nanocomposite (Fig. 5.3a) was better than that in N4 (Fig. 5.3c).

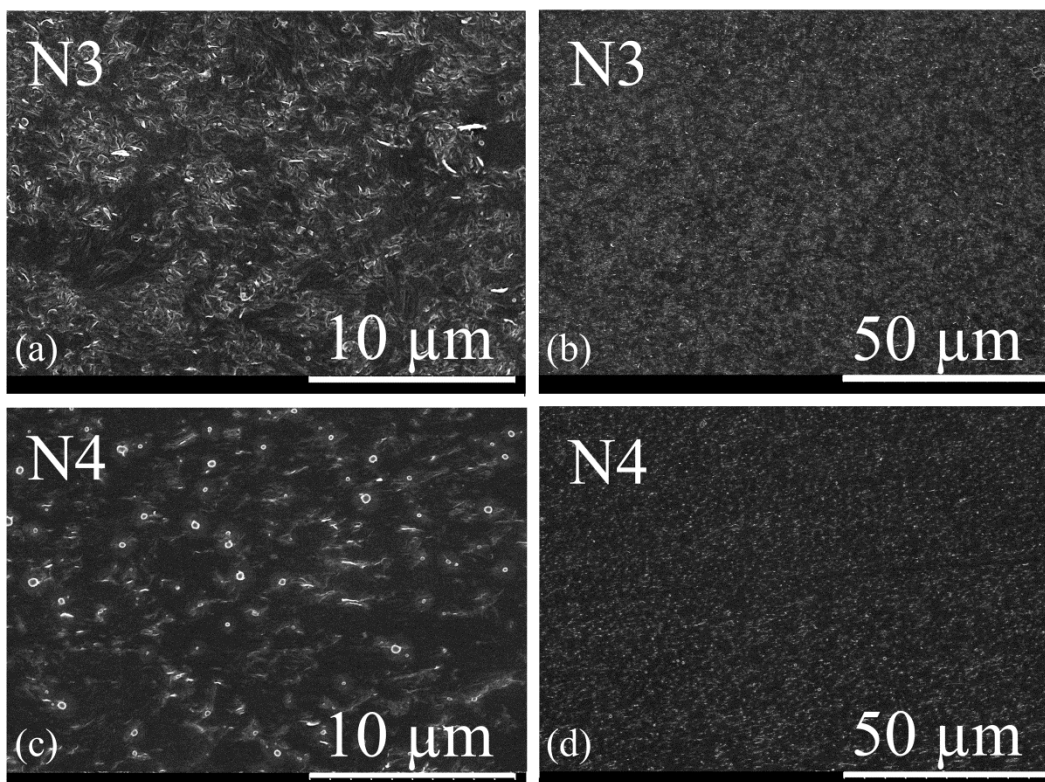


Figure 5-3. SEM images of PP Nanocomposites after removing the amorphous phase.

As shown in Fig. 5.1c, the peak at  $2\theta=2.42^\circ$  in XRD patterns of TPVN4 nanocomposites prepared at screw speed of 200 rpm is broader than the corresponding narrow peak of N4 (Fig. 5.1b) due to the higher shear stress, which was exerted on the nanoclay layers during dynamic vulcanization. Intercalation of polymer chains into the interlayer galleries of the nanoclays is more pronounced for the samples prepared at higher screw speed (400 rpm) and, as seen in Fig. 5.1d, the first characteristic peak of nanoclay in TPVN4 nanocomposites shifted to the lower angle ( $2\theta=0.94^\circ$ , corresponding d-spacing is about 9.3 nm). It should be mentioned that by increasing EPDM content, polymer intercalation was not enhanced significantly.

## 6.4.2 The Extent of Crosslinking

### 6.4.2.1 Curve Analyzing and Gel Content Experiments

Preliminary tests were performed in an internal mixer at two different processing temperatures to evaluate the dynamic vulcanization. Fig. 5.4 presents the torque-time curves and temperature profiles. Just after adding the curative agent and catalyst to the molten mixture of PP

and EPDM, the torque value first decreased significantly due to the low viscosity of the phenolic resin. Then it increased within 80 s at 170 °C and 50 s at 200 °C to reach its maximum value, regardless of the sample composition. Since the high mixing efficiency of the twin-screw extruder favors the crosslinking reaction and since the residence time in the twin screw configuration ranges from about 45 s to 65 s, depending on the screw speed, the cross-linking reaction at 200 °C would be fast enough for scale-up to the extruder. It should be mentioned that the observed peak is related to high cross-linking level and shows the beginning of the mechanical break up of the co-continuous structure through the mechanical action of the rotors [5]. The gel content of TPVs at torque peak in Fig. 5.4 is in the range 50% to 70%, depending on rubber content. It rose to 80% to 90% at the end of the process.

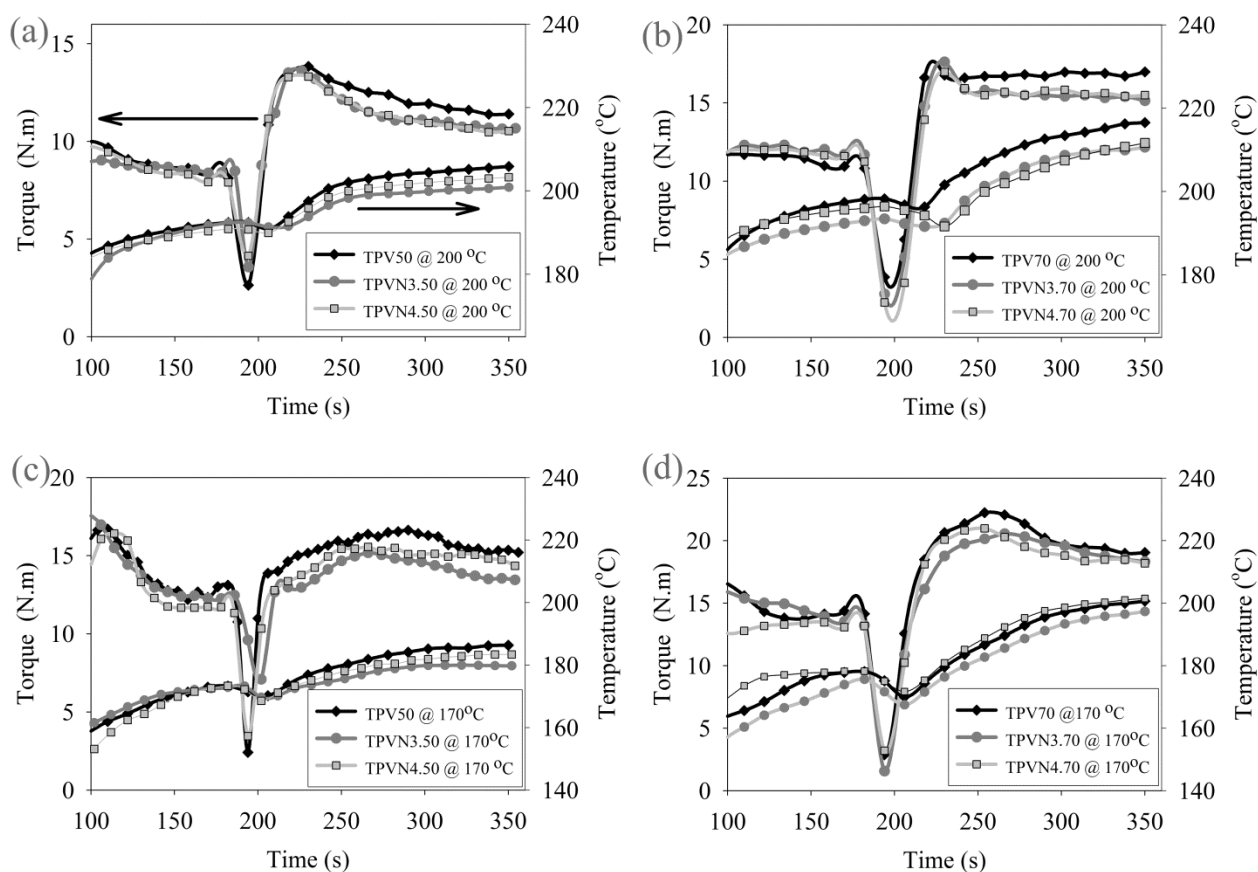


Figure 5-4. Torque-time curves and temperature profiles of the reactive blends.

It is suggested that the phase inversion along the screw length of the twin screw extruder occurs at the same gel content of the phase inversion in the internal mixer [17]. Therefore, as seen in Fig. 5.5, at least before the second mixing zone, co-continuous structure could be expected. In

other words, the co-continuity of the blends before the second mixing zone is not only controlled by dynamic vulcanization but also by the presence of nanoclay.

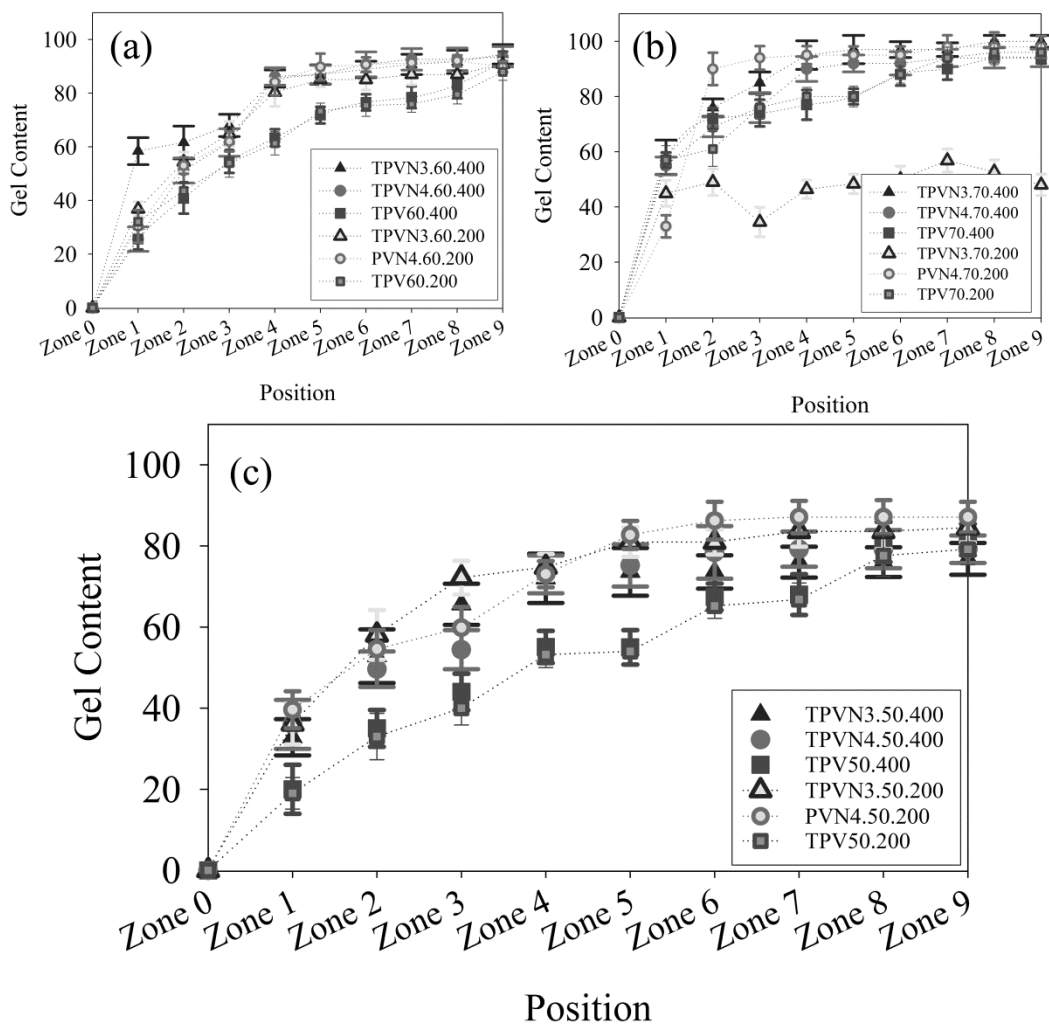


Figure 5-5. Gel content upon dynamic vulcanisation along the screw axis for the samples containing 60wt% (a), 70 wt% (b) and 50 wt% (c) of EPDM.

According to Fig. 5.5, in our experimental window, variation in the screw speed had virtually no influence on the gel content values along the screw axis. Moreover, it was more sensitive to the blend composition and nanoclay presence. Gel content increases significantly before the second mixing zone and remains constant to the end for TPV nanocomposites. It has been shown that the crosslinking reaction in dynamic vulcanization proceeds initially at the outer envelope of the EPDM phase, then it works its way toward the center of EPDM threads [24]. Therefore, the higher gel content in TPV nanocomposites, compared to TPV blends, during the

early stage of mixing should be related to higher local concentration of curative agent at the interface, due to the barrier effect of nanoclays in the thermoplastic phase. The low gel content of TPVN3.70 (TPV based on partially exfoliated PP) prepared at 400 rpm, indicates the occurrence of thermal degradation of the phenolic resin. The study of the evolution of gel content along the screw is helpful to obtain insight regarding the progression of cure in the extruder during dynamic vulcanization. However, such studies do not allow an accurate comparison among the final values of crosslinking extent in the various TPVs and TPV nanocomposites, because most of the systems show almost the same values of gel content at the extruder exit. Therefore, rheological and solid state NMR measurements were used to determine the effect of nanoclay and its dispersion level on the final state of cure.

#### **6.4.2.2 Rheological Characteristics**

Different rheological experiments could be used to evaluate the state of cure and the thermal stability of the dynamically crosslinked TPVs. The evolution of normalized storage modulus during time sweep tests may be related to the static vulcanization, due to the presence of unreacted phenolic resin in the blend. Therefore, higher residual unsaturated bonds of ENB lead to more thermal instability. Fig. 5.6 shows that the normalized storage modulus of TPV50, prepared at 200 °C in the internal mixer (gel content ~ 80%), increased by about  $6\pm 2\%$  in 6000 s (gel content ~ 100%), while that of TPVN4.50 and TPVN3.50 increased by about  $9\pm 3\%$  and  $13\pm 3\%$ , respectively. These deviations from an ideal stable system are more pronounced for the samples prepared at 170 °C. It is suggested that more residual ENB leads to higher instability of TPV nanocomposites. This is in agreement with the results obtained with the internal mixer. The torque and melt temperature for systems without nanoclay increase more than those for TPV nanocomposites after adding the curative system (Fig. 5.4). Increasing the EPDM content seems to reduce the influence of nanoclay presence. Thus, allowing for an error of 4 %, the normalized storage moduli of TPV70, TPVN3.70 and TPVN4.70 were enhanced by the same magnitude during the time sweep test. Accordingly, this criterion does not indicate the differences in extent of crosslinking reaction among the different extruded samples. However, it clearly indicates the high thermal stability of the samples prepared by reactive extrusion. Since the normalized storage modulus increased by less than 2% in the same time range, a higher extent of crosslinking reaction could be expected compared to the samples prepared in internal mixer.

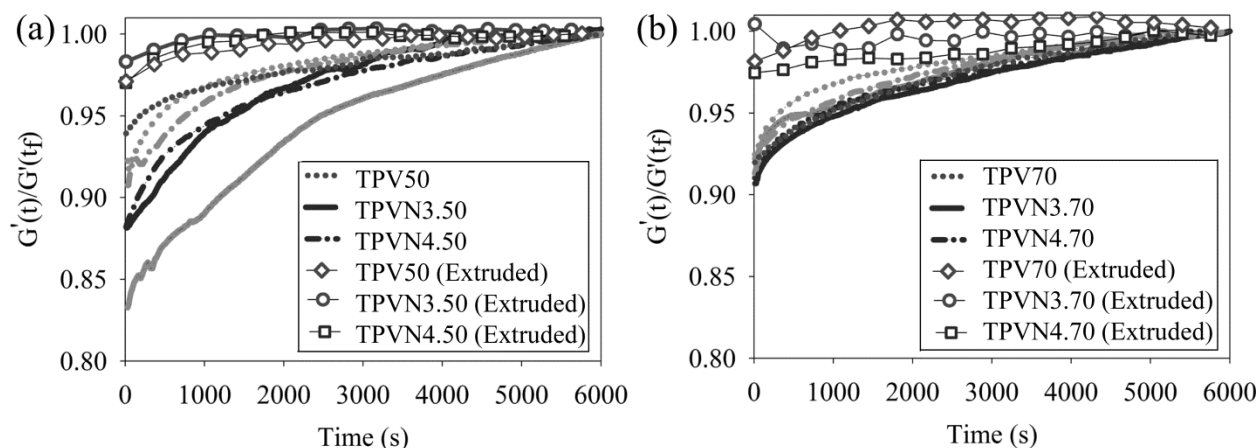


Figure 5-6. Figure 6. Evolution of the normalized storage modulus with time for the various reactive blends prepared by twin screw extruder, prepared by internal batch mixer at 200 °C (black) and 170 °C (gray) using 50wt% (a) and 70 wt% (b) of EPDM.

According to Fig. 5.7, it is obvious that rheological behavior of both dynamically vulcanized TPVs and TPV nanocomposites are strongly dependent on the rubber/plastic ratio. There is no indication of Newtonian-like behavior at low frequencies and the damping function is less than one for all the composition in our experimental window. In spite of the apparent similarity, there are meaningful differences. Fig. 7a shows that complex viscosity and storage modulus of TPVs without nanoclay increased with screw speed, probably because of higher extent of crosslinking.

The situation for TPV nanocomposites is more complicated. TPV nanocomposites based on intercalated system (TPVN4) exhibited higher values of dynamic properties, when prepared at lower screw speed (Fig. 5.7b). The complex viscosity of TPVN3.50 prepared at higher screw speed (400 rpm) was lower than for samples prepared at 200 rpm (Fig. 5.7c). The effect of screw speed is in the opposite direction by increasing rubber content to 60 wt %. Significant decrease in rheological properties of TPVN3.70 prepared at 400 rpm may be related to the thermal degradation of curative agent, because of the intensive exothermic reaction occurring in first mixing stage (Fig. 5.5). In the next section, we use NMR analysis to explain the effects of nanoclay dispersion level and the extent of crosslinking reaction on the observed rheological behavior of the blends. Particular emphasis is placed on the evolution of dynamic viscosity and storage modulus, as summarized in Fig. 5.7.

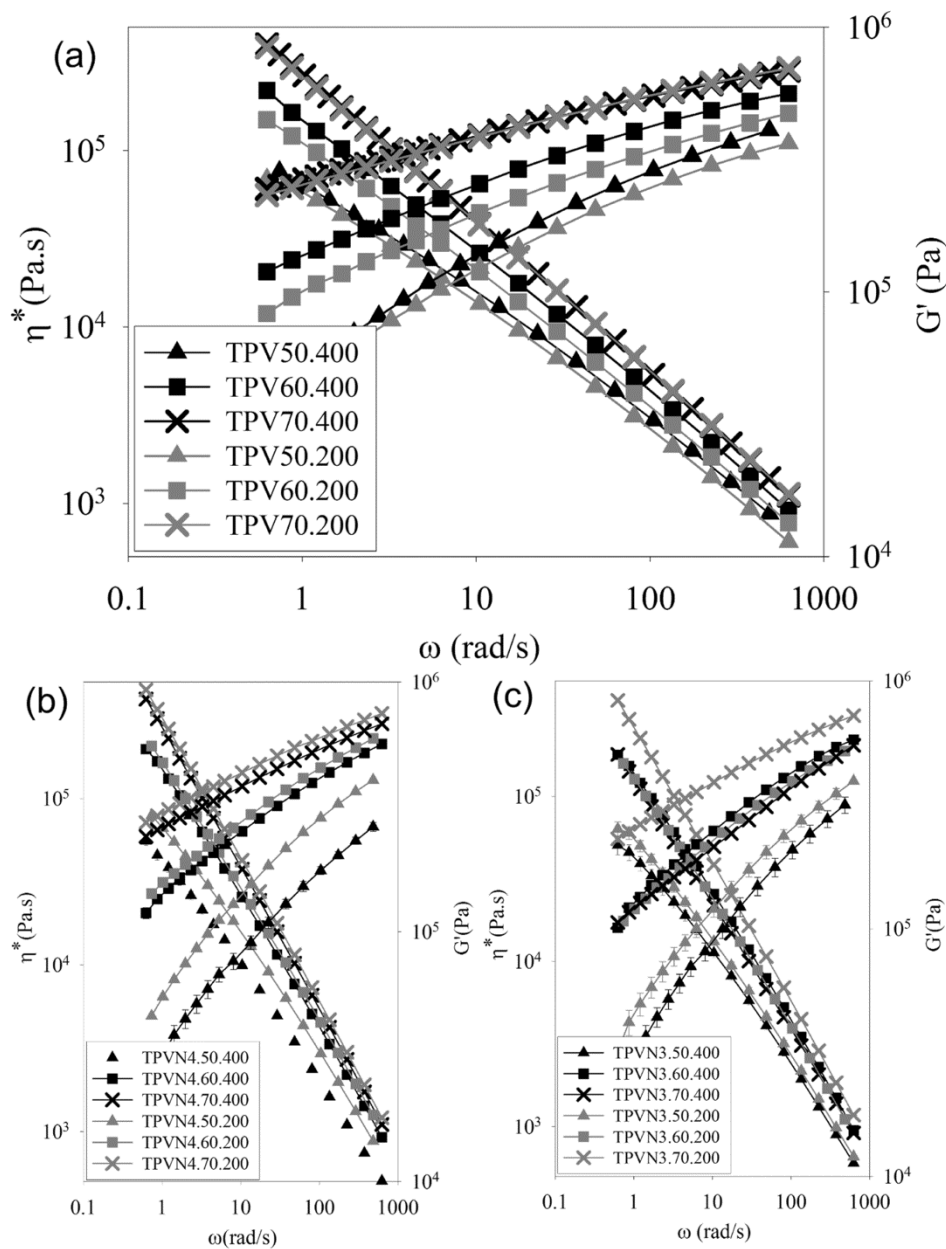


Figure 5-7. The evolution of dynamic viscosity and storage modulus with frequency.

### 6.4.2.3 Solid State NMR Analysis

The extent of crosslinking reaction was investigated, using solid state NMR spectra, in various studies. In particular, some investigations dealt with TPVs based on PP/EPDM prepared using phenolic resin curative [25, 26]. There are three characteristic peaks in the representative spectrum shown in Fig. 5.8. Signals at 1.0-1.4 are related to the methyl and methylene groups, the peak in range of 5.1–5.3 represents two isomers of ENB and the signal at

7.0 ppm is assigned to the aromatic components of phenolic resin [25]. The latter is not observed for the pure EPDM as expected (Fig. 5.8).

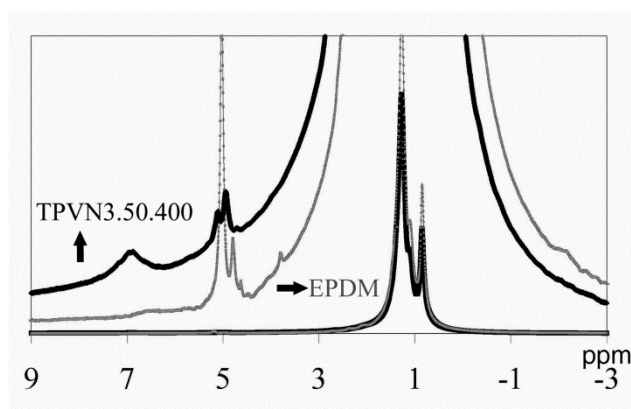


Figure 5-8.  $^1\text{H}$  MAS NMR spectrum of EPDM and TPVN3. The upper curves are the same spectrums as the lower curves but with higher amplification factor.

Among several proposed mechanisms for phenolic crosslinking, it seems that the 1,4 cyclic addition mechanism is more realistic [25]. According to this mechanism, dienes of ENB are consumed during the crosslinking reaction. Therefore, one can calculate residual ENB weight fraction as a measure of crosslinking extent. The calculation of residual ENB weight fraction involves using the area under the diene signal and the total area under the polymer backbone. According to the supplier, the ENB content of the EPDM grade provided is 3.9~5.1 wt%. On the other hand, the ENB content of the EPDM used in this study was determined, according to the method by A. G. Altenau et al. [27] using the NMR spectra. The measured ENB content was ~4 wt% and this nominal value was used to determine the residual ENB in TPVs. More detail is given elsewhere [25]. Fig. 5.9 shows these fractions for extracted samples that were collected at the end of extruder (gel content ~ 100%). To interpret these results and to establish a relation between nanoclay presence and crosslinking extent, two facts should be considered. Firstly, as mentioned before, according to gel content experiments along the screw axis, the co-continuous structure exists at least before the second mixing zone. This co-continuity is also controlled by the presence of nanoclay and its dispersion level. As shown in earlier work for corresponding non-reactive blends, the presence of nanoclay lowered the EPDM continuity index. This effect was more pronounced for systems prepared based on intercalated PP nanocomposites (Table 5.3) [18].

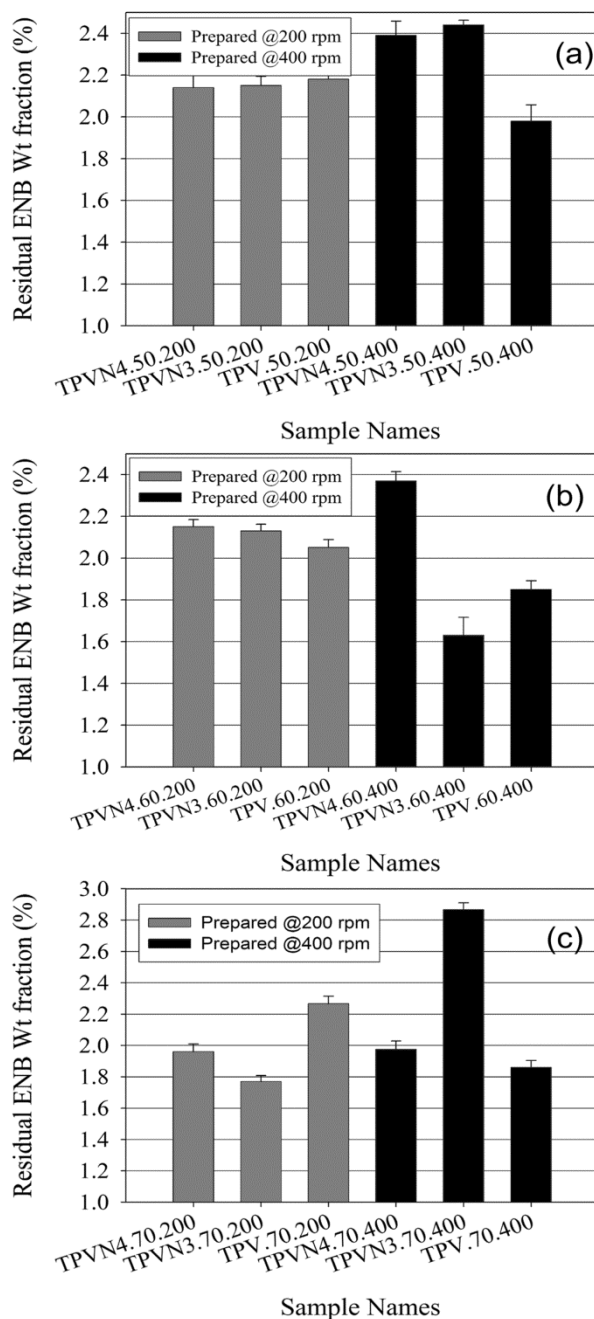


Figure 5-9. Residual diene contents of TPVs and TPV nanocomposites.

Higher continuity index of EPDM would probably result in better dispersion of the curing system. It would also provide higher interfacial surface that favors the diffusion process of phenolic resin, considering the point that the crosslinking reaction, as mentioned before, proceeds initially at the outer envelope of the EPDM phase, and works its way toward the center of EPDM threads in dynamic vulcanization [24].

Fig. 5.9a shows the residual ENB fraction of TPVs and TPV nanocomposites at 50 weight percent of EPDM. It seems that there is no significant difference in extent of crosslinking reaction for the samples prepared at lower screw speed (residence time of ~ 65 s). Also, the effect of nanoclay presence on the crosslinking reaction is more pronounced for the samples prepared at higher screw speed (residence time of ~ 45 s). As seen in Table 5.3, at 50 wt% EPDM, the continuity index of the rubber phase for intercalated and partially exfoliated system is about 0.6 and 0.85, respectively, while it is equal to 1 for the system without nanoclay. Therefore, the extent of crosslinking decreases significantly, compared to the TPV without nanoclay. By increasing the EPDM content to 60 wt%, before the second mixing zone, EPDM would be almost a fully continuous phase for the system based on "partially exfoliated" PP (TPVN3.60) and the system without nanoclay (TPV60), while the continuity index of TPVN4.60 would be about 0.8.

Residual ENB weight fractions indicate the same state of cure for the samples prepared at lower screw speed (Fig 5.9b). However, the crosslinking extent increased unexpectedly for the TPVN3.60 (TPV prepared based on partially exfoliated PP nanocomposite) and the curing state of TPV.60 lies between the curing states of intercalated TPV (TPVN4.60) and "partially exfoliated" one (TPVN3.60). It seems that, when co-continuity of two blends is similar, the barrier effect of nanoclays increases the local concentration of curing agent and intensifies the crosslinking reaction. By increasing the EPDM weight fraction to 70 wt%, continuity of the EPDM phase is uniform everywhere thus, the effect of nanoclay presence was observed even at the lower screw speed, such that the residual ENB of TPV without clay was higher than that of TPV nanocomposites. Also, a higher curing state was observed for TPVN3.70 compared to TPVN4.70, probably due to the better dispersion level of nanoclay. The degradation of phenolic resin caused about 3% of ENB to remain in TPVN3.70 prepared at 400 rpm.

Table 5-3. The continuity indices of EPDM from non-crosslinked specimens

Continuity index of EPDM in :	50 wt% of EPDM.	60 wt% of EPDM	70 wt% of EPDM
TPE (PP/EPDM)	1	1	1
TPEN3 (N3/EPDM)	~0.85	~1	1
TPEN4 (N4/EPDM)	~0.6	~0.8	1

It has been demonstrated that the phenolic content can be used as a measure of the crosslink density [25]. In the  $^1\text{H}$  spectra of extracted samples, the area under the signal of 7 ppm

relates to aromatic component of the reacted phenolic resin. Normalization of this area is carried out using the total area under the backbone peaks. The results are presented in Fig. 5.10.

The results are in complete agreement with the results of residual ENB. Generally, increasing the screw rotational speed generates higher shear stresses and improves the dispersion processes. Also, shear viscous heating that favors the exothermic crosslinking reaction increases. However, the time available for the crosslinking reaction is reduced. In the present study, According to Fig. 5.9 and Fig. 5.10, if EPDM in the corresponding non-reactive system is a continuous phase, the extent of crosslinking reaction appears to be more dependent on the screw speed. Otherwise, higher residence time would increase the extent of crosslinking.

Table 5-4. The backbone peak base width for the TPV and TPV nanocomposites.

Sample name	Backbone peak base width (Hz) @ 1% maximum	Standard deviation
TPVN4.50.200	991	5.41
TPVN3.50.200	1034	4.95
TPV.50.200	984	4.83
TPVN4.50.400	1149	4.14
TPVN3.50.400	1241	4.83
TPV.50.400	1007	4.81
TPVN4.60.200	1708	4.83
TPVN3.60.200	1703	7.07
TPV.60.200	1593	6.36
TPVN4.60.400	1763	4.12
TPVN3.60.400	1791	9.19
TPV.60.400	1639	4.83
TPVN4.70.200	1722	11.31
TPVN3.70.200	1680	4.12
TPV.70.200	1598	4.41
TPVN4.70.400	1791	12.02
TPVN3.70.400	1877	4.83
TPV.70.400	1624	4.19

In this study, the backbone peak base width at 1% of maximum was used as a measure of the crosslinking extent. Segments close to the crosslinks have low mobility. They contribute more to the base of the peak. Therefore, the samples with the higher curing state show wider signal line width. Table 5.4 shows the backbone peak base width values for the TPV and TPV nanocomposites. Due to the influence of the presence of clay on the mobility of the backbone of EPDM, the results in this table cannot be used to compare the extent of crosslinking in the various nanocomposites. However, they may be used to compare the extent of crosslinking in the

TPVs in the absence of clay. Therefore, in Table 5.4, TPVs prepared at screw speed of 400 rpm without nanoclay showed larger backbone peak base, indicating higher extent of crosslinking compared to the TPVs prepared at 200 rpm. This is in agreement with the results in Fig. 5.9 and Fig. 5.10.

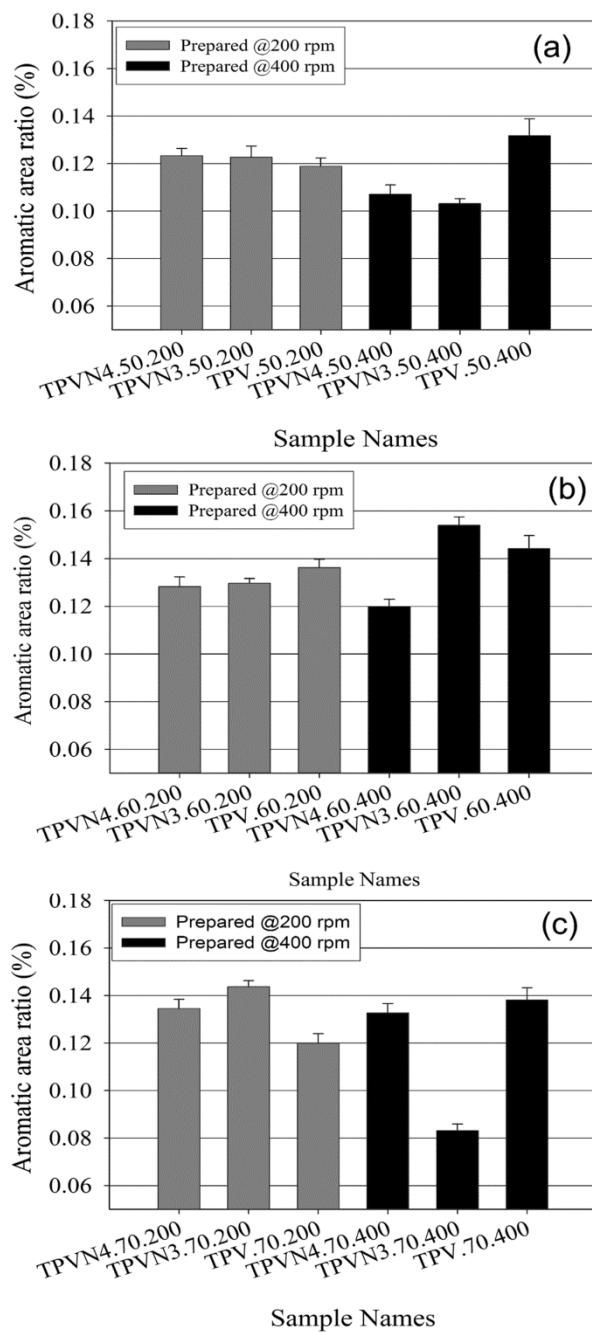


Figure 5-10. Aromatic area ratio of TPVs and TPV nanocomposites after extraction.

## 6.5 Conclusion

The effects of the presence and dispersion level of nanoclay on the extent of crosslinking in TPV nanocomposites were investigated, using a variety of characterization techniques, including rheology, gel content and NMR. It was found that a combination of all three techniques is required, in order to compare the values of the extent of crosslinking obtained under various reactive extrusion conditions. Dynamic vulcanization contributed to improved dispersion and intercalation, and, in some cases, it was possible to obtain partially exfoliated TPV nanocomposites. It was also found that the presence of nanoclay affects the crosslinking reaction not only through its barrier effect that increases the local concentration of curative agent but, more significantly, through its effect on the continuity index of the EPDM phase. In turn, the level of co-continuity, as reported in earlier work, depends on the degree of dispersion of nanoclay.

### Acknowledgements

The authors would like to acknowledge financial support from the Natural Sciences and Engineering Research Council of Canada (NSERC). We would like to thank Melina Hamdine and Leelapornpisit Weawkamol for experimental assistance.

## 6.6 References

1. A. M. Gessler and H. Haslee, United States Patent, 3037954, (1962).
2. W. K. Fischer and C. Woodbury, United States Patent, 284521, (1974).
3. P. K. Han and J. L. White, Rubber Chem. Technol. , 68,728 (1995).
4. S. Mishra, B. Baweja and R. Chandra, J. Appl. Polym. Sci., 74,2756 (1999).
5. I. Pesneau, M. F. Champagne and M. A. Huneault, Polym. Eng. Sci., 42,2016 (2002).
6. A. Y. Coran and R. P. Patel, United States Patent, 4104210, (1978).
7. C. Nakason, P. Wannavilai and A. Kaesaman, Polymer Testing, 25,34 (2006).
8. C. Nakason, P. Wannavilai and A. Kaesaman, J. Appl. Polym. Sci., 101,3046 (2006).
9. A. V. Machado and M. Van Duin, Polymer, 46,6575 (2005).
10. M. Van Duin and A. V. Machado, Polym. Degrad. Stabil. , 90,340 (2005).
11. K. Y. Lee and L. A. Goettler, Polym. Eng. Sci. , 44,1103 (2004).
12. A. A. Katbab and H. Mirzazadeh, Polym. Advan. Technol. , 17,975 (2006).
13. H. Thakkar, K. Y. Lee and L. A. Goettler, Phase Reinforcement Effects in TPV Nanocomposites. Society of Plastics Engineers, Nashville, TN, United States, pp. 3009 (2003).
14. G. Naderi, P. G. Lafleur and C. Dubois, Polym. Eng. Sci., 47,207 (2007).
15. G. Naderi, Thermoplastic elastomer nanocomposites based polypropylene and ethylene propylene diene terpolymer (PP/EPDM), in Thèse de doctorat (Ecole polytechnique de Montréal). École polytechnique de Montréal. Département de génie chimique pp. 203 (2006).
16. L. A. Utracki, Polymer blends handbook volume 2, Kluwer Academic Publishers, Dordrecht; London (2002).
17. A. Verbois, P. Cassagnau, A. Michel, J. Guillet and C. Raveyre, Polym. Int., 53,523 (2004).
18. A. Mirzadeh, P. G. Lafleur, M. R. Kamal and C. Dubois, Polym. Eng. Sci., 50,2131 (2010).

- 19.J. Lyngaae-Jorgensen, K. Lunde Rasmussen, E. A. Chtcherbakova and L. A. Utracki, *Polym. Eng. Sci.*, 39,1060 (1999).
- 20.J. Lyngaae-Jorgensen and L. A. Utracki, *Polymer*, 44,1661 (2003).
- 21.P. Potschke and D. R. Paul, *Polymer Reviews*, 43,87 (2003).
- 22.G. Dell'Anno, Development of a new class of hybrid reinforced thermoplastic composites based on nanoclays and woven glass fibers. University of Pisa (2004).
- 23.J. Park, K. Eom, O. Kwon and S. Woo, *Microsc. microana.*, 7,276 (2001).
- 24.P. A. Bhadane, N. Virgilio, B. D. Favis, M. F. Champagne, M. A. Huneault and F. Tofan, *AIChE J.*, 52,3411 (2006).
- 25.M. D. Ellul, A. H. Tsou and W. Hu, *Polymer*, 45,3351 (2004).
- 26.V. M. Litvinov, *Macromolecules*, 39,8727 (2006).
- 27.A. G. Altenau, L. M. Headley, C. O. Jones and H. C. Ransaw, *Anal.Chem.*, 42,1280 (1970).

**Chapter 7 MORPHOLOGY EVOLUTION AND THERMO MECHANICAL  
CHARACTERISTICS OF TPV NANOCOMPOSITES BASED ON  
PP/EPDM PREPARED BY REACTIVE EXTRUSION**

Amin Mirzadeh, Pierre G. Lafleur, Musa R. Kamal\* and Charles Dubois

Chemical Engineering Department, Ecole Polytechnique, PO Box 6079, Stn Centre- Ville,  
Montreal, QC H3C 3A7, Canada

\* Chemical Engineering Department, McGill University, 3610 University, Montreal, QC H3A  
2B2, Canada

## 7.1 Abstract

The rubber-like behaviour of thermoplastic vulcanizates (TPV), based on polypropylene/ethylene-propylene-diene M-class rubber (PP/EPDM), and their corresponding nanocomposites was investigated. The temperature Scanning Stress Relaxation (TSSR) method was used. Polypropylene nanocomposites, with different nanoclay dispersion levels, ranging from intercalated structures to a mixture of intercalated montmorillonite tactoids and exfoliated layers were used as the thermoplastic phase. A phenolic curing system was used to crosslink the rubber phase during the reactive extrusion process. The TSSR method provided useful information about the extent of the crosslinking reaction. Based on mechanical properties and the different criteria obtained by TSSR analysis, it was found that the presence of nanoclay would be more beneficial at high EPDM content in which the morphological studies suggested the existence of a network consisting of irregular shape rubber particles in vicinity of a small amount of the rubber droplets.

## 7.2 Introduction

The incorporation of nanoclay in polymer matrices is a more effective way to upgrade engineering properties of the materials and to expand their field of application, compared to the use of conventional micro composites<sup>1-8</sup>. More particularly, in the case of thermoplastic vulcanizate (TPV) production based on ethylene-propylene-diene-monomer/polypropylene (EPDM/PP), it is desirable to improve these properties by using the PP nanocomposites as the thermoplastic phase<sup>9-13</sup>. Since nanocomposite formation is thermodynamically driven, it can occur only with a negative free energy change. Therefore, maleic anhydride grafted polypropylene (PP-g-MA) is generally used as a compatibilizer<sup>1, 5, 14</sup>. The different grades of PP-g-MA affect the viscosity ratio, interfacial tension, mobility of the interface and the degree of exfoliation. Consequently, the co-continuous composition range changes<sup>15, 16</sup>. It has been shown that the two latter factors also affect the extent of crosslinking reaction<sup>17</sup>. Therefore different TPV characteristics and morphologies could be expected.

The present study attempts to characterize the rubber-like behaviour and engineering properties of TPVs and TPV nanocomposites with different dispersion levels of nanoclay in the precursor thermoplastic phase. The recently developed method temperature scanning stress

relaxation (TSSR) technique is used. The TSSR method is based on the stress relaxation test, which is conducted under non-isothermal conditions and has been developed recently to characterize the thermal-mechanical behaviour of thermoplastic elastomers. It has been suggested that certain useful characteristic parameters, such as the temperatures at which the initial force during the last step of TSSR decreases by 10%, 50% and 90% (namely  $T_{10}$ ,  $T_{50}$ ,  $T_{90}$  respectively) could be obtained from the resulting force–temperature curve of TSSR test<sup>18-21</sup>.  $T_{90}$  could be considered as the temperature limit. It has been shown that  $T_{50}$  correlates with compression set for the crosslinked rubber. Therefore, it has been proposed that this parameter could be considered as an alternative to the poorly reproducible compression set test method<sup>22</sup>.  $T_{10}$  is considered to be the temperature at which the relaxation process overcompensates the entropy effect<sup>20, 21</sup>. Furthermore, the rubber index (RI), which is a measure of rubber like behaviour, is calculated using the area under the force-temperature curve as follows<sup>19</sup>:

$$RI = \frac{\int_{T_0}^{T_f} \frac{F(T)}{F_0} dT}{T_f - T_0} \quad (6-1)$$

where  $T_0$  and  $T_f$  indicate the temperature interval (in the experimental window) and  $\frac{F(T)}{F_0}$  is the normalized force with respect to the initial force. No stress relaxation even at high temperature is expected for an ideal crosslinked elastomer. In this case, the area under the experimental curve divided by the length of the temperature interval becomes unity. Thus, a greater rubber index value reflects more rubber-like temperature behaviour of the examined TPV<sup>20</sup>. The TSSR test yields additional information about the crosslink density of the material.

Vennemann et al.<sup>19</sup> based on the theory of rubber elasticity determined the crosslink density of the EPDM phase. The results were in good agreement with results obtained from conventional swell measurements. However, it was pointed out that more studies should be carried out on TPVs with complex formulations, in order to establish the method for commercial materials. It was suggested that the maximum slope of the force-temperature curve in the initial part of the curve could be used to determine the temperature coefficient ( $\kappa$ ), according the following equation when strain ratio ( $\lambda$ ) is higher than 1.1<sup>19, 23</sup>.

$$\kappa = \left(\frac{\partial \sigma}{\partial T}\right)_{\lambda, P} \quad (6-2)$$

where  $\sigma$  is the mechanical stress and  $T$  is absolute temperature. On the other hand, crosslink density can be calculated according to the theory of rubber elasticity and the experimentally obtained temperature coefficient <sup>24</sup>:

$$\frac{\rho}{M_c} = \frac{\kappa}{R \cdot (\lambda - \lambda^{-2})} \quad (6-3)$$

where  $\rho$  is the mass density,  $\lambda$  is the strain ratio of the sample and  $R$  the universal gas constant.  $M_c$  is the effective molar mass of chains between elastically active junction points.

The present study is a continuation of our previous work on TPE and TPV nanocomposites. According to these early results <sup>16</sup>, the following observations were made: *(i)* the mobility of the compatibilizer is the key parameter that determines the dispersion level in nanocomposites; higher relaxation times of the compatibilizer were associated with better dispersion of nanoclay. This observation was considered in the material selection part of this work, in order to prepare polypropylene nanocomposites with different dispersion levels as the thermoplastic component besides neat polypropylene. *(ii)* The incorporation of clay resulted in a reduction of the continuity index of the EPDM phase in corresponding TPEs. The effect was more pronounced in the intercalated nanocomposites than in partially exfoliated nanocomposites. *(iii)* The presence of nanoclay affects the crosslinking reaction, not only through its barrier effect that increases the local concentration of curative agent, but, more significantly, through its effect on the continuity index of the EPDM phase in the corresponding TPEs formed during the initial step of TPV production <sup>17</sup>.

In the present paper, we attempt to determine how the dispersion level of nanoclay and, consequently, the extent of crosslinking change the rubber-like behaviour and the morphology of the prepared TPVs.

## 7.3 Experimental Procedures

### 7.3.1 Materials

The materials selected for the present study were chosen, in view of our previous works<sup>16, 17</sup>. General purpose polypropylene (PP) homopolymer resin, “Profax” 6523 (Basell Polyolefins), was used as the thermoplastic phase. “Buna” EP T 6470 (LANXESS Corporation) ethylene-propylene-diene M-class rubber (EPDM), with ethylidene norbornene (ENB) as diene was used as the rubber phase. Cloisite 15A (Southern Clay Products), which is a surface modified montmorillonite with di-methyl, di-hydrogenated tallow ammonium chloride, was used as the nanoclay. The decomposition temperature of the modifier (240 °C) is higher than the processing temperature used in this study. On the other hand, the modifier is more compatible with polyolefins, as compared to the modifiers used with other grades of Cloisite. Two grades of maleic anhydride-grafted-polypropylene (PP-g-MA), Orevac CA 100 and Orevac 18750 (Arkema), were chosen as compatibilizers, based on our previous study<sup>16</sup>, to prepare polypropylene nanocomposites with different clay dispersion levels. Irganox B 225 (Ciba) antioxidant was used, in order to prevent oxidative degradation of the thermoplastic phase. Dimethylol phenolic resin or octylphenol-formaldehyde resin (SP-1045) manufactured by Schenectady International Inc. was used as the curing agent, along with stannous chloride dihydrate ( $\text{SnCl}_2 \cdot 2\text{H}_2\text{O}$ ; Merck) as the catalyst.

### 7.3.2 Blend Preparation and Nomenclature

Initially, a laboratory scale co-rotating, closely intermeshing, twin-screw extruder (Liestritz ZSE-18HP) was used to prepare masterbatches consisting of PP/PP-g-MA/Cloisite15A with the same composition (60/30/10 wt %) and different compatibilizer grades. The nanoclay was fed to the extruder through the side feeder, in the zone where the granules were partially melted. The temperature profile of the extruder was maintained at 185, 190, 195, 195, 195 and 190 °C from the hopper to the die and the screw was fixed at 200 rpm. Then, in order to prepare polypropylene nanocomposites with 5 wt% of Cloisite 15A, the pellets of the masterbatches were mixed with the PP, using the same twin screw extruder. Here the temperature profile in the extruder was 175,180,185,190,190,185 °C from the hopper to the die and the screw speed was held at 600 rpm. A small amount (0.5 wt.%) of Irganox B 225 antioxidant was added to the

mixture to reduce the oxidative degradation of PP. Polypropylene nanocomposites were designated as N3 and N4, where numbers 3 & 4 refer to the compatibilizer used in the composition (Orevac CA100 and Orevac 18750, respectively). Finally TPVs and TPV nanocomposites were prepared at 50, 60 and 70 wt% of EPDM using the above mentioned twin screw extruder at screw rotation speeds of 200 and 400 rpm. The rubber phase was dynamically vulcanized using 5 phr phenolic curing agent (SP-1045, Schenectady) in combination with 1 phr Stannous Chloride. Everywhere throughout this article, TPVs and TPV nanocomposites will be respectively referred to as the TPV.xx.yy and TPVN.c.xx.yyy. Here “c” determines the nanocomposite used in the composition (N3 or N4). “xx” and “yyy” represent the EPDM content (wt%) and screw rotation speed, respectively. Therefore, for example, TPV.50.400 stands for the blend prepared based on neat PP (without nanoclay) with 50 wt% of EPDM prepared at screw speed of 400 rpm.

### **7.3.3 Sample Preparation and Characterization Steps**

#### **7.3.3.1 X-ray Diffraction**

To evaluate the dispersion of nanoclay in the prepared compounds, X-ray diffraction (XRD) was performed at room temperature using an X-ray diffractometer (Philips model X'PER) in the low angle range of  $2\theta$ . The X-ray source was Cu-K<sub>a</sub> radiation ( $\lambda = 1.540598$  angstroms) using a 50 kV voltage generator and a 40 mA current. The angular step size was  $0.005^\circ$  with a step time equal to 1 second from  $2^\circ$  to  $10^\circ$  and  $0.5^\circ$  to  $4^\circ$ . A simplified model of the system suggested by Dell'Anno<sup>25</sup> to reduce the X-ray beam intensity in the range of  $0.5^\circ$  to  $4^\circ$  was used. The setup comprised of a thin steel knife and cylindrical base as a sample holder to prevent edge effect. Great care was taken to adjust the setup in a manner that the upper surface of the sample touched the edge of the knife entirely and to align the edge of the knife with the X-ray generator and detector. More detail could be found in previous publications<sup>16, 25</sup>.

#### **7.3.3.2 Electron Microscopy**

Scanning electron microscopy (SEM) and transmission electron microscopy (TEM) were used to study nanoclay dispersion in the thermoplastic phase. A Leica-Jung RM 2065 microtome equipped with a cryochamber was used to cut the samples, using a glass knife under liquid nitrogen. In order to observe nanoclay dispersion, the amorphous phase of polypropylene was

removed chemically by the method provided by Park et. al.<sup>26</sup>. Subsequently, the samples were coated with gold–palladium alloy to obtain SEM micrographs using a scanning electron microscope (JSM 840, Jeol). To observe the morphology of the prepared TPVs, samples taken along the screw axis were quenched in liquid nitrogen and then embedded in the amine based epoxy resin. Finally they were microtomed and etched using the vapour of boiling xylene. Different exposure times (i.e. 1,3,5,7,15 (s)) were examined to find out the proper etching time. The samples were held about 2 cm away from the boiling xylene surface level. The proper exposure time was found 3-5 (s). The prepared samples were coated with gold–palladium alloy to obtain SEM micrographs using a scanning electron microscope. For TEM, trimmed polypropylene nanocomposites were ultra-microtomed at -130 °C using a diamond knife to prepare samples with thickness of 50 nm. A water bath was used to transfer the micro-thin sections to 200-mesh copper grids. TEM micrographs were recorded with a digital camera of the transmission electron microscope (JEM-2100F, Jeol).

### **7.3.3.3 Temperature Scanning Stress Relaxation (TSSR) and Tensile Testing**

The TSSR was performed in three steps, using the tensile machine equipped with programmable and electrically heated test chamber. In the first step, a constant tensile strain of at least 50% was applied to the dumbbell test piece. It was followed by preconditioning at room temperature for two hours to reach a quasi equilibrium state and to take place the short time relaxation processes. Finally, the sample was heated at a constant low rate of 2 °C/min from room temperature to 150 °C linearly. Using at least six dumbbells (type 5, ASTM D412) of each sample, the tensile properties also were determined using a strain rate of 100 mm/min.

## **7.4 Results and Discussion**

### **7.4.1 Nanocomposite Characterization**

Three characteristic peaks are shown in Fig. 1a for Cloisite 15A. The first one at  $2\theta = 2.85^\circ$  (corresponding d-spacing is 3.1 nm), the second is a shoulder in vicinity of the first one at  $2\theta = 4.6^\circ$  (corresponding d-spacing is 1.9 nm), and the third peak at  $2\theta = 7.17^\circ$  (corresponding d-spacing is 1.1 nm). The d-spacing of the clay is 1.1 nm therefore the latter is attributed to the portion of the clay that remained unmodified.

According to the XRD pattern of N4 (Fig. 6.1a), the intercalation of polymer chains into galleries of nanoclay shifts the first peak of Cloisite 15A to the lower angle of  $2\theta = 2.42^\circ$  (corresponding d-spacing of 3.8 nm; original  $2\theta \cong 2.85^\circ$ , d-spacing of about 3.1 nm). However the second and the third peaks of Cloisite 15A could be found almost at their original angles.

On the other hand, N3 nanocomposites show only two peaks in the range of  $2^\circ$  to  $10^\circ$  (Fig. 6.1a). The first observed peak at  $2\theta \cong 2.64^\circ$  corresponds to d-spacing of about 3.3 nm and the second peak is at  $2\theta \cong 6.5^\circ$ . It is likely that these two peaks are related to the second and third peaks of Cloisite 15A at  $2\theta \cong 4.6^\circ$  and  $2\theta \cong 7^\circ$ , respectively. The evidences like TEM and SEM micrographs (Fig. 6.2 and Fig. 6.3) show better dispersion level of nanoclay in N3 compared to N4 nanocomposites. Therefore, it can be inferred that the first characteristic peak of Cloisite 15 A was shifted to the angle lower than  $2\theta = 2^\circ$  and the detector could not detect this portion of nanoclay layers due to the high intensity of the X-ray beam.

To examine this assumption, using the setup described in the experimental section and after optimization of sample thickness, slit size, frame size, starting angle and scan rate to obtain reproducible data, X-ray scans were performed in the range of  $2\theta = 0.5^\circ$  to  $2\theta = 4^\circ$  (Fig. 6.1b).

It is suggested that the peak observed in Fig. 6.1b at  $2\theta = 1.05^\circ$  corresponding to d-spacing of 8.5 nm for N3 (in the range of  $2\theta = 0.5^\circ$  to  $2\theta = 2^\circ$ ) is attributable to some exfoliation of Cloisite 15A, with the original d-spacing of about 3.1 nm (at  $2\theta \cong 2.8^\circ$ ). As expected no peak in the range of  $2\theta = 0.5^\circ$  to  $2\theta = 2^\circ$  was found in pure polypropylene and N4 nanocomposites.

Therefore, the XRD analysis (Fig. 6.1b) suggests a coexistence of intercalated MMT tactoids and exfoliated MMT layers in N3 nanocomposite. For the purpose of further discussion, this PP nanocomposite (N3) will be referred to as the “partially exfoliated” nanocomposite.

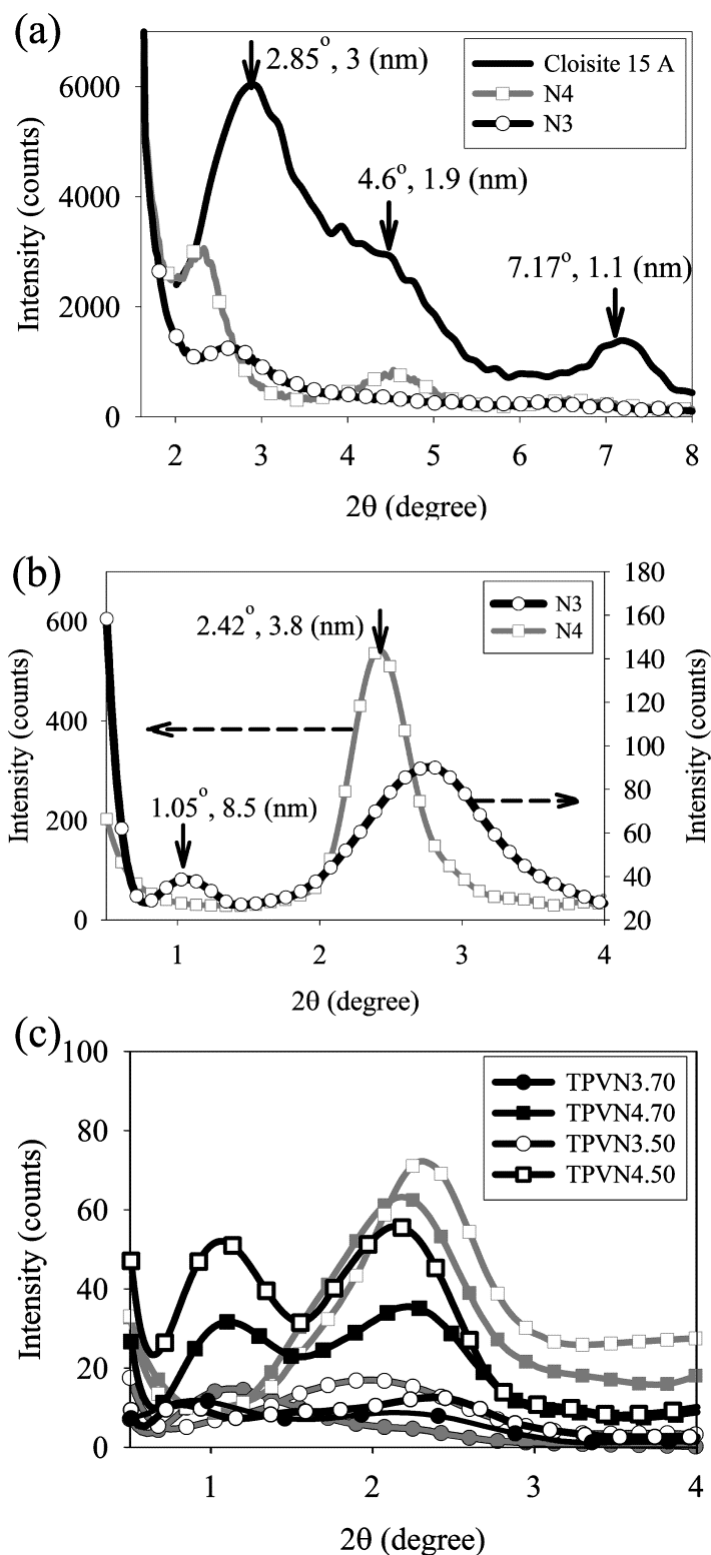


Figure 6-1. XRD patterns of Cloisite 15A, PP nanocomposites and TPV nanocomposites prepared at screw speed of 200 rpm (gray) and 400 rpm (black).

The TEM images shown in Fig. 6.2b and Fig. 6.2c confirm the “partially exfoliated” structure of N3 as suggested by XRD results obtained by the mentioned setup.

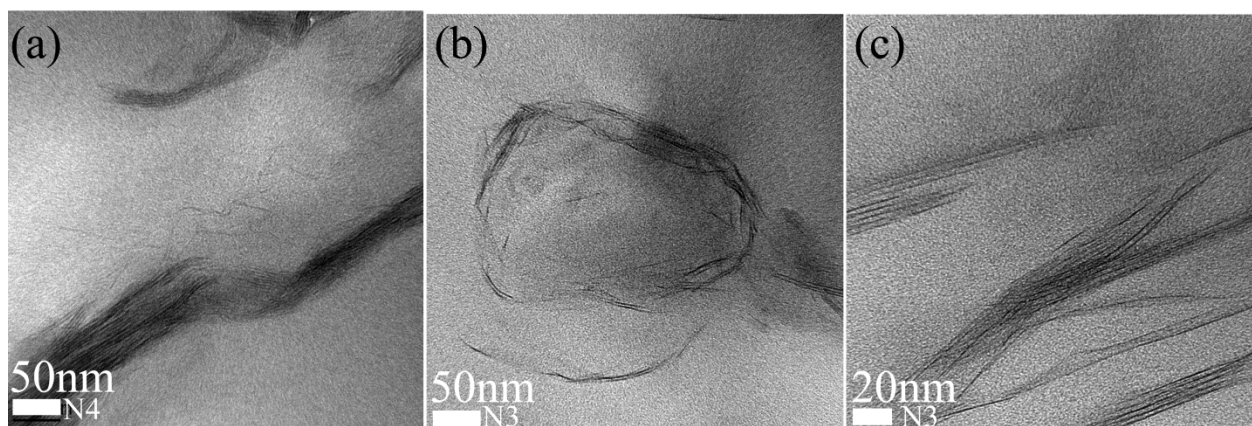


Figure 6-2. TEM micrographs of N4 (a) and N3 (b and c) polypropylene nanocomposites.

The larger intercalated tactoids could be observed in TEM micrographs (Fig. 6.2a) for N4 nanocomposite. Since the XRD results could be altered by the low quality of nanoclay dispersion, the uniformity of the prepared samples was also investigated by SEM. Fig. 6.3 reflects good mixing quality and shows that the agglomerates were uniformly dispersed in the matrix.

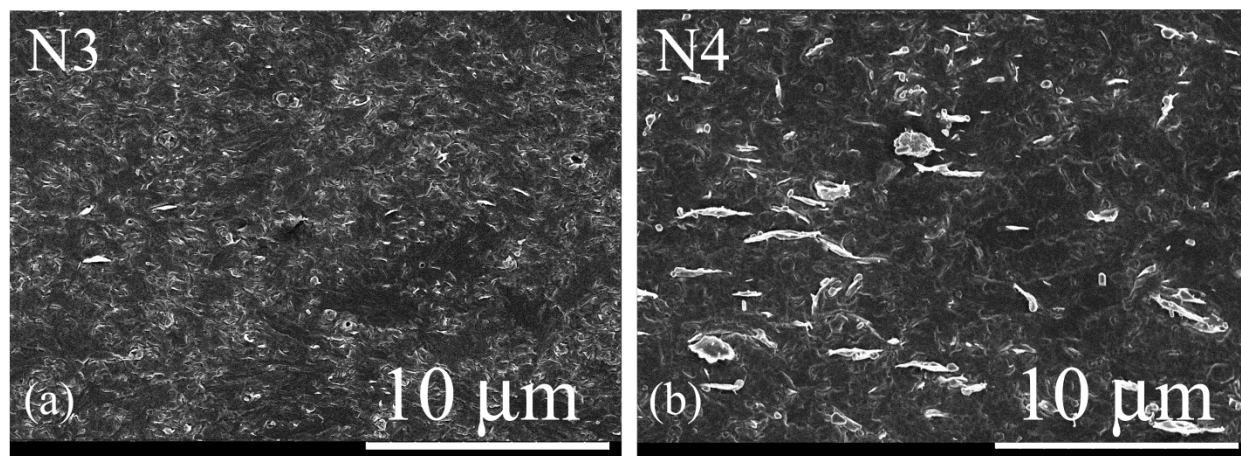


Figure 6-3. SEM images of N3 (a) and N4 (b) polypropylene nanocomposites after removing the amorphous phase.

It seems that a higher shear stress is applied on the nanoclay layers during dynamic vulcanization. Hence, the peak at  $2\theta = 2.42^\circ$  in XRD patterns of TPVN4 nanocomposites prepared at screw speed of 200 rpm (Fig. 6.1c) is broader than the corresponding narrow peak of N4 (Fig. 6.1b). By increasing EPDM content, polymer intercalation was enhanced slightly.

Intercalation of polymer chains into the interlayer galleries of the nanoclays is more pronounced for the samples prepared at higher screw speed (400 rpm). The observed peak at  $2\theta = 0.94^\circ$  (corresponding d-spacing is about 9.3 nm) is related to the portion of nanoclay layers in N4 nanocomposites that their corresponding peak had been observed at  $2\theta = 2.42^\circ$  before dynamic vulcanization.

#### 7.4.2 Crosslink Density of TPVs

It is known that with increasing the strain ratio, the slope of the nearly linear stress-temperature curves changes from negative to positive values<sup>27</sup>. According to the definition, thermoelastic inversion is a point at which this slope is zero. Under the condition of the present TSSR technique, where the strain ratio is constant and exceeds a value of 1.1 (above the thermoelastic inversion point), the thermal expansion coefficient of the stretched TPV is also negative<sup>19, 20</sup>. The thermal stress relaxation of the thermoplastic phase over-compensates the entropy effect at higher temperatures. Therefore, an increase of stress with temperature is recognized only in the initial part of the stress-temperature curve. Thus, the maximum slope in this range (below 40 °C) was used to calculate the crosslink density according to Eq. 6.3.

Fig. 6.4 shows the crosslink density of the TPVs and TPV nanocomposites prepared at screw speeds of 200 rpm and 400 rpm. The effect of nanoclay presence and processing conditions on the extent of crosslinking reaction was investigated in our previous publication using other methods<sup>17</sup>. Here, we discuss the present results regarding crosslink density values reported in Fig. 6.4, in light of the previous findings obtained with solid state NMR for the same samples.

At the lower screw speed (residence time of ~ 65 s), Fig. 6.4 shows negligible difference in crosslink density for the samples containing 50 and 60 wt% of EPDM. It seems that the effect of the presence of nanoclay on the crosslink density is more pronounced for the samples prepared at higher screw speed (residence time of ~ 45 s). Crosslink density decreases by incorporation of the nanoclay in the system containing 50 wt% of EPDM (Fig. 6.4). The previous work showed that the reduction in extent of crosslinking is associated with the lower continuity index of EPDM in the corresponding precursor TPE nanocomposites<sup>17</sup>. The definition and the method to evaluate the co-continuity index could be found elsewhere<sup>15, 16</sup>.

The observed co-continuous structure (Fig. 6.5), which is formed before the second mixing zone, is not only controlled by initiation of dynamic vulcanization but also by the presence of nanoclay. The continuity index values of the rubber phase were reported as  $\sim 0.6$ ,  $\sim 0.85$  and  $\sim 1$  for the corresponding blends based on N4 (intercalated nanocomposite), N3 (partially exfoliated nanocomposite) and neat PP when prepared at 50wt% of EPDM, respectively<sup>17</sup>. The lower continuity index of EPDM in co-continuous blend leads the lower interfacial surface halting the curative diffusion process and crosslinking reaction.

Since the reduction in EPDM continuity by nanoclay presence is more prominent in the system based on intercalated nanocomposite (N4)<sup>16</sup>, by increasing the EPDM content to 60wt%, continuity index of EPDM remains less than unity ( $\sim 0.8$ ) but EPDM becomes a continuous rubber phase in the blends based on partially exfoliated PP nanocomposites. Therefore, as seen in Fig. 6.4, crosslink density of TPVN4.60.400 is lower than TPV.60.400, while it increases significantly for TPVN3.60.400 (TPV based on partially exfoliated nanocomposite).

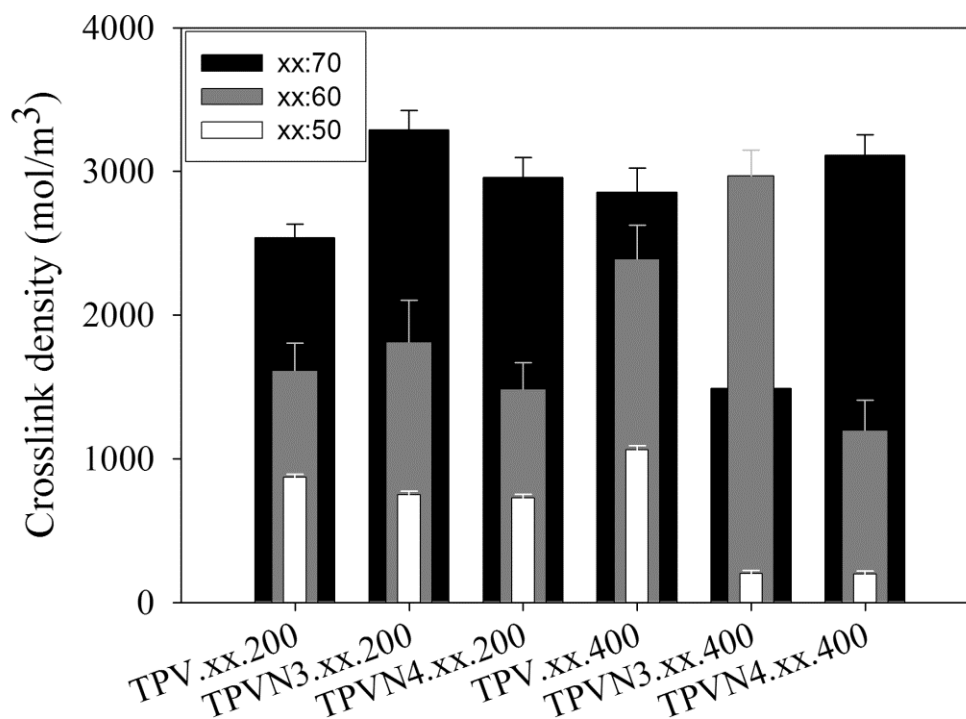


Figure 6-4. Crosslink density values of the TPVs and TPV nanocomposites containing 50 wt%(white), 60 wt%(gray) and 70 wt%(black) of EPDM prepared by twin screw extruder.

It should be mentioned here that the crosslinking reaction proceeds initially at the outer envelope of the EPDM phase, and continues toward the center of EPDM threads in dynamic vulcanization<sup>28</sup>. Therefore, the higher crosslink density of the partially exfoliated TPV nanocomposites (TPVN3.60.400), as compared to TPV.60.400, is probably related to the barrier effect caused by nanoclay, which results in higher local concentration of the curative agent in the outer envelope of EPDM domains. This explanation is supported by the fact that the extent of crosslinking reaction increases by increasing the curative concentration, as reported for different systems<sup>19, 29-31</sup>. The barrier effect leads to greater crosslink density for all the TPV nanocomposites, compared to TPVs at 70 wt% EPDM, where the rubber phase is fully continuous in all the corresponding TPEs (Fig. 6.4). The degradation of the phenolic resin at the beginning step of intensive exothermic reaction could explain the low crosslink density value for TPVN3.70.400.

### **7.4.3 Correlation between Morphology and Rubber like Behavior**

In this section, we investigate the correlation between the thermo-mechanical properties (the rubber like behaviour) of the blends with morphology evolution. This would allow us to evaluate the advantages of incorporating the nanoclay in the system.

#### **7.4.3.1 TPVs Containing 50 wt% and 60 wt% of EPDM**

By definition, the final morphology of TPVs is characterized by fully cured rubber particles dispersed in a continuous thermoplastic matrix. The results show that morphology development along the extruder axis is somehow similar for the blends incorporating 50 wt% and 60 wt% EPDM.

Figure 6.5 depicts the evolution of morphology along the extrusion direction for TPVs and TPV nanocomposites at 60 wt% EPDM during dynamic vulcanization. These results show the blend morphology of samples taken in the first mixing zone, the second mixing zone, the third mixing zone and the die exit for TPV and TPV nanocomposites prepared at screw speed of 400 rpm.

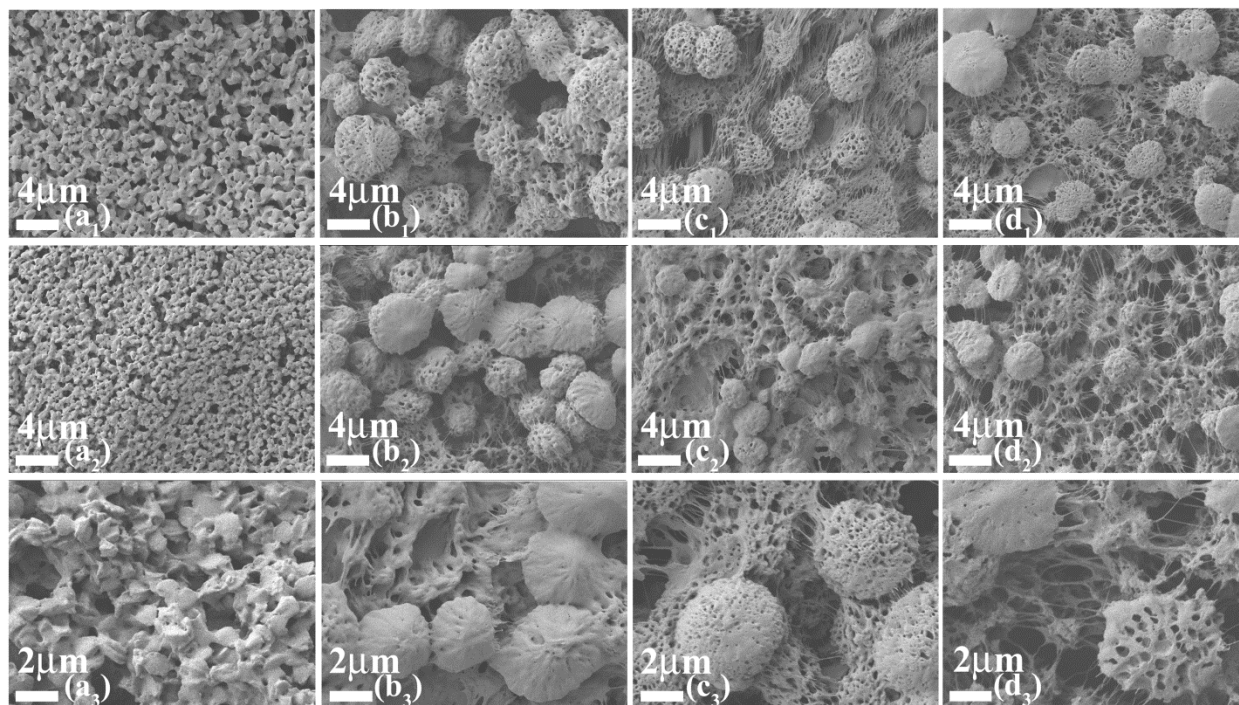


Figure 6-5. SEM micrographs of TPV60 ( $X_1$ ; the first row ), TPVN3.60 ( $X_2$ :the second row) and TPVN4.60 ( $X_3$ :the third row) for the samples taken at the first mixing zone (a), the second mixing zone (b), the third mixing zone (c) and the die exit (d).

The coarse co-continuous structure observed in the first mixing zone changes to droplet matrix morphology, as a result of dynamic vulcanization. The break-up of highly elongated threads leads to a line of small droplets (Fig. 6.5). Morphology evolution continues by the break-up of these droplets into smaller droplets and their transition to a network made by irregular rubber particles in the second and the third mixing zones. The SEM micrographs of the samples taken from the die exit depict the coexistence of rubber droplets in vicinity of the smaller irregular rubber particles that are connected to each other by some rubber fibrils (Fig. 6.5). The existence of irregular shape rubber particles was also observed by Shahbikian et al. using the AFM technique<sup>32</sup>.

In the blends containing 50 wt%, the network of irregular shape rubber particles is not fully developed and there is a number of rubber droplets in the SEM micrographs. The number of the droplet-like domains decreases in the blends containing 60 wt% EPDM (more irregular shape rubber particles were formed). As seen in Fig 6.5, the droplets are not smooth. The nanometer size voids on their surface had been filled by PP chains prior to the extraction process.

According to the SEM micrographs, incorporation of nanoclay causes the rubber particle size to decrease (the number average droplet diameter was found to be  $\sim 4.1 \mu\text{m}$ ,  $3.8 \mu\text{m}$  and  $\sim 3.1 \mu\text{m}$  for TPV60.400, TPVN4.60.400 and TPVN3.60.400, respectively). It should be pointed out that in estimating the droplet size, only the droplet-like rubber domains were used, not the irregular rubber particles forming the network. Upon lowering screw speed, the increase in number average droplet diameter was more pronounced for TPV without nanoclay, which reached  $\sim 5.2 \mu\text{m}$ , while it remained almost unchanged for TPV nanocomposites.

The above morphological observations could be used to explain the behavior of the blends with 50 wt% and 60 wt% in TSSR analysis, which is a very important criterion with respect to TPV applications, especially at elevated temperatures. Since the rubber phase is not a fully developed continuous phase at the end of the reactive extrusion, stress relaxation upon increasing the temperature occurs by retraction (short time) and reptation (long time) mechanism. According to Fig. 6.6, it seems that rubber index does not correlate directly with the crosslink density for the blends containing 50wt% and 60 wt% EPDM. In turn the observed behavior could be explained by considering the rubber droplet size, the crosslink density and using the deformation mechanism models for TPVs that are based on the deformation of thin PP films between the elastomer particles<sup>33, 34</sup>. It has been shown that the PP films yield in the equatorial region of the elastomer particles during deformation. Upon temperature increase and thermoplastic phase relaxation, the crosslinked rubber droplets retract due to the entropy effect. Therefore, at the beginning stage of the curves, force is slightly increased with increasing temperature. Thereafter, at higher temperature, more retraction of the rubber phase causes the wrinkling and buckling of the softened and constrain-released thermoplastic chains that cannot deform elastically<sup>34-36</sup>. This buckling mechanism has been confirmed by tensile testing and AFM studies during deformation of TPVs<sup>33, 36, 37</sup>. Therefore, by increasing the crosslink density (increasing the retraction force) and/or decreasing the rubber particle size (increasing the number of retracting droplets) the wrinkling and buckling phenomenon causes severe stress relaxation in the blends, showing the droplet matrix morphology. However, the presence of nanoclay could hinder PP chain buckling to some extent. As seen in Fig. 6.6a, TPV.50.200 ( $D_n \approx 5.6 \mu\text{m}$ ) shows higher rubber index compared to the corresponding TPV nanocomposites (TPVN4.50.200;  $D_n \approx 4.1 \mu\text{m}$  TPVN3.50.200;  $D_n \approx 3.6 \mu\text{m}$ ), whereas their crosslink densities are in the same range.

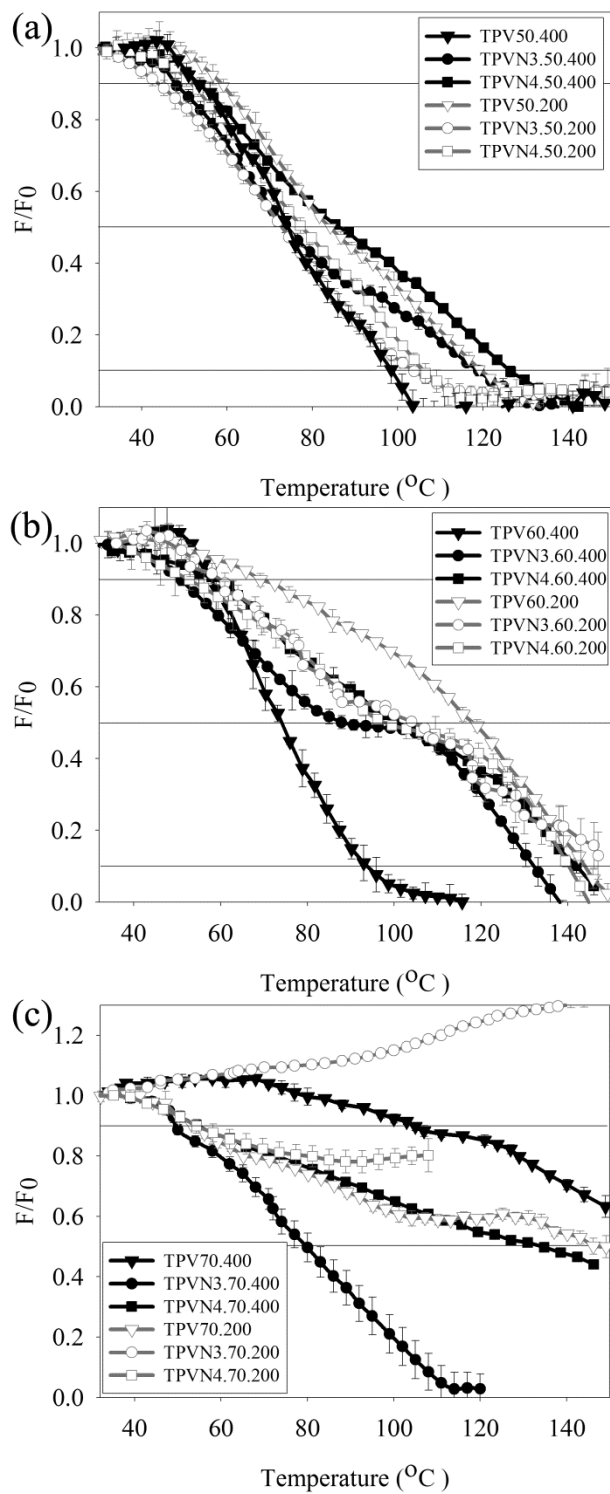


Figure 6-6. Normalized force – temperature curves of TPVs and TPV nanocomposites samples containing 50 wt%(a), 60 wt%(b) and 70 wt%(c) of EPDM obtained from TSSR measurements.

By increasing the screw speed, the reduction in crosslink density of the TPV nanocomposites (TPVN3.50.400 and TPVN4.50.400) compared to the corresponding nanocomposites prepared at lower screw speed (TPVN3.50.200 and TPVN4.50.200) leads to detectable improvement in rubber-like behaviour, because the droplet size in TPV nanocomposites changes slightly at different screw speed (200 rpm and 400 rpm). On the other hand, the increase in crosslink density, along with rubber droplet size reduction in TPV50.400 ( $D_n \approx 4.4 \mu\text{m}$ ) (compared to TPV50.200;  $D_n \approx 5.6 \mu\text{m}$ ) results in the lowest rubber index among corresponding blends.

A similar explanation could be used for the TSSR analyses of the TPVs prepared at 60 wt% EPDM. As seen in Fig. 6.6b, the rubber index values (the area under the normalized force-temperature curves) for TPV nanocomposites with 60wt% EPDM are almost in the same range and remain between those of TPV60.200 and TPV60.400. This could be meaningful from manufacturing point of view.

#### **7.4.3.2 TPVs Containing 70 wt% of EPDM**

The results of TSSR analyses for TPVs prepared at 70wt% of EPDM (Fig. 6c) show that the stress does not relax completely within the experimental window, except for the TPV based on partially exfoliated PP nanocomposite. This sample was prepared at high screw speed (TPVN3.70.400), and possibly experienced thermal degradation of the curing agent.

Fig. 6.7 demonstrates that, in the TPV (without nanoclay) containing 70 wt% EPDM, the thick threads of EPDM in the first mixing zone become thinner in the second mixing zone. The breakup of these thin threads to become a line of small droplets happens in the third mixing zone. Thus, the TPV nanocomposites reach this morphological state sooner (in the second mixing zone) than TPVs without clay (in the third mixing zone).

The deformation of these droplets under the high shear stress produces much finer morphology and a more extensive network formed by small irregular rubber particles, compared to the blends prepared at lower EPDM content. The observed morphology evolution seems to be in agreement with the conceptual mechanism of morphology development in thermoplastic vulcanizates proposed by Bhadane et al.<sup>28</sup>. They mentioned that a network (namely  $\beta$ -network) forms as a result of the viscosity mismatch between the non-crosslinked (in the center of rubber

phase) and crosslinked EPDM (at the outer envelope of the rubber domains), during the dynamic crosslinking.

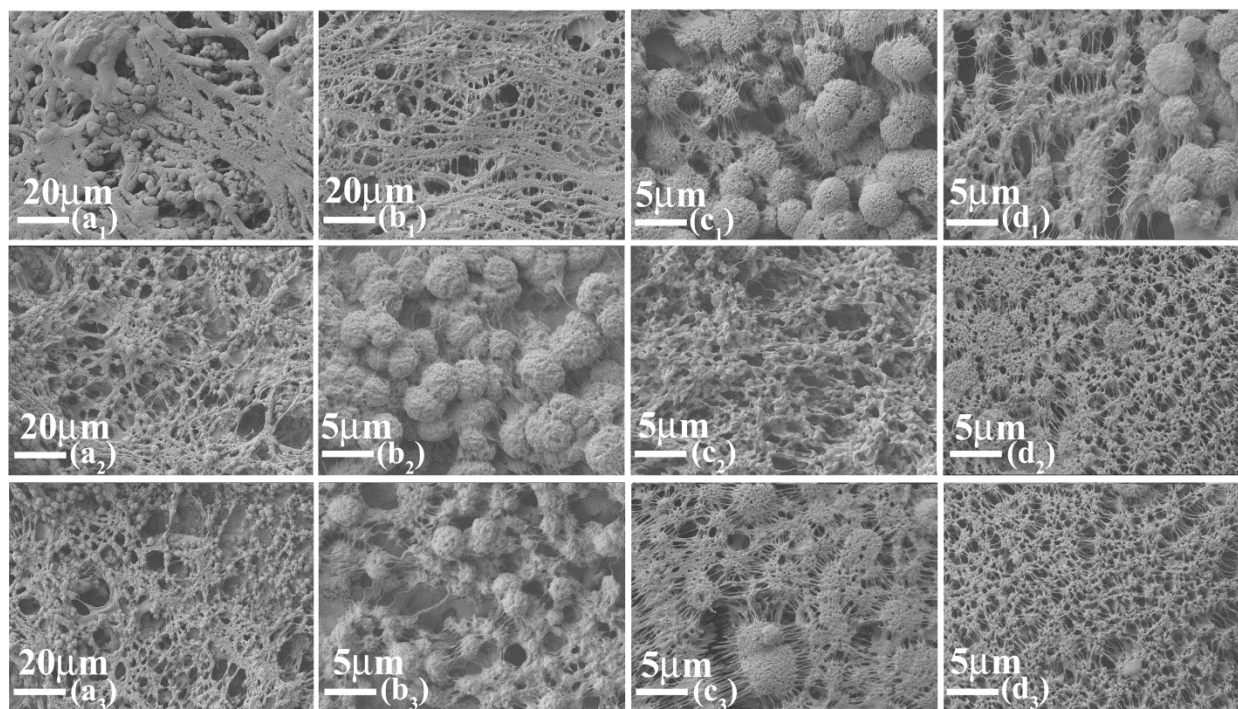


Figure 6-7. Figure 7. SEM micrographs of TPV70 ( $X_1$ ; the first row), TPVN4.70 ( $X_2$ ; the second row) and TPVN3.70 ( $X_3$ ; the third row) for the samples taken at the first mixing zone (a), the second mixing zone (b), the third mixing zone (c) and the die exit (d).

This kind of network and high crosslink density value are responsible for the observed high rubber like behaviour for these blends, especially for the sample based on semi exfoliated nanocomposite (TPVN3.70.200). The rubber network is constrained and cannot retract easily during TSSR tests. Therefore, thermal stress relaxation takes place more slowly and not under the influence of the buckling mechanism. According to Fig. 6.4 and Fig. 6.6c, a direct relation was found between the crosslink densities and rubber index values for the blends showing fully developed extensive network between irregular shape rubber domains (blends containing 70 wt% EPDM).

#### 7.4.4 Tensile Properties

The tensile properties of the TPVs and TPV nanocomposites are summarized in Table 6.1. For TPVs without nanoclay, tensile moduli are slightly higher for the blends prepared at screw speed of 400 rpm, compared to those of TPVs prepared at lower screw speed (200 rpm).

Table 6-1. Tensile properties of TPVs and TPV nanocomposites.

Sample name	Tensile modulus (MPa)	Elongation at break (%)	Tensile strength (MPa)
TPVN4.50.200	87.4	105	10.1
TPVN3.50.200	126.8	131	12.8
TPV.50.200	68.5	609	14.0
TPVN4.50.400	76.0	208	9.7
TPVN3.50.400	94.3	224	10.4
TPV.50.400	74.1	873	17.5
TPVN4.60.200	50.2	180	8.4
TPVN3.60.200	55.2	454	10.7
TPV.60.200	32.5	737	11.3
TPVN4.60.400	48.0	293	9.0
TPVN3.60.400	58.0	525	11.2
TPV.60.400	35.1	810	13.8
TPVN4.70.200	24.4	343	7.0
TPVN3.70.200	26.9	768	11.4
TPV.70.200	17.8	861	11.7
TPVN4.70.400	26.2	569	9.1
TPVN3.70.400	13.4	1435	9.7
TPV.70.400	21.0	1023	14.3

According to the literature, an increase in tensile modulus would be always expected upon incorporating the nanoclay in non-reactive TPVs (adding nanoclay to the commercially available TPVs) <sup>10, 13</sup>. However, in the reactive blends, the effect of nanoclay presence on the tensile modulus is more complicated, due to the effect of clay on the extent of crosslinking reaction. The tensile moduli of the TPV nanocomposites prepared at high screw speed are lower or higher (~0.63 to ~1.7 times, depending on blend composition) than those of the corresponding TPVs. However, for the TPV nanocomposites prepared at lower screw speed (200 rpm) showing almost the same extent of crosslinking, the tensile moduli of the nanocomposites are always higher (up to ~1.85 times) than those of corresponding TPVs without nanoclay. The increase is more pronounced for the samples prepared based on partially exfoliated PP (TPVN3).

Table 6.1 shows that elongation at break for TPV nanocomposites is significantly lower than that of corresponding TPVs without nanoclay, especially at 50 wt% of EPDM. However, by

increasing the EPDM content, elongation at break reaches levels comparable to those of commercial TPV materials. The tensile strength at break of TPV nanocomposites with 50 wt% of EPDM was lower than for the corresponding TPV without nanoclay. The presence of nanoclay tactoids causes an induced local stress concentration within the blends<sup>13</sup>. Accordingly, the response of TPV nanocomposites during tensile deformation leads to the observed lower tensile strength. By increasing EPDM content to 60 wt% and 70 wt%, stress hardening behaviour was observed, even for TPV nanocomposites. Thus, the tensile strength was in the same level or slightly lower, compared to the corresponding blends without nanoclay.

## 7.5 Conclusion

Temperature scanning stress relaxation (TSSR) was used to evaluate the effect of nanoclay presence and its dispersion level on the crosslink density and rubber like behaviour of the TPV nanocomposites based on PP/EPDM prepared by reactive extrusion. SEM micrographs for some samples suggested the presence of irregular shape rubber particles in the vicinity of the rubber droplets with a low level of interconnectivity (blends containing 50wt% and 60wt% of EPDM). For these samples, the rubber like behaviour correlates with the rubber droplet size. Therefore, nanoclay presence affects the rubber index values mainly through its effect on the size of the rubber droplets that controls the number of retraction points in the proposed buckling mechanism.

In this composition range, the screw speed does not change the rubber droplet size in nanocomposites significantly. Thus, the rubber like behaviour of TPV nanocomposites is limited between those of the corresponding TPVs prepared at the different screw speeds (200 and 400 rpm). On the other hand, the direct relation between rubber index values and the crosslink density was observed only for those TPVs showing a fully developed extensive network between irregular shape rubber domains (blends containing 70wt% of EPDM). Hence, the effect of nanoclay presence and its dispersion level on the rubber-like behaviour is through its effect on the crosslink density.

## Acknowledgments

The authors would like to acknowledge financial support from the Natural Sciences and Engineering Research Council of Canada (NSERC). The authors would also like to thank Prof.

Vladimir Brailovski and Karina Inaekyan from École de Technologie Supérieure (Montreal) for TSSR measurements.

## 7.6 References

1. P. Reichert, H. r. Nitz, S. Klinke, R. Brandsch, R. Thomannand R. Mülhaupt, *Macromolecular Materials and Engineering*, 275, 8-17 (2000).
2. P. Svoboda, C. Zeng, H. Wang, L. J. Leeand D. L. Tomasko, *Journal of Applied Polymer Science*, 85, 1562-1570 (2002).
3. S. Sinha Rayand M. Okamoto, *Progress in Polymer Science (Oxford)*, 28, 1539-1641 (2003).
4. F. P.-S. M. Ton-That, K C. Cole,M N. Bureau,J Denault, *Polymer Engineering and Science*, 44, 1212-1219 (2004).
5. A. Mirzadehand M. Kokabi, *European Polymer Journal*, 43, 3757-3765 (2007).
6. L. A. Utracki, M. Sepehrand E. Boccaleri, *Polymers for Advanced Technologies*, 18, 1-37 (2007).
7. Q. Zhang, W. Zhuang, H.-T. Shan, J.-H. Zhang, B.-X. Huand J. Shen, *Gaofenzi Cailiao Kexue Yu Gongcheng/Polymeric Materials Science and Engineering*, 23, 242-245 (2007).
8. D. W. K. Ho, J. H. Koo, J. C. Leeand O. A. Ezekoye. Hartford, CT, United states, 2008.
9. H. Thakkar, K. Y. Leeand L. A. Goettler. Nashville, TN, United States, 2003, pp 3009-3013.
10. I. K. Joy K Mishra, Chang-Sik Ha, Jin-Ho Ryou, Gue-Hyun Kim., *Rubber Chemistry and Technology*, 78, 42-54 (2005).
11. G. Naderi. in Thèse de doctorat (Ecole polytechnique de Montréal); École polytechnique de Montréal. Département de génie chimique  
2006, p 203.
12. G. Naderi, P. G. Lafleur and C. Dubois, *Polymer Engineering and Science*, 47, 207-217 (2007).

13. J. K. Mishra, G.-H. Kim, I. Kim, I.-J. Chung and C.-S. Ha, *Journal of Polymer Science Part B: Polymer Physics*, 42, 2900-2908 (2004).
14. W. Lertwimolnun and B. Vergnes, *Polymer*, 46, 3462-3471 (2005).
15. P. Potschke and D. R. Paul, *Polymer Reviews*, 43, 87-141 (2003).
16. A. Mirzadeh, P. G. Lafleur, M. R. Kamal and C. Dubois, *Polymer Engineering & Science*, 50, 2131-2142 (2010).
17. A. Mirzadeh, P. G. Lafleur, M. R. Kamal and C. Dubois, *Polymer Engineering & Science*, In press, (2011).
18. M. Narathichat, C. Kummerlöwe, N. Vennemann and C. Nakason, *Journal of Applied Polymer Science*, 121, 805-814.
19. N. Vennemann, K. Bökamp and D. Bröker, *Macromolecular Symposia*, 245-246, 641-650 (2006).
20. A. Barbe, K. Bökamp, C. Kummerlöwe, H. Sollmann, N. Vennemann and S. Vinzelberg, *Polymer Engineering & Science*, 45, 1498-1507 (2005).
21. K. G. Cai, C. G. Reid, S. Srinivasan and N. Vennemann. Chicago, IL., United States, 2004, pp 4239-4243.
22. K. G. Cai, C. G. Reid, T. H. and N. Vennemann, *Kautsch. Gummi Kunstst.*, 57, 227-234 (2004).
23. R. L. Anthony, R. H. Caston and E. Guth, *The Journal of Physical Chemistry*, 46, 826-840 (1942).
24. P. J. Flory, *Principles of Polymer Chemistry*, Cornell University Press, Ithaca, NY, 1990.
25. G. Dell'Anno. University of Pisa 2004.
26. J. Park, K. Eom, O. Kwon and S. Woo, *Microscopy and Microanalysis*, 7, 276-286 (2001).
27. H. M. James and E. Guth, *Journal of Chemical Physics*, 11, 455-481 (1943).
28. P. A. Bhadane, N. Virgilio, B. D. Favis, M. F. Champagne, M. A. Huneault and F. Tofan, *AIChE Journal*, 52, 3411-3420 (2006).
29. M. D. Ellul, A. H. Tsou and W. Hu, *Polymer*, 45, 3351-3358 (2004).

30. I. Pesneau, M. F. Champagne and M. A. Huneault, *Polymer Engineering & Science*, 42, 2016-2031 (2002).
31. A. Verbois, P. Cassagnau, A. Michel, J. Guillet and C. Raveyre, *Polymer International*, 53, 523-535 (2004).
32. S. Shahbikian, P. J. Carreau, M. C. Heuzey, M. D. Ellul, H. P. Nadella, J. Cheng and P. Shirodkar, *Polymer Engineering & Science*, n/a-n/a (2011).
33. G. Groeninckx, J. Oderkerk, G. De Schaetzen, B. Goderis and L. Hellemans, *Macromolecules*, 35, 6623-6629 (2002).
34. W. G. F. Sengers. in *Applied Sciences*; Delft University of Technology, 2005, p 171.
35. M. Van Duin, *Macromolecular Symposia*, 233, 11-16 (2006).
36. M. C. Boyce, S. Socrate, K. Kear, O. Yeh and K. Shaw, *Journal of the Mechanics and Physics of Solids*, 49, 1323-1342 (2001).
37. Y. Kikuchi, T. Fukui, T. Okada and T. Inoue, *Polymer Engineering & Science*, 31, 1029-1032 (1991).

## Chapter 8 GENERAL DISCUSSIONS AND CONCLUSIONS

### 8.1 Scientific Contributions and Concluding Remarks

Generally, the available literature related to the thermoplastic vulcanizates materials can be divided into two main categories; the first group deals with TPV production and their morphological, rheological and mechanical properties prepared either by extrusion process or using the internal batch mixers. The second one investigates the aforementioned properties for the TPV nanocomposites prepared by internal batch mixer. However, even though there are a few studies regarding the preparation of TPV nanocomposites using extrusion process in nonreactive system (i.e. incorporating the nanoclay into commercially available TPVs), the effects of nanoclay presence and particularly its dispersion level on dynamic vulcanisation had not been considered. The present study, for the first time, investigated systematically the TPV nanocomposites based PP/EPDM prepared by reactive extrusion process.

For this purpose, initially, to have a better insight about the formation of co-continuous structure in the corresponding TPE blends it was necessary to address the effect of various nanoclay dispersion levels on the co-continuity of the nonreactive blends.

Considering the studies in the second group, it seems that incorporating the nanoclay into the thermoplastic phase would be well-matched with what was defined as the main objective of this project to increase the functional and engineering properties of the final products. On the other hand, to disperse the nanoclay in the thermoplastic phase (PP) and to enhance nanocomposite formation, the use of PP-g-MA as the compatibilizer is an essential requirement.

The combination of the rheological studies and nanocomposite characterization methods reveals that the relaxation behaviour of compatibilizer controls the compatibilizer's efficiency to form a nanocomposite; as the relaxation time of the compatibilizer increases, the extent of intercalation in the corresponding nanocomposite improves. The mobility of the compatibilizer seems to take into account all other factors regarding PP-g-MA effectiveness such as molecular weight, viscosity and MA-content.

In this study, a special setup was employed to allow diffraction measurements at very small angles in wide angle X-ray diffraction measurements. The use of this modification is

recommended to characterize the nanocomposites in which the descriptions of changes in their XRD spectra are vague.

Considering the specific objectives defined in the first chapter, the effect of nanoclay dispersion level on the co-continuity of the TPE nanocomposite based on PP/EPDM was also investigated.

The results of the solvent extraction and gravimetry depict that the continuity index of the EPDM phase is decreased by the incorporation of nanoclay. As the processing conditions used in nanocomposite preparation were the same and also the viscosity ratios did not change significantly, the observed reduction in the continuity index might be related to an increase in the local apparent interfacial tension due to the presence of a portion of the nanoclay layers and intercalated montmorillonite tactoids at the interface. For that reason, the mentioned effect is more pronounced in the intercalated nanocomposites than in the partially exfoliated nanocomposites. On the other hand, our attempt to find a connection between these results and the rheological material functions reveals that a higher EPDM continuity index leads to a lower overshoot of normalized stress growth viscosity when the PP is the continuous phase.

Using the gamma irradiated samples for the thermoplastic phase continuity measurements; it was found that the rate of reduction in the thermoplastic continuity index by increasing the EPDM content decreases when the dispersion level improves. The higher continuity of PP in partially exfoliated systems is related to the higher thread stability; the presence of nanoclay layers in partially exfoliated PP nanocomposite increases elongational viscosity and contributes to melt strength. It leads to a lower value of the Tomokita function and consequently the break-up time increases. On the other hand, larger intercalated tactoids act as defects and reduce break-up times. A condition to satisfy this interpretation is that the nanoclay continues to reside in the thermoplastic phase. Therefore, some evidences were provided (see sec. 4.4.5.2) that clay remains mainly in the PP phase.

Another important research question is how different dispersion levels of nanoclay affect the crosslinking reaction of thermoplastic vulcanizate nanocomposites. The focus lies here on the reactive extrusion process. It should be recalled that the screw speed limits were chosen based on the technical restrictions (torque limit exerted on the twin screw extruder's shafts and the feeding rate limit of the used feeder). Based on the conclusions regarding compatibilizer optimization,

two grades of PP-g-MA were chosen among the others to prepare PP nanocomposites with different nanoclay dispersion levels as the models besides the neat PP as the thermoplastic phase to prepare TPVs. Among the various methods available to evaluate the extent of crosslinking for these complex systems, the solvent swelling method was not employed due to its low reliability and the AFM force modulation amplitude analysis was also discarded due to the technical restriction related to the presence of nanoclay. However, based on the strategy presented in the literature review (chapter 2) the dynamic vulcanization of the prepared models were characterized by different criteria such as gel content, viscosity and storage modulus, NMR signal line width, bound curative content and residual diene concentration. On the other hand, based on the data obtained from the initial part of the TSSR analysis, the crosslink density of the prepared samples was also determined.

Contrary to the results obtained from the blends prepared in internal batch mixer in which the extent of crosslinking in TPV nanocomposites is always lower than that of corresponding TPVs (in agreement with the available studies), the effect of nanoclay presence in the samples prepared by reactive extrusion is more complicated.

The combination of all the previously mentioned criteria provides sufficient information about the extent of crosslinking in each blend. However, without considering the co-continuity data, the elucidation of the effect of nanoclay presence and its dispersion level remains ambiguous. In other words, it is not clear whether the nanoclay presence increases or decreases or even does not change the crosslinking reaction significantly. Therefore, to draw a conclusion, one should take into account that the co-continuous structure exists at least before the second mixing zone of the twin screw extruder as confirmed by the torque-time curve analysing obtained from internal batch mixer, gel content experiments and SEM micrographs along the extruder axis for the reactive blends. Thus, the co-continuity of the blends before the second mixing zone is not only controlled by dynamic vulcanization but also by the presence of nanoclay.

It is suggested that the higher extent of crosslinking is associated with higher continuity index of EPDM in the mentioned structure. In turn, the nanoclay dispersion level, as pointed out earlier, determines the level of co-continuity. Higher continuity index of EPDM would probably result in a better dispersion of the curing system and a higher interfacial surface that favours the diffusion controlled reaction.

On the other hand, when the continuity of EPDM phase of two blends is in the same range, the barrier effect of nanoclays intensifies the crosslinking reaction by limiting the diffusion of the curing system into the thermoplastic phase and increasing the local concentration of the curative agent and the catalyst.

No significant difference was found between the extent of crosslinking reaction of TPVs and TPV nanocomposites for the samples prepared at lower screw speed (200 rpm, residence time of  $\sim 65$  s). Whereas the difference is more pronounced for the samples prepared at higher screw speed (400 rpm, residence time of  $\sim 45$  s). Moreover, if EPDM in the corresponding non-reactive system is a continuous phase, the extent of crosslinking reaction appears to be more dependent on the screw speed. Otherwise, higher residence time would increase the extent of crosslinking (when comparing between similar compositions processed at different screw speeds).

It is shown that NMR signal line width (backbone peak base) may be used to compare the extent of crosslinking in the TPVs in the absence of clay; however, the accumulated nanoclay agglomerates inside the EPDM domains, after complete dissolution of the thermoplastic phase, influence the mobility of the backbone of EPDM. Therefore, it cannot be used to compare the extent of crosslinking in the various nanocomposites. It is rather suggested to consider this criterion as the new measure of the nanoclay dispersion level for future studies.

In some cases, partially exfoliated TPV nanocomposites even for those prepared based on intercalated nanocomposite were obtained as a result of the high shear stress exerted by the dynamic vulcanization.

Finally, among different methods to characterize the elastomeric properties (sec. 2.3.1), recently developed temperature scanning stress relaxation (TSSR) analysis was chosen because of its importance in connection with the TPVs applications especially at elevated temperatures. The rubber like behaviour of the thermoplastic vulcanizate and their corresponding nanocomposites was explained by the morphological observations.

According to the morphological studies the prepared blends can be divided into two series; the blends showing the matrix-dispersed particle structure with a low level of interconnectivity of the rubber phase (blends containing 50 wt% and 60 wt% of EPDM) and the

blends with the fully developed extensive network between irregular shape rubber domains (blends containing 70wt% of EPDM).

For the first group, according to the SEM micrographs, the rubber particle size decreases by incorporation of nanoclay. By increasing the screw speed, the reduction in the number average droplet diameter is more pronounced for TPV without nanoclay while it remains almost in the same range for TPV nanocomposites. Here, the rubber index values correlate with the rubber droplet size. Therefore, nanoclay presence influences the rubber like behaviour mainly through its effect on the size of the rubber droplets that controls the number of retraction points in the proposed buckling mechanism during the TSSR test.

On the other hand, for the second group, rubber index values are associated with the crosslink density. Hence, the nanoclay presence and its dispersion level affect the rubber like behaviour through their effect on the extent of crosslinking reaction as indicated earlier.

The results obtained in this project could be used to optimize the TPV production and their properties according to their final applications and to fulfill the economical concerns in a scientific manner.

## 8.2 Recommendations

Based on the present research the following recommendations are proposed:

1. In this project we investigated the blends in which the interfacial tension between the thermoplastic phase and the rubber phase is too low. It is interesting to investigate the effect of different dispersion level of nanoclay on the TPE morphology and crosslinking reaction of the corresponding TPV for the system with higher interfacial tension between its components.
2. In this work, TPV nanocomposite production has been done by a three-step mixing process in twin screw extruder (Masterbatch preparation, PP nanocomposite preparation and TPV preparation). Comparative studies for one-step production would be interesting.
3. It is unclear how the TPVs with highly crosslinked rubber network are still processable. It needs to be clarified and their processability should be addressed.

4. It would be interesting subject to study the effect of different dispersion level of nanoclay on the non-linear viscoelastic behaviour of TPE nanocomposite and their corresponding TPVs using single and multiple start-up transient experiments.
5. A limitation of the work was that the clay was incorporated only into the PP phase. Furthermore, it was verified that it continues to reside in that phase. It would be recommended to investigate the nanoclay incorporating in the rubber phase.

## REFERENCES

- Abdou-Sabet, S., & Patel, R. P. (1991). Morphology of elastomeric alloys. *Rubber Chemistry and Technology*, 64(5), 769-779.
- Agnès Verbois, P. C. A. M. J. G. C. R. (2004). New thermoplastic vulcanizate, composed of polypropylene and ethylene-vinyl acetate copolymer crosslinked by tetrapropoxysilane: evolution of the blend morphology with respect to the crosslinking reaction conversion. *Polymer International*, 53(5), 523-535.
- Araki, T., & White, J. L. (1998). Shear viscosity of rubber modified thermoplastics: Dynamically vulcanized thermoplastic elastomers and ABS resins at very low stress. *Polymer Engineering and Science*, 38(4), 590-595.
- Aranda, P., & Ruiz-Hitzky, E. (1992). Poly(ethylene oxide)-silicate intercalation materials. *Chemistry of Materials*, 4(6), 1395-1403.
- Avella, M., Cosco, S., della Volpe, G., & Errico, M. E. (2005). Crystallization behavior and properties of exfoliated isotactic polypropylene/organoclay nanocomposites. *Advances in Polymer Technology*, 24(2), 132-144.
- Avgeropoulos, G. N., Weissert, F. C., Biddison, P. H., & Boehm, G. G. A. (1976). HETEROGENEOUS BLENDS OF POLYMERS. RHEOLOGY AND MORPHOLOGY. *Rubber Chemistry and Technology*, 49(1), 93-104.
- Barbe, A., Bökamp, K., Kummerlöwe, C., Sollmann, H., Vennemann, N., & Vinzelberg, S. (2005). Investigation of modified SEBS-based thermoplastic elastomers by temperature scanning stress relaxation measurements. *Polymer Engineering & Science*, 45(11), 1498-1507.
- Bhadane, P. (2005). *Morphology of ethylene-propylene-diene terpolymer/polypropylene (EPDM/PP) blends and their thermoplastic vulcanizates*. École polytechnique de Montréal. Département de génie chimique.
- Bhadane, P., Champagne, M., Huneault, M., Tofan, F., & Favis, B. (2006). Continuity development in polymer blends of very low interfacial tension. *Polymer*, 47(8), 2760-2771.
- Bhadane, P. A., Champagne, M. F., Huneault, M. A., Tofan, F., & Favis, B. D. (2006). Erosion-dependant continuity development in high viscosity ratio blends of very low interfacial tension. *Journal of Polymer Science, Part B (Polymer Physics)*, 44(14), 1919-1929.
- Bharadwaj, R. K. (2001). Modeling the Barrier Properties of Polymer-Layered Silicate Nanocomposites. *Macromolecules*, 34(26), 9189-9192.
- Biswas, M., & Ray, S. (2001). Recent Progress in Synthesis and Evaluation of Polymer-Montmorillonite Nanocomposites. In (Vol. 155, pp. 167-221): Springer Berlin / Heidelberg.
- Borcea, V. (2008). *Radioactive ion implantation of thermoplastic elastomers*: Presses univ. de Louvain.

- Bourry, D., & Favis, B. D. (1998). Cocontinuity and phase inversion in HDPE/PS blends: Influence of interfacial modification and elasticity. *Journal of Polymer Science, Part B: Polymer Physics*, 36(11), 1889-1899.
- C. Boyce, M., Socrate, S., Kear, K., Yeh, O., & Shaw, K. (2001). Micromechanisms of deformation and recovery in thermoplastic vulcanizates. *Journal of the Mechanics and Physics of Solids*, 49(6), 1323-1342.
- Cai, K. G., Reid, C. G., Srinivasan, S., & Vennemann, N. (2004). *Elastomeric property characterization of thermoplastic elastomers*, Chicago, IL., United States.
- Coran, A. (1982). Rubber-Thermoplastic Compositions. Part V. Selecting Polymers for Thermoplastic Vulcanizates. *Rubber Chem. Technol.*, 55(1), 116.
- Coran, A. Y., & Patel, R. P. (1978). United States Patent No. 4104210.
- Coran, A. Y., Patel, R. P., & William, S. (1981a). RUBBER-THERMOPLASTIC COMPOSITIONS - 4. THERMOPLASTIC VULCANIZATES FROM VARIOUS RUBBER-PLASTIC COMBINATIONS. *Rubber Chemistry and Technology*, 54(4), 892-903.
- Coran, A. Y., Patel, R. P., & William, S. (1981b). RUBBER-THERMOPLASTIC COMPOSITIONS - 5. SELECTING POLYMERS FOR THERMOPLASTIC VULCANIZATES. *Rubber Chemistry and Technology*, 55(1), 116-136.
- de Bussetti, S. G., & Ferreira, E. A. (2004). ADSORPTION OF POLY(VINYL ALCOHOL) ON MONTMORILLONITE. *Clays and Clay Minerals*, 52(3), 334-340.
- Dell'Anno, G. (2004). *Development of a new class of hybrid reinforced thermoplastic composites based on nanoclays and woven glass fibers*. University of Pisa
- Dietrich, S., & Amnon, A. (1994). *Introduction to percolation theory*: Taylor & Francis.
- Dikland, H. (1992). *Co-agents in peroxide vulcanizations of EPDM rubber*. Unpublished Ph.D. Thesis, University of Twente, The Netherlands.
- Drobny, J. G. (2007). *Handbook of Thermoplastic Elastomers*: William Andrew Pub.
- Ellul, M. D., Tsou, A. H., & Hu, W. (2004). Crosslink densities and phase morphologies in thermoplastic vulcanizates. *Polymer*, 45(10), 3351-3358.
- Fischer, W. K., & Woodbury, C. (1974). United States Patent No. 284521.
- Galuska, A. A., Poulter, R. R., & McElrath, K. O. (1997). Force Modulation AFM of Elastomer Blends: Morphology, Fillers and Cross-linking. *Surface and Interface Analysis*, 25(6), 418-429.
- Gessler, A. M., & Haslee, H. (1962). United States Patent No. 3037954.
- Giannelis, E., Krishnamoorti, R., Manias, E., Granick, S., Binder, K., de Gennes, P. G., et al. (1999). Polymer-Silicate Nanocomposites: Model Systems for Confined Polymers and Polymer Brushes

- Polymers in Confined Environments. In (Vol. 138, pp. 107-147): Springer Berlin / Heidelberg.
- Giannelis, E. P. (1996). Polymer Layered Silicate Nanocomposites. *Advanced Materials*, 8(1), 29-35.
- Giannelis, E. P. (1998). Polymer-layered silicate nanocomposites: Synthesis, properties and applications. *Applied Organometallic Chemistry*, 12(10-11), 675-680.
- Gilman, J. W., Jackson, C. L., Morgan, A. B., Harris, R., Manias, E., Giannelis, E. P., et al. (2000). Flammability Properties of Polymer Layered-Silicate Nanocomposites. Polypropylene and Polystyrene Nanocomposites *Chemistry of Materials*, 12(7), 1866-1873.
- Goettler, L. A., Richwine, J. R., & Wille, F. J. (1982). RHEOLOGY AND PROCESSING OF OLEFIN-BASED THERMOPLASTIC VULCANIZATES. *Rubber Chemistry and Technology*, 55(5), 1448-1463.
- Goharpey, F., Katbab, A. A., & Nazockdast, H. (2001). Mechanism of morphology development in dynamically cured EPDM/PP TPEs. I. effects of state of cure. *Journal of Applied Polymer Science*, 81(10), 2531-2544.
- Goharpey, F., Katbab, A. A., & Nazockdast, H. (2003). Formation of rubber particle agglomerates during morphology development in dynamically crosslinked EPDM/PP thermoplastic elastomers. Part 1: Effects of processing and polymer structural parameters. *Rubber Chemistry and Technology*, 76(1), 239-252.
- Goharpey, F., Nazockdast, H., & Katbab, A. A. (2005). Relationship between the rheology and morphology of dynamically vulcanized thermoplastic elastomers based on EPDM/PP. *Polymer Engineering and Science*, 45(1), 84-94.
- Grace, H. P. (1982). DISPERSION PHENOMENA IN HIGH VISCOSITY IMMISCIBLE FLUID SYSTEMS AND APPLICATION OF STATIC MIXERS AS DISPERSION DEVICES IN SUCH SYSTEMS. *Chemical Engineering Communications*, 14(3-6), 225-277.
- Groeninckx, G., Oderkerk, J., De Schaetzen, G., Goderis, B., & Hellemans, L. (2002). Micromechanical deformation and recovery processes of nylon-6/ rubber thermoplastic vulcanizates as studied by atomic force microscopy and transmission electron microscopy. *Macromolecules*, 35(17), 6623-6629.
- Hambir, S., Bulakh, N., & Jog, J. P. (2002). Polypropylene/clay nanocomposites: Effect of compatibilizer on the thermal, crystallization and dynamic mechanical behavior. *Polymer Engineering and Science*, 42(9), 1800-1807.
- Han, P. K., & White, J. L. (1995). Rheological studies of dynamically vulcanized and mechanical blends of polypropylene and ethylene-propylene rubber. *Rubber Chemistry and Technology*, 68(5), 728.
- Harrats, C., Thomas, S., & Groeninckx, G. (2006). *Micro- and nanostructured multiphase polymer blend systems: phase morphology and interfaces*: Taylor & Francis.
- Hasegawa, N., Kawasumi, M., Kato, M., Usuki, A., & Okada, A. (1998). Preparation and mechanical properties of polypropylene-clay hybrids using a maleic anhydride-modified polypropylene oligomer. *Journal of Applied Polymer Science*, 67(1), 87-92.

- Ho, R. M., Wu, C. H., & Su, A. C. (1990). Morphology of plastic/rubber blends. *Polymer Engineering and Science*, 30(9), 511-518.
- Jain, A. K., Gupta, N. K., & Nagpal, A. K. (2000). Effect of dynamic cross-linking on melt rheological properties of polypropylene/ethylene-propylene-diene rubber blends. *Journal of Applied Polymer Science*, 77(7), 1488-1505.
- Janssen, J. M. H., & Meijer, H. E. H. (1993). Droplet breakup mechanisms: Stepwise equilibrium versus transient dispersion. *Journal of Rheology*, 37(4), 12.
- Joy K Mishra, I. K., Chang-Sik Ha, Jin-Ho Ryou, Gue-Hyun Kim. (2005). STRUCTURE-PROPERTY RELATIONSHIP OF A THERMOPLASTIC VULCANIZATE (TPV)/LAYERED SILICATE NANOCOMPOSITES PREPARED USING MALEIC ANHYDRIDE MODIFIED POLYPROPYLENE AS A COMPATIBILIZER. *Rubber Chemistry and Technology*, 78(1), 42-54.
- Karger-Kocsis, J., Kallo, A., & Kuleznev, V. N. (1984). PHASE STRUCTURE OF IMPACT-MODIFIED POLYPROPYLENE BLENDS. *Polymer*, 25(2), 279-286.
- Katbab, A. A., & Mirzazadeh, H. (2006). PP/EPDM-based thermoplastic dynamic vulcanizates with organoclay: morphology, mechanical and viscoelastic properties. *Polymers for Advanced Technologies*, 17(11-12), 975-980.
- Kawasumi, M., Hasegawa, N., Kato, M., Usuki, A., & Okada, A. (1997). Preparation and Mechanical Properties of Polypropylene Clay Hybrids. *Macromolecules*, 30(20), 6333-6338.
- Kornmann, X. (1999). *Synthesis and characterisation of thermoset-clay nanocomposites* Unpublished Ph.D. Thesis, Lulea university of technology.
- Lattimer, R. P., Kinsey, R. A., Layer, R. W., & Rhee, C. K. (1989). Mechanism of phenolic resin vulcanization of unsaturated elastomers. *Rubber Chemistry and Technology*, 62(1), 107-123.
- Lebel, M. A. (1994). Factors fueling the growth of thermoplastic elastomers. *Plastics Engineering*, 50(1), 23-26.
- Lee, K. Y., & Goettler, L. A. (2004). Structure-property relationships in polymer blend nanocomposites. *Polymer Engineering and Science*, 44(6), 1103-1111.
- Leisen, J. (1999). <sup>1</sup>H NMR Relaxation Studies of Cured Natural Rubbers with Different Carbon Black Fillers. *Rubber Chem. Technol.*, 72(1), 1.
- Lertwimolnun, W., & Vergnes, B. (2005). Influence of compatibilizer and processing conditions on the dispersion of nanoclay in a polypropylene matrix. *Polymer*, 46(10), 3462-3471.
- Li, J., Ma, P. L., & Favis, B. D. (2002). The Role of the Blend Interface Type on Morphology in Cocontinuous Polymer Blends. *Macromolecules*, 35(6), 2005-2016.
- Litvinov, V. (1998). The Density of Chemical Crosslinks and Chain Entanglements in Unfilled EPDM Vulcanizates as Studied with Low Resolution, Solid State <sup>1</sup>H NMR. *Rubber Chem. Technol.*, 71(1), 105.

- Litvinov, V. M. (2006). EPDM/PP Thermoplastic Vulcanizates As Studied by Proton NMR Relaxation: Phase Composition, Molecular Mobility, Network Structure in the Rubbery Phase, and Network Heterogeneity. *Macromolecules*, 39(25), 8727-8741.
- Luciani, A., & Jarrin, J. (1996). Morphology development in immiscible polymer blends. *Polymer Engineering and Science*, 36(12), 1619-1626.
- Lyngaae-Jorgensen, J., Lunde Rasmussen, K., Chtcherbakova, E. A., & Utracki, L. A. (1999). Flow induced deformation of dual-phase continuity in polymer blends and alloys. Part I. *Polymer Engineering and Science*, 39(6), 1060-1071.
- Lyngaae-Jorgensen, J., & Utracki, L. A. (2003). Structuring polymer blends with bicontinuous phase morphology. Part II. Tailoring blends with ultralow critical volume fraction. *Polymer*, 44(5), 1661-1669.
- Machado, A. V., & Van Duin, M. (2005). Dynamic vulcanisation of EPDM/PE-based thermoplastic vulcanisates studied along the extruder axis. *Polymer*, 46(17), 6575-6586.
- Maiti, M., Patel, J., Naskar, K., & Bhowmick, A. K. (2006). Influence of various crosslinking systems on the mechanical properties of gas phase EPDM/PP thermoplastic vulcanizates. *Journal of Applied Polymer Science*, 102(6), 5463-5471.
- Mareanukroh, M. (2000). Use of Atomic Force Microscope as a Nanoindenter to Characterize Elastomers. *Rubber Chem. Technol.*, 73(5), 912.
- Metelkin, V. I., & Blekht, V. S. (1984). FORMATION OF A CONTINUOUS PHASE IN HETEROGENEOUS POLYMER MIXTURES. *Colloid Journal of the USSR (English Translation of Kolloidnyi Zhurnal)*, 46(3), 425-429.
- Mirzadeh, A., & Kokabi, M. (2007). The effect of composition and draw-down ratio on morphology and oxygen permeability of polypropylene nanocomposite blown films. *European Polymer Journal*, 43(9), 3757-3765.
- Naderi, G. (2006). *Thermoplastic elastomer nanocomposites based polypropylene and ethylene propylene diene terpolymer (PP/EPDM)*. École polytechnique de Montréal. Département de génie chimique
- Naderi, G., Lafleur, P. G., & Dubois, C. (2005). *Thermoplastic elastomer nanocomposites based on dynamically vulcanized PP/EPDM: Microstructure, mechanical and viscoelastic properties*, Boston, MA, United States.
- Naderi, G., Lafleur, P. G., & Dubois, C. (2007). Microstructure-properties correlations in dynamically vulcanized nanocomposite thermoplastic elastomers based on PP/EPDM. *Polymer Engineering and Science*, 47(3), 207-217.
- Nakason, C., Wannavilai, P., & Kaesaman, A. (2006). Effect of vulcanization system on properties of thermoplastic vulcanizates based on epoxidized natural rubber/polypropylene blends. *Polymer Testing*, 25(1), 34-41.
- Nakason, C., Wannavilai, P., & Kaesaman, A. (2006). Thermoplastic vulcanizates based on epoxidized natural rubber/polypropylene blends: Effect of epoxide levels in ENR molecules. *Journal of Applied Polymer Science*, 101(5), 3046-3052.

- Naskar, K. (2004). *Dynamically vulcanized PP/EPDM thermoplastic elastomers : exploring novel routes for crosslinking with peroxides*. Unpublished Ph.D. Thesis, University of Twente, Enschede.
- Naskar, K., & Noordermeer, J. W. M. (2004). Dynamically vulcanized PP/EPDM blends: Multifunctional peroxides as crosslinking agents - Part I. *Rubber Chemistry and Technology*, 77(5), 955-971.
- Okamoto, M., Morita, S., & Kotaka, T. (2001). Dispersed structure and ionic conductivity of smectic clay/polymer nanocomposites. *Polymer*, 42(6), 2685-2688.
- Okamoto, M., Morita, S., Taguchi, H., Kim, Y. H., Kotaka, T., & Tateyama, H. (2000). Synthesis and structure of smectic clay/poly(methyl methacrylate) and clay/polystyrene nanocomposites via in situ intercalative polymerization. *Polymer*, 41(10), 3887-3890.
- Özdemir, T. (2008). Gamma irradiation degradation/modification of 5-ethylidene 2-norbornene (ENB)-based ethylene propylene diene rubber (EPDM) depending on ENB content of EPDM and type/content of peroxides used in vulcanization *Radiation Physics and Chemistry*, 77(3), 787-793
- Peltola, P., Välikakka, E., Vuorinen, J., Syrjälä, S., & Hanhi, K. (2006). Effect of rotational speed of twin screw extruder on the microstructure and rheological and mechanical properties of nanoclay-reinforced polypropylene nanocomposites. *Polymer Engineering & Science*, 46(8), 995-1000.
- Pesneau, I., Champagne, M. F., & Huneault, M. A. (2002). PP/EMA TPV: Dynamic cross-linking through an alcoholysis reaction. *Polymer Engineering & Science*, 42(10), 2016-2031.
- Potschke, P., & Paul, D. R. (2003). Formation of Co-continuous Structures in Melt-Mixed Immiscible Polymer Blends. *Polymer Reviews*, 43(1), 87-141.
- Radhesh Kumar, C., Nair, S. V., George, K. E., Oommen, Z., & Thomas, S. (2003). Blends of Nylon/Acrylonitrile Butadiene Rubber: Effects of Blend Ratio, Dynamic Vulcanization and Reactive Compatibilization on Rheology and Extrudate Morphology. *Polymer Engineering and Science*, 43(9), 1555-1564.
- Radusch, H. J., & Pham, T. (1996). Morphology formation in dynamic vulcanized PP/EPDM blends. *Kautschuk Gummi Kunststoffe*, 49(4), 249-&.
- Reichert, P., Nitz, H. r., Klinke, S., Brandsch, R., Thomann, R., & Mülhaupt, R. (2000). Poly(propylene)/organoclay nanocomposite formation: Influence of compatibilizer functionality and organoclay modification. *Macromolecular Materials and Engineering*, 275(1), 8-17.
- Rivaton, A., Cambon, S., & Gardette, J. L. (2004). Radiochemical aging of ethylene-propylene-diene monomer elastomers. I. Mechanism of degradation under inert atmosphere. *Journal of Polymer Science Part A: Polymer Chemistry*, 42(5), 1239-1248.
- Sarazin, P., & Favis, B. D. (2003). Morphology control in co-continuous poly(L-lactide)/polystyrene blends: A route towards highly structured and interconnected porosity in poly(L-lactide) materials. *Biomacromolecules*, 4(6), 1669-1679.

- Sengers, W. G. F. (2005). *Rheological properties of olefinic thermoplastic elastomer blends*. Unpublished Ph.D. Thesis, Delft University of Technology.
- Shahbikian, S. (2010). *Phase morphology development and rheological behavior of non-plasticized and plasticized thermoplastic elastomer blends*. Ecole Polytechnique, Montreal.
- Shahbikian, S., Carreau, P. J., Heuzey, M. C., Ellul, M. D., Nadella, H. P., Cheng, J., et al. (2011a). Morphology and rheology of nonreactive and reactive EPDM/PP blends in transient shear flow: Plasticized versus nonplasticized blends. *Rubber Chemistry and Technology*, 84(3), 325-353.
- Shahbikian, S., Carreau, P. J., Heuzey, M. C., Ellul, M. D., Nadella, H. P., Cheng, J., et al. (2011b). Morphology development of EPDM/PP uncross-linked/dynamically cross-linked blends. *Polymer Engineering & Science*, n/a-n/a.
- Singh, C., & Balazs, A. C. (2000). Effect of polymer architecture on the miscibility of polymer/clay mixtures. *Polymer International*, 49(5), 469-471.
- Sinha Ray, S., & Okamoto, M. (2003). Polymer/layered silicate nanocomposites: A review from preparation to processing. *Progress in Polymer Science (Oxford)*, 28(11), 1539-1641.
- Steinmann, S., Gronski, W., & Friedrich, C. (2001). Cocontinuous polymer blends: Influence of viscosity and elasticity ratios of the constituent polymers on phase inversion. *Polymer*, 42(15), 6619-6629.
- Svoboda, P., Zeng, C., Wang, H., Lee, L. J., & Tomasko, D. L. (2002). Morphology and mechanical properties of polypropylene/organoclay nanocomposites. *Journal of Applied Polymer Science*, 85(7), 1562-1570.
- Thakkar, H., Lee, K. Y., & Goettler, L. A. (2003). *Phase Reinforcement Effects in TPV Nanocomposites*, Nashville, TN, United States.
- Thitithammawong, A., Nakason, C., Sahakaro, K., & Noordermeer, J. (2007). Effect of different types of peroxides on rheological, mechanical, and morphological properties of thermoplastic vulcanizates based on natural rubber/polypropylene blends. *Polymer Testing*, 26(4), 537-546.
- Tucker, C. L., III, & Moldenaers, P. (2002). Microstructural evolution in polymer blends. *Annual Review of Fluid Mechanics*, 34, 177-210.
- Utracki, L. A. (1991). On the viscosity-concentration dependence of immiscible polymer blends. *Journal of Rheology*, 35(8), 1615-1637.
- Utracki, L. A. (2002). *Polymer blends handbook volume 2*. Dordrecht; London: Kluwer Academic Publishers.
- Utracki, L. A., Sepehr, M., & Boccaleri, E. (2007). Synthetic, layered nanoparticles for polymeric nanocomposites (PNCs). *Polymers for Advanced Technologies*, 18(1), 1-37.
- van Duin, M. (1995). The Chemistry of Phenol-Formaldehyde Resin Vulcanization of EPDM: Part I. Evidence for Methylene Crosslinks. *Rubber Chem. Technol.*, 68(5), 717.
- Van Duin, M. (2006). Recent developments for EPDM-based thermoplastic vulcanisates. *Macromolecular Symposia*, 233, 11-16.

- Van Duin, M., & Machado, A. V. (2005). EPDM-based thermoplastic vulcanisates: Crosslinking chemistry and dynamic vulcanisation along the extruder axis. *Polymer Degradation and Stability*, 90(2), 340-345.
- Vennemann, N., Bökamp, K., & Bröker, D. (2006). Crosslink Density of Peroxide Cured TPV. *Macromolecular Symposia*, 245-246(1), 641-650.
- Verbois, A., Cassagnau, P., Michel, A., Guillet, J., & Raveyre, C. (2004). New thermoplastic vulcanizate, composed of polypropylene and ethylene-vinyl acetate copolymer crosslinked by tetrapropoxysilane: evolution of the blend morphology with respect to the crosslinking reaction conversion. *Polymer International*, 53(5), 523-535.
- Wang, D.-Q., Ma, J.-H., & Liang, B.-R. (2005). Crystallization kinetics and morphology of PP/PP-g-MAH/org-MMT nanocomposites. *Gaofenzi Cailiao Kexue Yu Gongcheng/Polymeric Materials Science and Engineering*, 21(3), 125-128.
- Wang, Y., Wu, K.-C., & Wang, J.-Z. (2007). Effect of maleated propylene on rheology of polypropylene nanocomposites. *Journal of Central South University of Technology (English Edition)*, 14(1 SUPPL), 160-164.
- Willemsse, R. C., de Boer, A. P., van Dam, J., & Gotsis, A. D. (1998). Co-continuous morphologies in polymer blends: A new model. *Polymer*, 39(24), 5879-5887.
- Willis, J. M., & Favis, B. D. (1988). Processing-morphology relationships of compatibilized polyolefin/polyamide blends. Part 1: The effect of an ionomer compatibilizer on blend morphology. *Polymer Engineering and Science*, 28(21), 1416-1426.
- Winters, R. (2002). *Mechanism of resol and sulfur vulcanization of EPDM: crosslink structure and kinetics of crosslinking resolved by 13C labeling and solid state NMR*: s.n.
- Xanthos, M. (1992). *Reactive Extrusion: Principles and Practice*: Hanser Gardner Pubns.
- Yano, K., Usuki, A., Okada, A., Kurauchi, T., & Kamigaito, O. (1993). Synthesis and properties of polyimide-clay hybrid. *Journal of Polymer Science Part A: Polymer Chemistry*, 31(10), 2493-2498.
- Zaharescu, T., Setnescu, R., Jipa, S., & Setnescu, T. (2000). Radiation processing of polyolefin blends. I. Crosslinking of EPDM-PP blends. *Journal of Applied Polymer Science*, 77(5), 982-987.
- Zhang, Q., Zhuang, W., Shan, H.-T., Zhang, J.-H., Hu, B.-X., & Shen, J. (2007). Preparation and characterization of polypropylene/montmorillonite nanocomposites. *Gaofenzi Cailiao Kexue Yu Gongcheng/Polymeric Materials Science and Engineering*, 23(5), 242-245.